A Mechanics Simulation of the Influence of Reinforcement Corrosion on RC Beam Behaviour

by

Qian Feng

A thesis submitted for the degree of Doctor of Philosophy

Department of Civil, Environment and Mining Engineering

The University of Adelaide

Australia

August 2016

TABLE OF CONTENTS

ABSTRACT

Corrosion influences both of the serviceability limit state and the ultimate limit state of the reinforced concrete structures. The mass loss of reinforcement caused by corrosion not only reduces cross sectional area of the reinforcement but also the bond between the steel reinforcement and surrounding concrete. By reducing the bond between the reinforcement and surrounding concrete, at serviceability limit state, corrosion may lead to an increase crack width and deflection, while at the ultimate limit state it may lead to reinforcement debonding. Hence, knowledge of the influence of corrosion on the bond between reinforcement and concrete is required to evaluate structural behaviour and extend the life span of the reinforced concrete structures.

This thesis first investigates the influence of corrosion on bond properties yielding a new bond-slip material model which has been developed from the analysis of a large data base of 377 individual test results obtained from published experimental results. From the resulting bond-slip model it is shown the debonding of reinforcement may occur at relatively low levels of corrosion and that the influence of corrosion on bond is more significant corrosion for large bar diameters.

Having developed a material model illustrating how corrosion influences the bond-slip relationship, the impact of corrosion on reinforced concrete beams is considered. Firstly the performance of beams at the ultimate limit state is considered through the development of a numerical segmental analysis technique to simulate member behaviour prior to and post debonding. Importantly this model shows that although debonding of reinforcement may occur at a relatively low level of corrosion, it does not always negatively impact member strength or ductility.

The impact of reinforcement corrosion at the serviceability limit state is then considered through the extension of the segmental approach to incorporate not only the influence of bond but also concrete creep and shrinkage. The resulting model couples concrete creep and shrinkage with reinforcement corrosion and predicts the influence of each on crack width and member deflection. Significantly it is shown that reinforcement corrosion can be much more easily monitored through measurement of crack widths over time rather than through consideration of member deflection and the approach proposed may be used to provide guidance on the variation in reinforcement corrosion along a span.

STATEMENT OF ORIGINALITY

I certify that this work contains no material which has been accepted for the award of any other degree or diploma in my name, in any university or other tertiary institution and, to the best of my knowledge and belief, contains no material previously published or written by another person, except where due reference has been made in the text. In addition, I certify that no part of this work will, in the future, be used in a submission in my name, for any other degree or diploma in any university or other tertiary institution without the prior approval of the University of Adelaide and where applicable, any partner institution responsible for the joint-award of this degree.

I give consent to this copy of my thesis when deposited in the University Library, being made available for loan and photocopying, subject to the provisions of the Copyright Act 1968.

The author acknowledges that copyright of published works contained within this thesis resides with the copyright holder(s) of those works.

I also give permission for the digital version of my thesis to be made available on the web, via the University's digital research repository, the Library Search and also through web search engines, unless permission has been granted by the University to restrict access for a period of time.

LIST OF PUBLICATIONS

Feng, Q, Visintin, P and Oehlers, DJ (2016) Deterioration of bond–slip due to corrosion of steel reinforcement in reinforced concrete. Magazine of Concrete Research, 68(15): 768-781.

Feng, Q, Visintin, P and Oehlers, D (2016) Quantifying through bond mechanics the effect of steel bar corrosion on the flexural capacity of RC beams. Submitted to Proceedings of the Institution of Civil Engineers-Structures and Buildings.

Feng, Q, Visintin, P and Oehlers, D (2016) A mechanics prediction of reinforcement corrosion in RC beams through the measurement of crack widths. Submitted to Structural Concrete.

ACKNOWLEDGEMENTS

I would like to express my sincere thanks to Professor Deric Oehlers for guiding my Ph.D study with his patience, passion and knowledge. His attitude towards details in research inspires me always. I thank him for his great effort to attend meetings every week, his helpful thoughts and the procedures that he helped me to build for my research work. Because of his involvement, the Ph.D study for me is not only doing research work, but also a training of brain which would be beneficial for me in the future. I feel very lucky to have him as my supervisor.

Besides, I would like to thank Dr. Phillip Visintin for his involvement in supervising me and also his encouragement when I was faced with difficulties. Furthermore, his suggestions on computer and programming techniques enhanced my efficiency largely towards research.

My sincere thanks also goes to Professor Michael Griffith who has been very helpful and nice towards the examinations of my Ph.D work. His kindness helped me adapt to this environment.

Finally, I would like to thank my parents, my husband back in China and my friends in Adelaide. Supports from them provides me with great energy overcoming obstacles.

INTRODUCTION

This thesis collects one published paper and 2 submitted papers to show (i) how bond-slip relationship between concrete and reinforcement changes with corrosion; (ii) how corrosion influences the serviceability and ultimate limit states of reinforced concrete structures; (iii) how to monitor the level of reinforcement corrosion.

The first chapter develops a material model to predict the bond-slip relationship between corroded reinforcement and concrete. A large database of existing test data is collected and the influence of concrete compressive strength, concrete cover and reinforcing bar diameter is investigated. Importantly, based on partial interaction theory, this paper quantifies the level of corrosion required to cause the reinforcement to debond and shows that relatively low levels of corrosion lead to debonding of reinforcement prior to yielding. Examples of analysis with different bar diameters are presented and it is shown from mechanics that reinforcement of larger diameters is more susceptible to the debonding induced by corrosion.

Having quantified the corrosion required to cause debonding of reinforcement in chapter 1, chapter 2 develops analytical procedures to calculate the flexural capacity and ductility of members with corroded reinforcement. Significantly the analysis procedures developed consider behaviour prior to dobonding of corroded reinforcement as well as analysis after debonding occurs by treating the unbonded reinforcement in a similar way to unbonded post-tensioned tendons. Importantly, the results of the analysis indicate that, despite the existence of debonding, members may still have significant capacity and ductility due to deformation compatibility between the reinforcement and concrete. This chapter tells reader that debonding caused by corrosion may not be a catastrophic problem in terms of beam strength and ductility.

Chapter 2 affords a model to analyse the problems caused by corrosion in ultimate limit states while Chapter 3 provides a monitoring way to quantify the corrosion effects in serviceability limit states. As is widely known, concrete creep and shrinkage have significant impact at the serviceability limit state of reinforced concrete leading to increased deflection and crack widths. In this chapter is shown how the additional time dependent action of reinforcement corrosion can be coupled with concrete creep and shrinkage. Significantly, this chapter provides a methodology for predicting variation in corrosion along the span of a member by monitoring crack widths over time.

CHAPTER 1

Manuscript

Feng, Q, Visintin, P and Oehlers, DJ (2016) Deterioration of bond–slip due to corrosion of steel reinforcement in reinforced concrete. Magazine of Concrete Research, 68(15): 768-781.

Statement of Authorship

Title of Paper	Deterioration of bond-slip due to corrosion of steel reinforcement in reinforced concrete
Publication Status	☑ Published ☐ Accepted for Publication ☐ Submitted for Publication ☐ Unpublished and Unsubmitted work written in manuscript style
Publication Details	Feng, Q, Visintin, P & Oehlers, DJ 2016, 'Deterioration of bond–slip due to corrosion of steel reinforcement in reinforced concrete', *Magazine of Concrete Research*, vol. 68, no. 15, pp. 768-781.

Principal Author

Name of Principal Author (Candidate)	Qian Feng		
Contribution to the Paper	Performed analysis on data base building and data processing, interpreted data and wrote manuscript.		
Overall percentage (%)	75%		
Certification:	This paper reports on original research I conducted during the period of my Higher Degree by Research candidature and is not subject to any obligations or contractual agreements with a third party that would constrain its inclusion in this thesis. I am the primary author of this paper.		
Signature		Date	19/08/2016

Co-Author Contributions

By signing the Statement of Authorship, each author certifies that:

i. the candidate's stated contribution to the publication is accurate (as detailed above);

ii. permission is granted for the candidate in include the publication in the thesis; and

iii. the sum of all co-author contributions is equal to 100% less the candidate's stated contribution.

Name of Co-Author	Phillip Visintin		
Contribution to the Paper	Supervised development of work, helped process data and acted as corresponding author.		
Signature		Date	19/08/2016

Name of Co-Author	Deric Oehlers		
Contribution to the Paper	Supervised development of work, helped edit manuscript and helped check details.		
Signature		Date	19/08/2016

Please cut and paste additional co-author panels here as required.

Deterioration of bond-slip due to corrosion of steel reinforcement in RC

Qian Feng, Phillip Visintin and Deric John Oehlers

Abstract

Corrosion of steel reinforcement in RC members is a common occurrence and a major concern as it can significantly affect both the serviceability and ultimate limit states. In order to simulate the effects of corrosion through mechanics, it is necessary to quantify the effects of corrosion on the material bond-slip properties, which is the subject of this paper. A large data base of 377 data points, is used to quantify the effect of corrosion on the bond-strength and on the bond-slip in a form that can be used in numerical analyses. This research concentrates on the changes in bond-strength and bond-slip due to corrosion and hence the changes relative to the uncorroded properties because these are already well quantified. Furthermore, it does not consider the clamping action of stirrups encasing the reinforcement. As an illustration of the application of these bond properties of corroded steel reinforcement, they are used in a mechanics analysis to show that large diameter bars are much more susceptible to the effects of corrosion than small diameter bars.

Keywords: bond-slip; bond-strength; steel reinforcement; corrosion; debonding.

Notation

A_r = cross-sectional area of reinforcing bar allowing for reduction in area due to corrosion

C = % corrosion; % loss of mass due to corrosion

C_{pk} = C at peak τ_{max}

C_{tran} = C at transition from yield to P_{IC}

$C_{1\text{-}2}$ = C at transition from Stage 1 to Stage 2 where k_t = 0

$C_{2\text{-}3}$ = C at transition from Stage 2 to Stage 3

c = reinforcing bar cover

d_b = reinforcing bar diameter

E_r = modulus of reinforcing bar

f_c = concrete cylinder strength

f_y = yield strength of reinforcing bar

K_s = slope of τ/δ descending branch

K_{s1} = K_s divided by τ_{max0}

K_{2D} = slope of Stage 2 Descending branch

$k_t = \tau_{max}/\tau_{max0}$

$(k_t)_{pk}$ = maximum or peak value of k_t

$k_{t\text{-}1A}$ = k_t in Stage 1 Ascending branch

$k_{t\text{-}2D}$ = k_t in Stage 2 Descending branch

$(k_{t\text{-}2D})_{exp}$ = experimental value of $k_{t\text{-}2D}$

$(k_{t\text{-}2D})_{the}$ = theoretical value of $k_{t\text{-}2D}$ from Eq. 5

$k_{t\text{-}3}$ = k_t in Stage 3 branch

L_{emb} = reinforcement embedment length

L_{per} = perimeter of uncorroded reinforcing bar; πd_b

P_{IC} = intermediate crack debonding resistance

P_{yld} = yield strength of reinforcing bar; $A_r f_y$

P_{yld0} = P_{yld} of uncorroded bar

α = exponent of ascending τ/δ model

δ = interface bond slip

δ_{max} = δ at zero shear

δ_1 = δ at τ_{max}

τ = interface bond shear; shear stress

τ_{max} = maximum shear stress; bond-strength

τ_{max0} = τ_{max} at zero corrosion

τ/δ = bond-slip variation

Figures

Figure 1: Idealised bond-slip

Figure 2: Idealised bond-strength variation with corrosion

Figure 3: Variation of bond-strength with corrosion

Figure 4: Variations of bond-slip

Figure 5: Stage 3 Descending

Tables

1. Introduction

The bond between the reinforcement and adjacent concrete in RC members affects the flexural behaviour at both the serviceability and ultimate limit states, as well as the shear capacity. Needless to say, the deterioration of this bond due to corrosion of the steel reinforcement can cause both increased deflections and reduced strengths and consequently lead to failure. Thus there is a clear need for accurately predicting the deteriorated bond-slip for use in mechanics models that use the bond-slip properties directly to simulate the flexural and shear capacity of beams (Visintin et al. 2012; Zhang et al. 2014) as well as the long term deflection (Visintin et al. 2013). Hence although not the purpose of this paper, with an improved definition of the change in bond properties due to corrosion these models can assist in predicting the performance of a structure deteriorated by reinforcement corrosion.

There is already a very large number of publications experimentally investigating or empirically quantifying: (1) the deterioration due to corrosion of the bond-strength (Johnston and Cox 1940;

Peattie and Pope 1956; Kemp et al 1968; Chapman and Shah 1987; Al-Sulaimani et al 1990; Maslehuddin et al 1990; Giuriani et al 1991; Cabrera and Ghoddoussi 1992; Almusallam et al 1996; Ihekwaba et al 1996; Fu and Chung 1997; Amleh and Mirza 1999; Auyeung et al 2000; Jin and Zhao 2001; Lee et al 2002; Lundgren 2002; Al-Negheimish and Al-Zaid 2004; Fang et al 2004; Amleh and Ghosh 2006; Cairns et al 2006; Fang et al 2006; Ouglova et al 2008; Kobayashi et al 2010; Shang et al 2011; Yalciner et al 2012; Fischer and Ožbolt 2013), that is the maximum interface shear τ_{max} that can be resisted after corrosion; (2) the change in the bond-slip (τ/δ) characteristics due to corrosion, that is the relationship between the interface shear stress τ and interface slip δ with corrosion (Al-Sulaimani et al 1990; Almusallam et al 1996; Lee et al 2002). Additionally there exist a number of studies deriving semi-empirical approaches for predicting the bond-strength τ_{max} as a function of corrosion. These models are derived through regression analyses of varying complexity and typically take a linear (Cabrera 1996), non-linear (Jin and Zhao 2001; Chung et al 2008) or exponential (Lee et al 2002; Bhargava et al 2007; Yalciner et al 2012) form. As with most empirical models they are generally accurate within the bounds of the experimental population from which they were derived. However, they are less accurate or inaccurate beyond these bounds and importantly and in general, existing models are derived from limited data sets.

In this study, the very large amount of published data referenced above has been scrutinised to extract that which gives sufficient information for the extraction of the changes in the bond properties due to corrosion. This refined data is then used to derive expressions for the changes in the bond-strength and bond-slip due to corrosion and which are compared with published values. It should be emphasised here that the purpose of this work is not to provide the practitioner with guidance on predicting the level of corrosion, but rather once the level of corrosion in a structure is determined to provide guidance on how the bond is affected. The outcomes of this research can be used directly in numerical simulations. However as just one example of their application, they are used in published partial-interaction mechanics analyses to quantify the debonding resistance of corroded reinforcement; such that it can be shown that there exists a transition whereby failure is no longer initiated by yielding of the reinforcement but rather debonding. Full details of all the papers considered, the reasons for eliminating papers and the results of all the statistical regression analyses are given elsewhere (Feng 2014).

2. Data bases

2.1 Idealisation of bond models

The variation of the bond-slip (τ/δ) is idealised as in Fig. 1. In theory any ascending branch can be used. For convenience the following model is used (CEB-FIP 1993)

$$\tau = \tau_{max}(\frac{\delta}{\delta_1})^{\alpha} \tag{1}$$

in which the maximum shear stress or bond-strength τ_{max} occurs at a slip δ_1 and in which α can be taken as 0.4 (CEB-FIP 1993). The slope of the descending branch in Fig. 1 is defined as K_s and the slip at zero shear $\delta_{max.}$

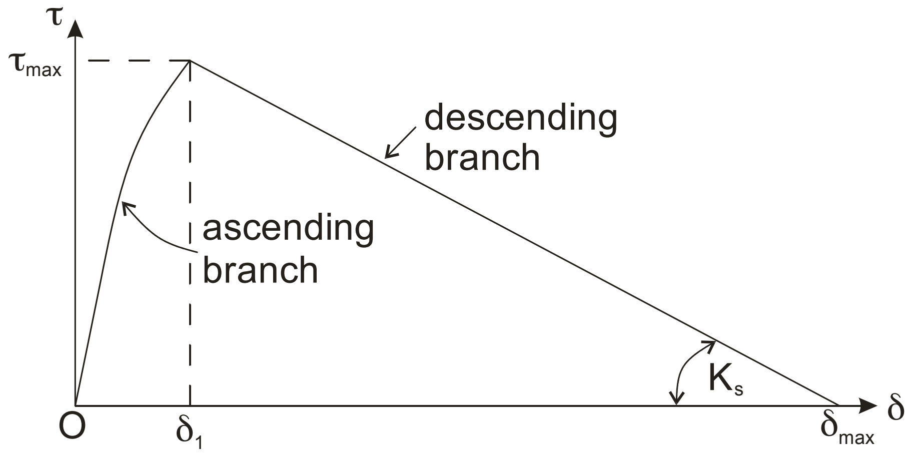

Figure 1 Idealised bond-slip

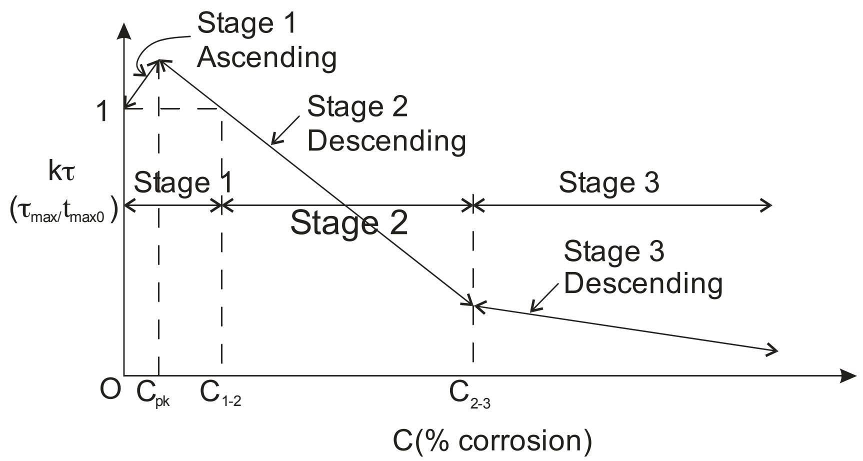

Figure 2 Idealised bond-strength variation with corrosion

The variation of the bond-strength (τ_{max}) with the percentage mass loss due to corrosion (C) is idealised as the tri-linear variation in Fig. 2 where k_t is the bond-strength τ_{max} as a proportion of the bond-strength with zero corrosion τ_{max0} (Mirza and Houde 1979; Howe 1979; Eligehausen et al 1982; CEB-FIP 1993 Wu and Zhao 2012). It should be noted that in this work the different forms of corrosion are not distinguished and it is assumed that corrosion quantified as a percentage of mass loss is uniform along the reinforcing bar. Within Stage 1, which is bounded by the peak bond-strength which occurs at a corrosion level C_{pk}, corrosion enhances the bond strength and thus a conservative design would be to ignore this benefit. Stage 2 is associated with a rapid reduction in the bond-strength below τ_{max0}. The transition from Stage 1 to Stage 2 occurs at a corrosion percentage C_{1-2}. Stage 3 is associated with very low bond-strengths that only reduce gradually. The transition from Stage 2 to Stage 3 occurs at a corrosion percentage of C_{2-3}.

It is a question of quantifying each linear variation of the tri-linear variation in Fig. 2. The first linear variation is the ascending branch in Stage 1 and will be referred to as 'Stage 1 Ascending'. Only a small part of the second linear variation occurs in Stage 1 so it will be referred to as 'Stage 2 Descending'. The third linear variation will be referred to as 'Stage 3'.

2.2 Limitations to test data

To allow the bond properties in Figs. 1 and 2 to be quantified, it was necessary to restrict the data base to tests in which there was enough information from which these bond properties could be extracted. Hence test data that did not conform with the following requirements or limitations were not used in the statistical analyses.

1. Limited to deformed or ribbed reinforcing bars.
2. Accelerated corrosion was achieved by inducing corrosion following the encasement of the bar in concrete, that is, tests in which bars were pre-corroded have been excluded.
3. The level of corrosion is calculated as the proportion of the mass loss as opposed to exposure time or the severity of the environment.
4. Pull-tests had short embedment lengths. Such that the average bond stress was close to the actual bond stress. This was confirmed through partial-interaction tension-stiffening analyses (Haskett et al. 2008; Knight et al. 2013; Feng 2014).
5. The ribbed bars were not entrapped by stirrups as the presence of stirrups is an additional anchor or confinement that should be dealt with as an alternative bond such as a mechanical anchor.
6. The concrete strength (f_c), concrete cover (c) and bar diameter (d_b) had been stated as these were considered important parameters.
7. The bond-strength at zero corrosion τ_{max0} had been measured within the series of tests. This was considered important as the aim of this research is to determine the change due to corrosion from this reference point.
8. When dealing with Stage 2 in Fig. 2, only test series in which there was sufficient test data to quantify the slope of the descending branch were included.

Full details of all the data collected and the reasons for omitting specific data are given elsewhere (Feng 2014). However in general most test data was excluded in the present study due to insufficient information to be able to determine the corrosion level as a function of mass loss. Additionally, tests were excluded if the bonded length, according to a tension stiffening analysis (Haskett et al. 2008), was found to be of a length such that the average bond stress could not be taken as the actual bond stress.

2.3 Bond-strength corrosion data base

Based on the requirements in Section 2.2, the data sets for the bond-strength are listed in Table 1. It can be seen that there are 15 data sets from 7 publications. Furthermore there is a wide range in the variables: f_c varied from 22 to 60 MPa; cover c from 8 to 70 mm; bar diameter d_b from 10 to 20 mm; and the embedment length L_{emb} from 40 to 208 mm.

Table 1 Bond-strength data sets

Data sets	References	f_c (MPa)	c (mm)	d_b (mm)	L_{emb} (mm)
M1	Almusallam et al. (1996)	30	64	12	102
M2	Al-Sulaimani et al. (1990)	30	70	10	40
M3	Al-Sulaimani et al. (1990)	30	68	14	56
M4	Al-Sulaimani et al. (1990)	30	65	20	80
M5	Yalciner et al. (2012)	23	8	14	50
M6	Yalciner et al. (2012)	23	23	14	50
M7	Yalciner et al. (2012)	23	38	14	50
M8	Yalciner et al. (2012)	51	8	14	50
M9	Yalciner et al. (2012)	51	23	14	50
M10	Yalciner et al. (2012)	51	38	14	50
M11	Fang et al. (2006)	52	60	20	80
M12	Jin and Zhao (2001)	22	44	12	80
M13	Cabrera and Ghoddoussi (1992)	56	69	12	48
M14	Amleh and Ghosh (2006)	60	25	20	208
M15	Amleh and Ghosh (2006)	50	25	20	208

The individual data points from the papers in Table 1 are given in Table A in the Appendix. There are a total of 196 results in which: there is always within a series a bond-strength at 0% corrosion that is τ_{max0} as this is the datum by which all other values are compared; the percentage corrosion C reached 80%; τ_{max} ranged between 0.67 MPa and 30.7 MPa; and k_t between 0.088 and 1.54. The bond-strengths τ_{max} in Table A are divided by their respective strengths at zero corrosion, that is at C equal to 0%, to determine k_t. Hence

$$\tau_{max} = k_t \tau_{max0} \tag{2}$$

which are plotted in Fig. 3 as the square points.

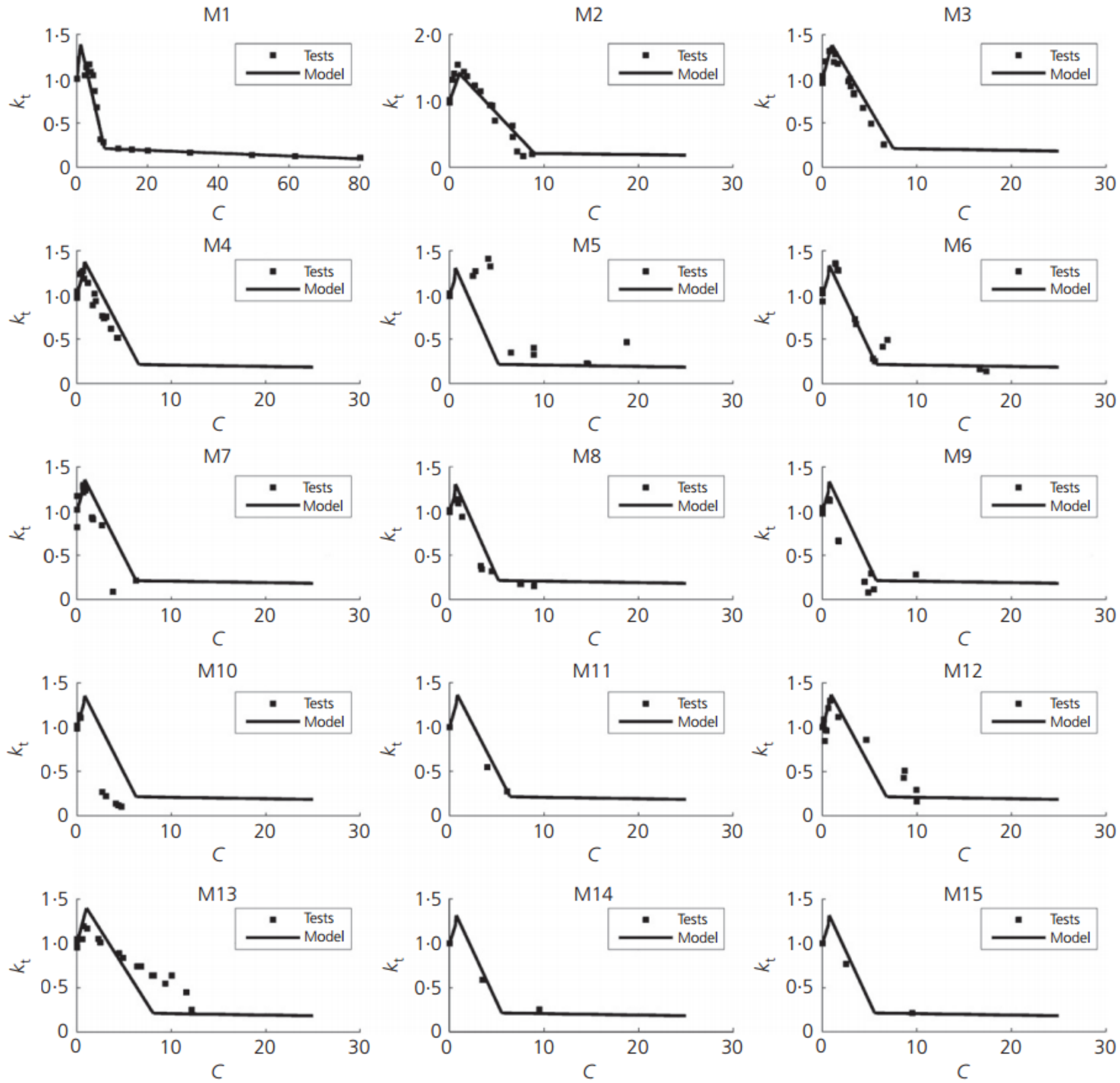

Figure 3 Variation of bond-strength with corrosion

2.4 Bond-slip corrosion data base

Based on the limitations in Section 2.2, the data base in Table 2 of 21 bond-slip curves from 3 publications was collected. The individual load-slip curves are shown as unbroken lines in Fig. 4. From each data set in Fig. 4, the maximum shear stress τ_{max} and the slip δ_1 at τ_{max} is listed in Table 3.

Furthermore from a linear regression analysis of the falling branches (Feng 2014) of each data set which is plotted as the 'Regression' line in Fig. 4 was extracted the slope of the falling branches K_s and these are also listed in Table 3.

Table 2 Bond-slip data sets

Data Set	Reference	C	f_c (MPa)	c (mm)	d_b (mm)	L_{emb}
N1	Almusallam et al. (1996)	0	30	63.5	12	102
N2	Almusallam et al. (1996)	3.6	30	63.5	12	102
N3	Almusallam et al. (1996)	4	30	63.5	12	102
N4	Almusallam et al. (1996)	4.78	30	63.5	12	102
N5	Almusallam et al. (1996)	5.09	30	63.5	12	102
N6	Almusallam et al. (1996)	7	30	63.5	12	102
N7	Almusallam et al. (1996)	15.7	30	63.5	12	102
N8	Almusallam et al. (1996)	20.5	30	63.5	12	102
N9	Almusallam et al. (1996)	32.5	30	63.5	12	102
N10	Al-Sulaimani et al. (1990)	0	30	70	10	40
N11	Al-Sulaimani et al. (1990)	0.87	30	70	10	40
N12	Al-Sulaimani et al. (1990)	1.5	30	70	10	40
N13	Al-Sulaimani et al. (1990)	4.27	30	70	10	40
N14	Al-Sulaimani et al. (1990)	6.7	30	70	10	40
N15	Al-Sulaimani et al. (1990)	7.8	30	70	10	40
N16	Al-Sulaimani et al. (1990)	1.62	30	68	14	56
N17	Al-Sulaimani et al. (1990)	2.75	30	68	14	56
N18	Al-Sulaimani et al. (1990)	5.45	30	68	14	56
N19	Lee et al (2002)	0	24.7	39	13	78
N20	Lee et al (2002)	3.2	24.7	39	13	78
N21	Lee et al (2002)	16.8	24.7	39	13	78

3. Bond-strength corrosion model

It is now a question of quantifying the variation of the bond-strength parameter k_t in Fig. 2 that is τ_{max} as a proportion of τ_{max0}.

3.1 Stage 2 Descending

First consider the falling branch in Fig. 2 that is between the percentage corrosions C_{pk} and $C_{2\text{-}3}$. From Fig. 3, it can be seen that the seven data sets M1-M4, M6, M12 and M13 have comparatively clearly defined falling branches. The falling branch in each of these sets of data points was subjected to a linear regression analysis from which was extracted and tabulated in Table 4: the individual slopes K_{2D}; and the percentage corrosion $C_{1\text{-}2}$ at k_t equal to one, that is when τ_{max} equalled that of the uncorroded specimen τ_{max0} that is $C_{1\text{-}2}$ in Fig. 2. Also listed is the non-dimensional cover parameter c/d_b and the concrete strength f_c.

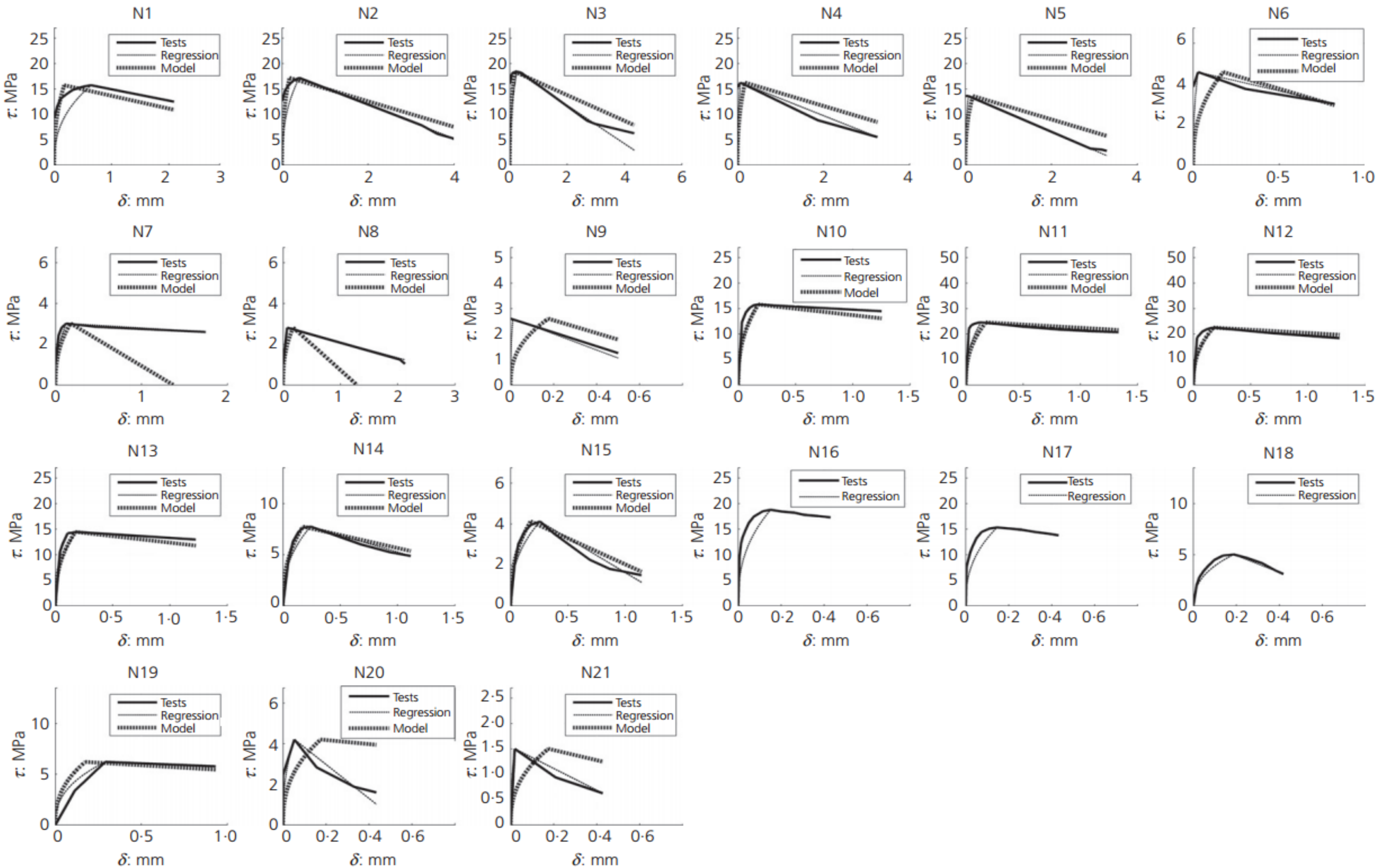

Figure 4 Variations of bond-slip

Table 3 Bond-slip properties

Data Set	C	τ_{max} (MPa)	δ_1 (mm)	K_s (N/mm^3)	Ks_{-1} (mm^{-1})
N1	0	15.7	0.643	-2.231	-2.527
N2	3.6	17.2	0.400	-3.325	-2.527
N3	4	18.4	0.250	-3.781	-2.527
N4	4.78	16.2	0.064	-3.365	-2.527
N5	5.09	13.6	0.071	-3.651	-2.527
N6	7	4.6	0.029	-1.969	-2.527
N7	15.7	3.0	0.125	-0.257	-2.527
N8	20.5	2.8	0.071	-0.767	-2.527
N9	32.5	2.6	0.010	-2.706	-2.527
N10	0	15.8	0.167	-1.223	-2.540
N11	0.87	24.5	0.133	-3.192	-2.540
N12	1.5	22.5	0.183	-3.779	-2.540
N13	4.27	14.5	0.183	-1.440	-2.540
N14	6.7	7.75	0.242	-3.292	-2.540
N15	7.8	4.13	0.258	-3.364	-2.540
N16	1.62	18. 8	0.151	-5.332	-
N17	2.75	15.3	0.146	-5.453	-
N18	5.45	5.0	0.188	-8.268	-
N19	0	6.22	0.291	-0.682	-1.000
N20	3.2	4.21	0.053	-8.356	-1.000
N21	16.8	1.50	0.019	-2.137	-1.000

Table 4: Stage 2 Descending statistical results

Data set	c/d_b	f_c (MPa)	$C_{1\text{-}2}$	K_{2D}
M1	5.29	30	4.30	-0.265
M2	7.00	30	3.82	-0.186
M3	4.86	30	2.51	-0.199
M4	3.25	30	1.69	-0.195
M6	1.64	23	2.63	-0.270
M12	3.67	22	3.15	-0.108
M13	5.75	56	3.00	-0.073

A linear regression analysis of the results in Table 4 Feng (2014) showed that neither $C_{1\text{-}2}$ nor K_{2D} were dependent on f_c. This is probably because the ordinate k_t in Fig. 2 is a function of τ_{max0} which itself is a function of f_c that is any dependency on f_c is already allowed for in τ_{max0}. However, the linear regression analyses Feng (2014) did show a strong dependency on c/d_b and the regressions are given below

$$C_{1-2} = 0.288\times\frac{c}{d_b} + 1.72 \tag{3}$$

$$K_{2D} = 0.0137\times\frac{c}{d_b} - 0.247 \tag{4}$$

from which can be derived the following linear variation of the Stage 2 Descending branch.

$$k_{t-2D} = \left(0.0137\frac{c}{d_b} - 0.247\right)C + 1.42 + 0.0475\frac{c}{d_b} - 3.94\times10^{-3}\left(\frac{c}{d_b}\right)^2 \tag{5}$$

The variation of k_{t-2D} from Equation 5 has been plotted in Fig. 3 as the 'Model' between C_{pk} and C_{1-2} for all the data sets and shows reasonably good correlation throughout. For only the data sets in Table 4, dividing the experimental values $(k_{t-SD})_{exp}$ by the theoretical values $(k_{t-2D})_{the}$ from Eq. 5 showed very good correlation up to a corrosion level of 6% (Feng 2014). Hence Eq. 5 should be limited to corrosion levels less than 6%; for this range the mean of $(k_{t-2D})_{exp}/(k_{t-2D})_{the}$ is 0.974 and the coefficient of variation 0.156.

3.2 Stage 1 Ascending

Consider the rising branch in Stage 1 in Fig. 2. The statistical analyses have been restricted to the data base in Section 3.1 which is listed in the first column in Table 5.

Table 5 Bond-strength Stage 1 statistical results

	Stage 1 Ascending ($k_{t-1A}=$)	Stage 2 Descending ($k_{t-2D}=$)	$(k_t)_{pk}$	C_{pk}	C_{1-2}	$\frac{C_{pk}}{C_{1-2}}$
M1	$0.0458C + 0.987$	$-0.265C + 2.14$	1.16	3.71	4.30	0.862
M2	$0.68C + 1.02$	$-0.186C + 1.71$	1.56	0.780	3.82	0.209
M3	$0.374C + 1.02$	$-0.199C + 1.5$	1.33	0.838	2.51	0.333
M4	$0.459C + 1.02$	$-0.195C + 1.33$	1.24	0.474	1.69	0.280
M6	$0.26C + 1$	$-0.27C + 1.71$	1.35	1.34	2.63	0.509
M12	$0.36C + 1$	$-0.108C + 1.34$	1.26	0.727	3.15	0.231
M13	$0.207C + 0.994$	$-0.0733C + 1.22$	1.16	0.806	3.00	0.269

The results of a linear regression analysis of the ascending branches of each data set are listed in Column 2 in Table 5, where, as would be expected the constant is close to unity. The descending branch in Column 3 is from a linear regression analysis of the data for that specific data set and not from Eq. 5. The intercept between the equations in Columns 2 and 3 is the maximum or peak bond-strength $(k_t)_{pk}$ in Column 4 which occurs at the corrosion level C_{pk} in Column 5. Substituting k_{t-2D} = 1 into Column 3 gives C_{1-2} in Column 6. Dividing C_{pk} in Column 5 by C_{1-2} in Column 6 gives Column 7.

The result for M1 in the Column 7 can be considered to be an outlier when compared with the remaining values which have a mean of 0.305. Rounding down to 0.3 gives

$$C_{pk} = 0.3C_{1\text{-}2} \tag{6}$$

which can be substituted into Eq. 5 to derive $(k_t)_{pk}$ for C_{pk}. A linear variation from this point (C_{pk}; $(k_t)_{pk}$) to the intercept on the ordinate (0,1) in Fig. 2 gives the following linear ascending branch in Stage 1

$$k_{t-1A} = \left(-0.0320\frac{c}{d_b} + 0.576\right)C + 1 \tag{7}$$

For data sets in Table 5, a comparison of the experimental data points with the theoretical predictions of Eqs. 5 and 7, that is $(k_t)_{exp}/(k_t)_{the}$, gave a mean of 0.97 and coefficient of variation of 0.16; these are listed in the second column in Table 6. Equations 5 and 7 are plotted for all the data sets in Fig. 3 with reasonable correlation.

Table 6 Comparison of experimental and theoretical bond strengths

	Proposed model	Bhargava et al. (2007)	Cabrera (1996)	Chung et al (2008)	Lee et al (2002)
Mean	0.97	1.12	1.14	1.17	1.12
COV	0.16	0.22	0.24	0.22	0.25
Confidence intervals	0.72 - 1.22	0.71 - 1.54	0.68 - 1.60	0.74 - 1.59	0.66 - 1.58

3.3 Stage 3

It can be seen in Fig. 3 that the transition from Stage 2 to Stage 3 is difficult to pinpoint as any scatter in the Stage 2 results may make the results appear to be Stage 3. To overcome this, only corrosion levels greater than 10% were used to quantify Stage 3 as shown in Fig. 5.

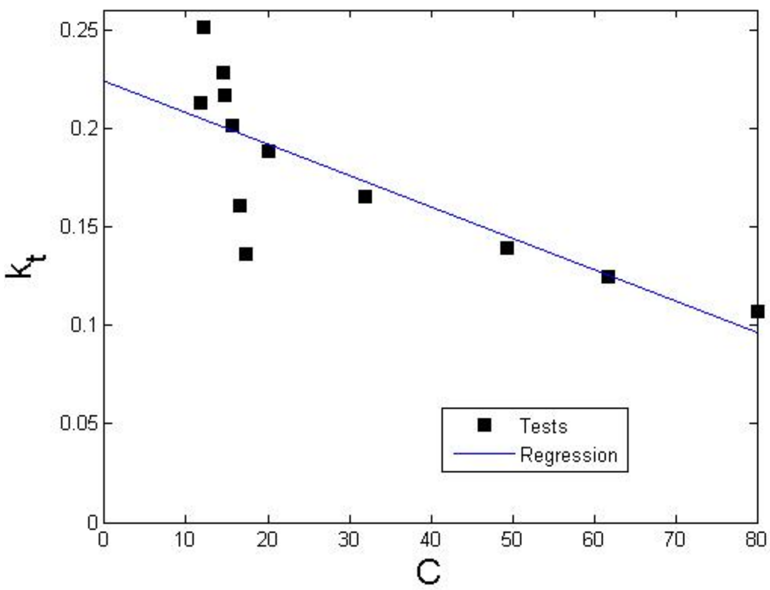

Figure 5 Stage 3 Descending

The linear regression is given by

$$k_{t-3} = -0.0016C + 0.224 \tag{8}$$

where the intercepts between Stages 2 and 3 occur at

$$C_{2-3} = \frac{-1.20-0.0475\frac{c}{d_b}+3.94\times10^{-3}\left(\frac{c}{d_b}\right)^2}{0.0137\frac{c}{d_b}-0.245} \tag{9}$$

which is plotted for all the data sets in Fig. 3.

3.4 Comparison with published models

The published models referenced in Table 6 apply to any strength of concrete, are based on mass loss due to corrosion and have been written in terms of k_t in Column 2 in Table 7. They have been compared with the Stage 2 data sets in Table 5; the statistical analysis of $(k_t)_{exp}/(k_t)_{the}$ are summarised in Table 6 where it can be seen that the new model has reduced the scatter.

Table 7: Published bond-strength models

References	
Cabrera (1996)	$k_t = \frac{\tau_{max}}{\tau_{max0}} = \frac{23.5-1.31C}{23.5}$
Bhargava et al. (2007)	$k_t = 1.0$, for $C \leq 1.5\%$

	$k_t = 1.192e^{-0.117C}$, for $C > 1.5\%$
Lee, Noguchi and Tomosawa (2002)	If $f_c \leq 21$MPa: $k_t = \frac{\tau_{max}}{\tau_{max0}}$=1, for $C < \frac{\ln(\frac{(0.34f_C-1.93)}{5.21})}{-0.0561}\%$ $k_t = \frac{\tau_{max}}{\tau_{max0}} = \frac{5.21e^{-0.0561C}}{0.34f_C-1.93}$, for $C \geq \frac{\ln(\frac{(0.34f_C-1.93)}{5.21})}{-0.0561}\%$ If $f_c > 21$MPa: $k_t = \frac{\tau_{max}}{\tau_{max0}} = \frac{5.21e^{-0.0561C}}{5.21}$
Chung, Kim and Yi (2008)	$k_t = 1$, for C$\leq$ 2.0% $k_t = \frac{24.7C^{-0.55}}{16.87}$, for $C > 2.0\%$

4. Bond-slip corrosion model

Having quantified in Section 3 the bond-strength τ_{max} in the bond-slip variation in Fig. 1, all that is now required is δ_1 and K_s; these have already been extracted from the data sets in Fig. 4 and are listed in Table 3. To mirror the research approach in Section 3, the ordinate in Fig. 4 has been normalised by dividing by τ_{max0}, which are the corresponding values in Table 3 at zero C. This adjustment to K_s in Table 3 is listed as K_{s1}; there are no values for N16-N18 as τ_{max0} had not been measured experimentally. A plot of K_{s1} against τ_{max}/τ_{max0} showed no correlation and, furthermore, that the points for N20 and N21 could be considered as outliers (Feng 2014). Ignoring the outliers, the average value for K_{s1} was -0.161 so that the slope K_s can be taken as the following in which the units are in N and mm.

$$k_s = -0.161 \times \tau_{max0} \tag{10}$$

A statistical analysis of δ_1 in Table 3 had an average value of 0.175 mm, showed large scatters and was unable to find a correlation (Feng 2014). It can be seen in Fig. 4 that the slip δ_1 at the maximum shear τ_{max} is very small compared with the slips associated with the falling branches and hence the measurement of these slips are prone to experimental error. It will be shown in the following section that although more research data is required to accurately quantify δ_1 is not an important parameter so that the average value can be taken, that is

$$\delta_1 = 0.175\,mm \tag{11}$$

Also shown in the following section, an important parameter for debonding is the slip limit δ_{max} in Fig. 1. It can be seen in Fig. 1 that δ_{max} depends on both δ_1 and K_s. Hence using Eqs. 10 and 11

$$\delta_{max} = 0.175 - \frac{\tau_{max0} k_t}{k_s} \tag{12}$$

where the units are in mm. The theoretical bond-slips from the above analyses are plotted as 'Model' in Fig. 4. A comparison with the experimental values in Fig. 4 that is the unbroken line shows that apart from N7 and N8 there appears to be good correlation.

5. Debonding of corroded reinforcing bars

The effect of corrosion on the degradation of the bond-slip properties has been quantified above. These properties can be used in numerical simulations such as finite element analyses or segmental analyses (Visintin et al. 2013; Zhang et al. 2014; Knight et al. 2014). However just as an example of its application as opposed to a detailed study, let us now consider the effect of the degradation of the bond-slip on the strength of the steel reinforcing bar.

The strength of a steel reinforcing bar is the lesser of either its yield capacity

$$P_{yld} = A_r f_y \tag{13}$$

or its resistance to debonding, that is its partial-interaction intermediate crack (IC) debonding resistance (Seracino et al. 2007; Haskett et al. 2008; Haskett et al. 2009; Muhamad et al. 2012; Visintin et al. 2012) of which one form (Haskett et al. 2009) is given by

$$P_{IC} = \sqrt{\tau_{max}\delta_{max}}\sqrt{L_{per}E_r A_r} \tag{14}$$

in which: A_r is the cross-sectional area of the bar allowing for loss of area due to corrosion; f_y is the yield capacity of the reinforcing bar; E_r is the modulus of the reinforcing bar; and L_{per} is the circumference of the reinforcing bar prior to corrosion that is πd_b. It can be seen in Eq. 14 that P_{IC} is proportional to the product $\tau_{max}\delta_{max.}$

To illustrate the effect of corrosion on P_{yld} and P_{IC}, consider reinforcing bars in RC members in which: the cover c is 40 mm; yield strength f_y = 500 MPa; bar modulus E_r = 200 GPa; and a concrete strength f_c = 40 MPa for which the peak bond stress for unconfined concrete was taken as τ_{max0} = 6.32 MPa (CEB-FIP 1993). The variations of the bond-slip properties for a 16 mm diameter bar are shown in Fig. 6 where the ascending branches are also shown as linear. For the uncorroded case that is C = 0: τ_{max} = 6.32 MPa; δ_{max}= 6.39 mm; and δ_1=0.175 mm. It can be seen in Fig. 6 that δ_1 is at least one order of magnitude smaller than δ_{max}. Hence any error in the estimation of δ_1 as discussed previously has only a very minor effect on the overall bond-slip. It can also be seen in Fig. 6 that the area under each bond-slip, that is $\tau_{max}\delta_{max}/2$, which is proportional to P_{IC} as in Eq. 14, rapidly diminishes with corrosion, that is the debonding resistance P_{IC} rapidly diminishes with corrosion.

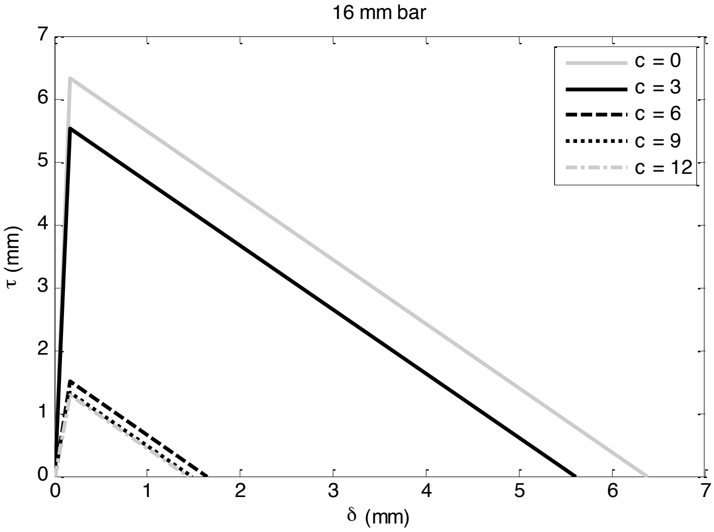

Figure 6 Variation of bond-slip with corrosion for 16 mm diameter bar

The variation of bond-slip with bar diameter at 6% corrosion is shown in Fig. 7. It can be seen that the areas under the plots $\tau_{max}\delta_{max}/2$ diminishes rapidly with increase in bar diameter such that large diameter bars are much more susceptible to debonding due to corrosion than small diameter bars.

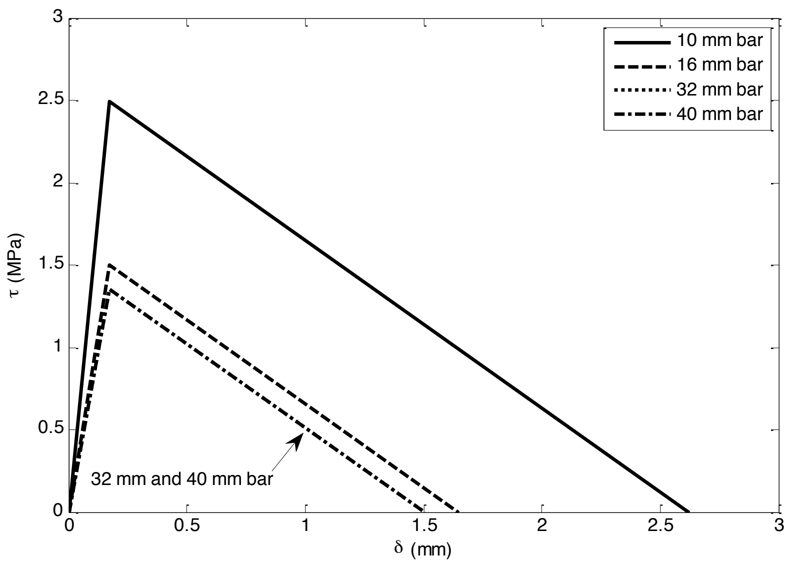

Figure 7 Variation of bond-slip with bar diameter

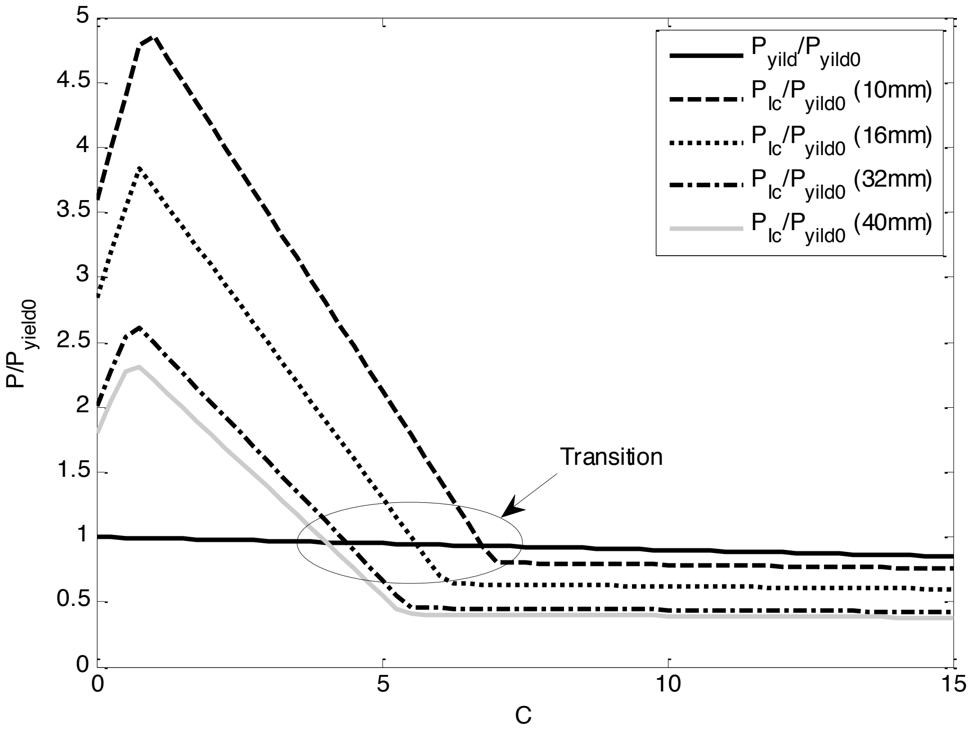

Figure 8 Debonded resistance

The effect of corrosion on the yield capacity from Eq. 13 and on the IC debonding resistance from Eq. 14 are plotted in Fig. 8. At zero corrosion, C = 0, P_{IC} is much larger that the yield capacity P_{yld} ranging from about twice as much for large diameter bars to 4¾ times for small diameter bars. Corrosion causes a small reduction in P_{yld} but a large reduction in P_{IC}. Where $P_{IC} > P_{yld}$, yielding limits the strength. Where $P_{IC} < P_{yld}$ debonding limits the strength. For large corrosions the 10 mm bars are only slightly below their yield capacity but for 40 mm bars they are about half. Hence large diameter bars are more likely to debond than small diameter bars and their debonding resistance is much less than their yield capacity.

The transition from yielding to IC debonding in Fig. 8 is shown in Fig. 9 where it can be seen that smaller diameter bars can resist higher corrosion levels than large diameter bars. This behaviour, which has also been noted by Fischer and Ožbolt (2013), arises because both the bond stress slip relationship and the partial interaction mechanics of IC debonding are dependent on the bar diameter.

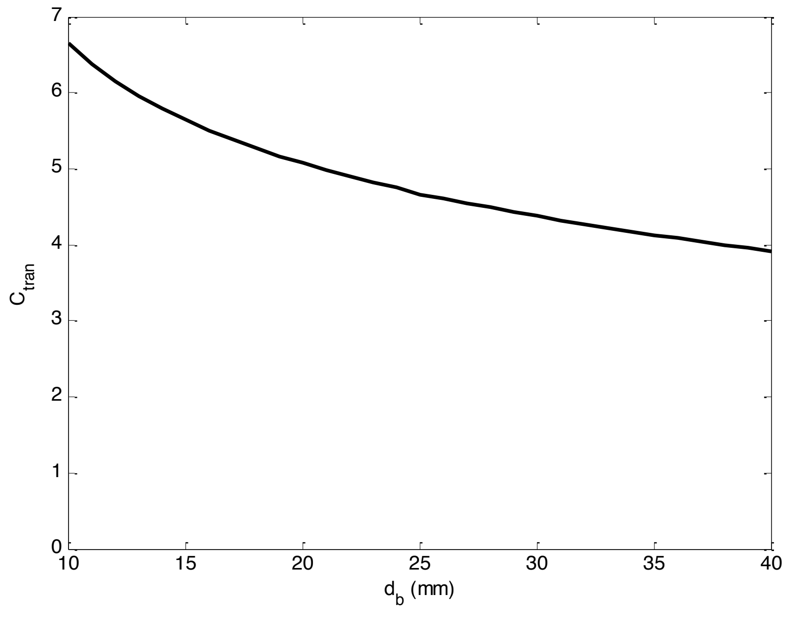

Figure 9 Transition from yield to debonding

The transition in Fig. 9 is given by the following equation

$$C_{tran} = 100 - 200\sqrt{\frac{E_r\delta_{max}\tau_{max}}{d_b f_y^2}} \tag{15}$$

which has been developed by equating the IC debonding resistance given by Eq. 14 with the reduced yield capacity of a corroded bar, and in which τ_{max} and δ_{max} can be determined from Eq. 2 and Eq. 12 respectively.

6. Conclusions

A model for determining the change in the bond-slip properties (τ/δ) of ribbed steel reinforcement due to corrosion has been developed. As this model quantifies the change, it can be used with existing published or code bond-slip models for uncorroded steel reinforcement to estimate the change due to various degrees of corrosion. As the model is based on the change in bond-slip, it was found that the only parameter that needs to be considered is the cover as a proportion of the bar diameter (c/d_b). The beneficial effect of early corrosion on the bond-strength (τ_{max}) has been quantified, as well as the ensuing rapid reduction in bond-strength followed by a very small region with slow deterioration of the bond. The quantified bond-strength of corroded reinforcement is then used in a bond-slip model where it is shown that the slip capacity (δ_{max}) is also reduced with corrosion. The research is completed with a study of the changes in τ_{max} and δ_{max} for different diameter bars and for different levels of corrosion. It is then shown through published partial-interaction mechanics how the parameter $\tau_{max}\delta_{max}$ can be used to quantify reinforcement debonding and how large diameter bars are prone to large reductions in strength compared with smaller diameter bars.

7. Appendix

Table A: Bond-strength individual data points

Data sets	Data points	C	τ_{max} (MPa)	k_t
M1	M1_1	0.000	15.8	1.00
	M1_2	2.22	16.4	1.04
	M1_3	2.67	17.9	1.13
	M1_4	3.44	18.4	1.16
	M1_5	3.89	17.1	1.08
	M1_6	4.56	16.4	1.04
	M1_7	5.00	13.6	0.86
	M1_8	5.56	10.7	0.68
	M1_9	6.67	5.00	0.32
	M1_10	7.50	4.49	0.28
	M1_11	11.7	3.37	0.21
	M1_12	15.6	3.17	0.20
	M1_13	20.0	2.97	0.19
	M1_14	31.9	2.60	0.17
	M1_15	49.4	2.20	0.14
	M1_16	61.7	1.97	0.13
	M1_17	80.0	1.69	0.11
M2	M2_1	0.00	15.1	0.97
	M2_2	0.00	15.70	1.01
	M2_3	0.00	15.1	0.97
	M2_4	0.30	20.4	1.32
	M2_5	0.50	21.9	1.41
	M2_6	0.87	23.9	1.54
	M2_7	1.50	22.3	1.44
	M2_8	1.83	21.2	1.37
	M2_9	2.66	19.1	1.23
	M2_10	3.25	17.7	1.14
	M2_11	4.27	14.5	0.94
	M2_12	4.52	14.4	0.93
	M2_13	4.81	10.9	0.70
	M2_14	6.67	9.70	0.63
	M2_15	6.70	7.10	0.46
	M2_16	7.15	3.70	0.24
	M2_17	7.80	2.60	0.17
	M2_18	8.75	3.10	0.20
M3	M3_1	0.00	16.3	1.02

	M3_2	0.00	15.2	0.95
	M3_3	0.00	16.5	1.03
	M3_4	0.30	19.1	1.19
	M3_5	0.76	21.0	1.31
	M3_6	0.90	21.1	1.32
	M3_7	1.22	19.0	1.19
	M3_8	1.36	20.4	1.28
	M3_9	1.62	18.7	1.17
	M3_10	2.75	15.5	0.97
	M3_11	2.89	16.0	1.00
	M3_12	3.00	14.6	0.91
	M3_13	3.33	13.2	0.83
	M3_14	3.33	13.4	0.84
	M3_15	4.29	10.7	0.67
	M3_16	5.15	7.90	0.49
	M3_17	5.45	4.80	0.30
	M3_18	6.50	4.10	0.26
M4	M4_1	0.00	15.0	0.97
	M4_2	0.00	16.1	1.04
	M4_3	0.00	15.4	0.99
	M4_4	0.30	19.1	1.23
	M4_5	0.50	19.4	1.25
	M4_6	0.65	19.7	1.27
	M4_7	0.78	18.3	1.18
	M4_8	1.16	17.6	1.14
	M4_9	1.67	13.7	0.88
	M4_10	1.86	15.7	1.01
	M4_11	2.00	14.4	0.93
	M4_12	2.69	11.8	0.76
	M4_13	2.87	11.4	0.74
	M4_14	3.08	11.6	0.75
	M4_15	3.13	11.7	0.76
	M4_16	3.60	9.60	0.62
	M4_17	4.25	8.00	0.52
	M4_18	4.35	8.00	0.52
M5	M5_1	0.00	9.10	0.99
	M5_2	0.00	9.40	1.02
	M5_3	0.00	9.20	1.00
	M5_4	2.47	11.2	1.21
	M5_5	2.72	11.7	1.27
	M5_6	4.09	13.0	1.41
	M5_7	4.10	13.0	1.41
	M5_8	4.32	12.2	1.32
	M5_9	4.33	12.2	1.32
	M5_10	6.51	3.20	0.35

	M5_11	8.90	3.70	0.40
	M5_12	8.90	3.00	0.33
	M5_13	14.5	2.10	0.23
	M5_14	14.7	2.00	0.22
	M5_15	18.8	4.30	0.47
M6	M6_1	0.00	14.0	1.06
	M6_2	0.00	12.3	0.93
	M6_3	0.00	13.5	1.02
	M6_4	1.37	18.0	1.36
	M6_5	1.40	17.9	1.35
	M6_6	1.60	17.0	1.28
	M6_7	1.69	16.9	1.27
	M6_8	3.45	9.60	0.72
	M6_9	3.57	8.90	0.67
	M6_10	5.36	3.70	0.28
	M6_11	5.56	3.30	0.25
	M6_12	6.40	5.50	0.41
	M6_13	6.87	6.50	0.49
	M6_14	16.7	2.13	0.16
	M6_15	17.3	1.80	0.14
M7	M7_1	0.00	12.1	0.82
	M7_2	0.00	17.3	1.17
	M7_3	0.00	15.0	1.01
	M7_4	0.66	18.9	1.28
	M7_5	0.68	17.9	1.21
	M7_6	0.68	18.0	1.22
	M7_7	0.69	19.1	1.29
	M7_8	0.84	18.3	1.24
	M7_9	0.88	18.2	1.23
	M7_10	1.60	13.7	0.93
	M7_11	1.69	13.4	0.91
	M7_12	2.66	12.4	0.84
	M7_13	3.81	1.30	0.09
	M7_14	3.81	1.30	0.09
	M7_15	6.27	3.20	0.22
M8	M8_1	0.00	19.6	0.99
	M8_2	0.00	20.0	1.01
	M8_3	0.77	22.3	1.13
	M8_4	0.80	22.4	1.13
	M8_5	0.90	21.7	1.10
	M8_6	0.94	21.5	1.09
	M8_7	1.33	18.5	0.93
	M8_8	3.30	7.50	0.38
	M8_9	3.41	6.80	0.34
	M8_10	4.47	6.30	0.32

	M8_11	7.48	3.50	0.18
	M8_12	7.56	3.50	0.18
	M8_13	8.95	3.00	0.15
M9	M9_1	0.00	20.9	1.00
	M9_2	0.00	21.7	1.03
	M9_3	0.00	21.0	1.00
	M9_4	0.00	20.4	0.97
	M9_5	0.65	23.8	1.13
	M9_6	0.77	23.5	1.12
	M9_7	0.77	23.4	1.11
	M9_8	1.70	14.0	0.67
	M9_9	1.72	13.8	0.66
	M9_10	4.45	4.20	0.20
	M9_11	4.86	1.70	0.08
	M9_12	5.14	6.20	0.30
	M9_13	5.46	2.40	0.11
	M9_14	9.90	5.90	0.28
M10	M10_1	0.00	27.3	0.98
	M10_2	0.00	27.7	1.00
	M10_3	0.00	28.3	1.02
	M10_4	0.31	31.5	1.14
	M10_5	0.39	30.7	1.11
	M10_6	2.69	7.43	0.27
	M10_7	3.08	6.10	0.22
	M10_8	4.12	3.81	0.14
	M10_9	4.39	3.24	0.12
	M10_10	4.71	2.86	0.10
M11	M11_1	0.00	21.8	1.00
	M11_2	4.00	11.9	0.55
	M11_3	6.10	6.00	0.28
M12	M12_1	0.00	8.74	1.00
	M12_2	0.12	8.92	1.02
	M12_3	0.16	9.48	1.09
	M12_4	0.24	7.36	0.84
	M12_5	0.32	8.45	0.97
	M12_6	0.43	8.39	0.96
	M12_7	0.62	10.6	1.21
	M12_8	0.81	11.3	1.30
	M12_9	1.66	9.72	1.11
	M12_10	4.64	7.50	0.86
	M12_11	5.97	5.68	0.65
	M12_12	8.70	4.45	0.51
	M12_13	8.60	3.75	0.43
	M12_14	9.95	2.54	0.29
	M12_15	9.99	1.40	0.16

M13	M13_1	0.00	18.5	0.95
	M13_2	0.00	19.4	1.00
	M13_3	0.00	20.3	1.05
	M13_4	0.31	20.3	1.05
	M13_5	0.56	20.3	1.05
	M13_6	0.71	23.2	1.19
	M13_7	1.09	22.6	1.16
	M13_8	2.28	20.4	1.05
	M13_9	2.48	19.6	1.01
	M13_10	4.46	17.2	0.89
	M13_11	4.87	16.2	0.84
	M13_12	6.41	14.3	0.74
	M13_13	6.80	14.3	0.74
	M13_14	7.95	12.4	0.64
	M13_15	8.16	12.4	0.64
	M13_16	9.35	10.6	0.55
	M13_17	10.0	12.4	0.64
	M13_18	11.6	8.68	0.45
	M13_19	12.1	4.87	0.25
M14	M14_1	0.00	5.10	1.00
	M14_2	3.50	3.00	0.59
	M14_3	9.50	1.30	0.26
M15	M15_1	0.00	3.11	1.00
	M15_2	2.50	2.39	0.77
	M15_3	9.50	0.67	0.22

References

Al-Negheimish AI and Al-Zaid RZ (2004) Effect of manufacturing process and rusting on the bond behavior of deformed bars in concrete. *Cement and concrete composites*, 26(6): 735-742.

Al-Sulaimani G, Kaleemullah M, Basunbul I and Rasheeduzzafar (1990) Influence of corrosion and cracking on bond behavior and strength of reinforced concrete members. *ACI Structural Journal*, 87(2):220-231.

Almusallam AA, Al-Gahtani AS, Aziz AR and Rasheeduzzafar (1996) Effect of reinforcement corrosion on bond strength. *Construction and Building Materials* 10(2): 123-129.

Amleh L and Ghosh A (2006) Modeling the effect of corrosion on bond strength at the steel-concrete interface with finite-element analysis. *Canadian Journal of Civil Engineering* 33(6): 673-682.

Amleh L and Mirza S (1999), 'Corrosion influence on bond between steel and concrete', *ACI Structural Journal* 96(3): 415-423.

Auyeung Y, Balaguru P and Chung L (2000) Bond behavior of corroded reinforcement bars. *ACI Materials Journal* 97(2): 214-220.

Bhargava K, Ghosh A, Mori Y and Ramanujam S (2007) Corrosion-induced bond strength degradation in reinforced concrete—Analytical and empirical models. *Nuclear engineering and design* 237(11): 1140-1157.

Cabrera J (1996) Deterioration of concrete due to reinforcement steel corrosion. *Cement and concrete composites* 18(1): 47-59.

Cabrera J and Ghoddoussi P (1992) The effect of reinforcement corrosion on the strength of the steel/concrete bond. *International conference on bond in concrete: from Research to Practice. CEB-RTU (Riga Technical University), Riga (Latvia)* 10/11-10/24.

Cairns J, Du Y and Law D (2006) Residual bond strength of corroded plain round bars. *Magazine of Concrete Research* 58(4): 221-231.

CEB-FIP (1993) Design of concrete structures. CEB-FIP-Model-Code 1990', *British Standard Institution, London, UK*.

Chapman RA and Shah SP (1987) Early-age bond strength in reinforced concrete. *ACI Materials Journal* 84(6): 501-510.

Chung L, Jay JH and Yi ST (2008) Bond strength prediction for reinforced concrete members with highly corroded reinforcing bars. *Cement and concrete composites* 30(7): 603-611.

Eligehausen R, Popov EP and Bertero, VV (1982) Local bond stress-slip relationships of deformed bars under generalized excitations'. Proceedings of the 7th European Conference on Earthquake Engineering 4:69-80.

Fang C, Lundgren K, Chen L and Zhu C (2004) Corrosion influence on bond in reinforced concrete. *Cement and concrete research* 34(11): 2159-2167.

Fang C, Lundgren K, Plos M and Gylltoft, K (2006) Bond behaviour of corroded reinforcing steel bars in concrete. *Cement and concrete research* 36(10): 1931-1938.

Feng Q. (2014) A mathematical model for the effect of corrosion on the bond-slip of reinforcement in RC structures without stirrups. School Report R190, August 2014. School of Civil, Environmental and Mining Engineering, The University of Adelaide, Australia.

Fischer C and Ožbolt J (2013) An appropriate indicator for bond strength degradation due to reinforcement corrosion. In Proceedings of VIII International Conference on Fracture Mechanics of Concrete and Concrete Structures.

Fu X and Chung D (1997) Effect of corrosion on the bond between concrete and steel rebar. *Cement and concrete research* 27(12): 1811-1815.

Giuriani E, Plizzari G and Schumm C (1991) Role of stirrups and residual tensile strength of cracked concrete on bond. *Journal of Structural Engineering* 117(1): 1-18.

Haskett M, Oehlers DJ, and Ali MM (2008). Local and global bond characteristics of steel reinforcing bars. *Engineering Structures*, 30(2): 376-383.

Ihekwaba N, Hope B and Hansson C (1996) Pull-out and bond degradation of steel rebars in ECE concrete. *Cement and concrete research* 26(2): 267-282.

Jin Wl and Zhao YX (2001) Effect of corrosion on bond behavior and bending strength of reinforced concrete beams', *Journal of Zhejiang University SCIENCE* 2(3): 298-308.

Johnston B and Cox KC (1940) The bond strength of rusted deformed bars. *ACI Journal Proceedings* 37: 57-72.

Kemp EL, Brezny F and Unterspan J (1968) Effect of Rust and Scale on the Bond Characteristcs of Deformed Reinforcing Bars. *ACI Journal Proceedings* 65(9): 743-756.

Knight D, Visintin P, Oehlers DJ and Jumaat MZ (2013): Incorporating residual strains in the flexural rigidity of RC members with varying degrees of prestress and cracking. *Advances in Structural Engineering* 16(10): 1701-1718.

Kobayashi K, Rokugo K, Sugiki K, Inaguma T and Maruyama S (2010) An experimental study on the effects of cracks on corrosion distribution and bond behavior of reinforcing bar. Proceeding of Fracture Mechanics of Concrete and Concrete Structures, Jeju South Korea, May 23-28.

Lee HS, Noguchi T and Tomosawa F (2002) Evaluation of the bond properties between concrete and reinforcement as a function of the degree of reinforcement corrosion. *Cement and concrete research* 32(8): 1313-1318.

Lundgren K (2002) Modelling the effect of corrosion on bond in reinforced concrete. *Magazine of Concrete Research* 54(3): 165-173.

Maslehuddin M, Allam IA, Al-Sulaimani GJ, Al-Mana A and Abduljauwad SN (1990) Effect of rusting of reinforcing steel on its mechanical properties and bond with concrete. *ACI Materials Journal* 87(5): 496-502.

Mirza SM and Houde J (1979) Study of bond stress-slip relationships in reinforced concrete. *ACI Journal Proceedings* 76(1): 19-46.

Ouglova A, Berthaud Y, Foct F, François M, Ragueneau F and Petre-Lazar I (2008) The influence of corrosion on bond properties between concrete and reinforcement in concrete structures. *Materials and structures* 41(5): 969-980.

Peattie K and Pope J (1956) Effect of age of concrete on bond resistance. *ACI Journal Proceedings* 52(2): 661-672.

Seracino R, Raizal Saifulnaz M, and Oehlers, D (2007) Generic Debonding Resistance of EB and NSM Plate-to-Concrete Joints. *ASCE Composites for Construction* 11(1), 62–70.

Shang F, An X, Mishima T and Maekawa K (2011) Three-dimensional nonlinear bond model incorporating transverse action in corroded RC members. *Journal of Advanced Concrete Technology* 9(1): 89-102.

Visintin P, Oehlers DJ, Wu C and Haskett M (2012) A mechanics solution for hinges in RC beams with multiple cracks. *Engineering Structures* 36: 61-69.

Visintin P, Oehlers DJ, and Haskett M (2013) Partial-interaction time dependent behaviour of reinforced concrete beams. *Engineering Structures* 49: 408-420.

Wu YF and Zhao XM (2012) Unified Bond Stress-Slip Model for Reinforced Concrete. *Journal of Structural Engineering* 139(11)*: 1951-1962*.

Yalciner H, Eren O and Sensoy S (2012) An experimental study on the bond strength between reinforcement bars and concrete as a function of concrete cover, strength and corrosion level. *Cement and concrete research* 42(5): 643-655.

Zhang T, Visintin P, Oehlers DJ and Griffith MC (2014) Presliding shear failure in prestressed RC beams. I: Partial-Interaction mechanism. *Journal of Structural Engineering* 140(10): 04014069.

CHAPTER 2

Manuscript

Feng, Q, Visintin, P and Oehlers, D (2016) Quantifying through bond mechanics the effect of steel bar corrosion on the flexural capacity of RC beams. Submitted to Proceedings of the Institution of Civil Engineers-Structures and Buildings.

Statement of Authorship

Title of Paper	Quantifying through bond mechanics the effect of steel bar corrosion on the flexural capacity of RC beams
Publication Status	☐ Published ☐ Accepted for Publication ☑ Submitted for Publication ☐ Unpublished and Unsubmitted work written in manuscript style
Publication Details	Feng, Q, Visintin, P & Oehlers, D 2016, 'Quantifying through bond mechanics the effect of steel bar corrosion on the flexural capacity of RC beams', *Submitted to Proceedings of the Institution of Civil Engineers-Structures and Buildings.*

Principal Author

Name of Principal Author (Candidate)	Qian Feng		
Contribution to the Paper	Analysed all the models in the manuscript, wrote the manuscript and edited		
Overall percentage (%)	75%		
Certification:	This paper reports on original research I conducted during the period of my Higher Degree by Research candidature and is not subject to any obligations or contractual agreements with a third party that would constrain its inclusion in this thesis. I am the primary author of this paper.		
Signature		Date	19/08/2016

Co-Author Contributions

By signing the Statement of Authorship, each author certifies that:

i. the candidate's stated contribution to the publication is accurate (as detailed above);
ii. permission is granted for the candidate in include the publication in the thesis; and
iii. the sum of all co-author contributions is equal to 100% less the candidate's stated contribution.

Name of Co-Author	Phillip Visintin		
Contribution to the Paper	Gave suggestions of data processing, supervised the work progress and acted as a corresponding author.		
Signature		Date	19/08/2016

Name of Co-Author	Deric Oehlers		
Contribution to the Paper	Supervised the research work, afforded opinions of the work, helped wrote and edited the manuscript.		
Signature		Date	19/08/2016

Please cut and paste additional co-author panels here as required.

Quantifying through bond mechanics the effect of steel bar corrosion on the flexural capacity of RC beams

Feng, Q., Visintin, P., Oehlers, D.J.

Abstract

Steel reinforcing bar corrosion is a major concern in reinforced concrete (RC) structures. Two problems have to be tackled: determining the rate of corrosion which is a material property; and secondly, determining the effect of corrosion on the behaviour of the RC structure not just at serviceability but also at the ultimate limit state which is a mechanics problem. This paper deals with the latter at the ultimate limit state, that is, the quantification through mechanics of the effect of a known amount of corrosion on the flexural capacity of RC beams with corroded longitudinal steel reinforcement. A partial interaction numerical procedure is described for quantifying the effect of corrosion at the ultimate limit state. The procedure quantifies: the flexural capacity and ductility prior to debonding that is whilst the corroded bars are still acting as reinforcement; the onset of debonding; and the flexural capacity and ductility after debonding whilst the corroded bars are acting as tendons. Hence the partial interaction numerical model can be used in design to quantify the effect of gradual corrosion on RC structures and also in assessment to quantify the effect of known corrosion within an existing member. It is shown through mechanics that the onset of debonding through the deterioration of the bond through corrosion is not necessarily a major or catastrophic problem as the RC beam can still have significant strength and ductility both of which are quantifiable. Furthermore, it is shown that corrosion has to occur in critical regions and over large critical lengths, also quantifiable, to significantly affect the behaviour at the ultimate limit state.

Keywords: reinforced concrete; beams; steel corrosion; durability; debonding; flexural strength; and flexural ductility.

Notation

b = width of prism

c = cover to reinforcing bar

$C(x\%)$ = x% corrosion by mass

d = diameter of bar

d_{NA} = depth from compression face to neutral axis

d_{tend} = distance from neutral of debonded bar acting as a tendon

E_c = elastic modulus of concrete

E_s = elastic modulus of steel reinforcement

E_{sh} = strain hardening modulus of steel reinforcement

$(EA)_r$ = axial rigidity of corroded reinforcement

FI = full interaction i.e. no interface slip

FRP = fibre reinforced polymer

f_c = concrete compressive cylinder strength

f_y = yield strength of steel reinforcement

h = depth of prism

IC = intermediate crack

K = crack opening stiffness

K_t = K of top layer of tension reinforcing bars

$K_{x\%}$ = K of bar with x% corrosion

L = half span of simply supported beam

L_{crt} = bond length required to develop P_{IC}

L_{db} = debonded length of reinforcing bar

L_{def} = half length of segment over which Euler-Bernoulli deformation occurs

L_{FI} = length over which there is no interface slip i.e. full interaction

L_{per} = perimeter length of uncorroded reinforcing bar

L_{PI} = length over which there is interface slap that is partial interaction

L_{wdg} = length of softening wedge

M = moment

M_{asc} = moment at which the concrete ascending branch is fully developed; moment at the onset of hinge formation

M_{des} = moment at which the concrete descending branch is fully developed; moment when hinge is fully formed

M_{fail} = maximum stable moment after which the moment capacity reduces rapidly

M_{IC} = moment at which P_{IC} is first achieved

M_{max} = maximum moment of the moment distribution applied to beam

P = force; force profile; force in reinforcing bar

P_{cc} = force in concrete in compression

P_{IC} = IC debonding resistance of reinforcing bar; maximum force in bar that can be developed by bond stresses alone

$P_{IC\text{-}x\%}$ = P_{IC} of bar with x% corrosion

P_{rc} = force in reinforcement in compression

P_{rtt} = force in reinforcement in tension at top layer

P_{rtb} = force in reinforcement in tension in bottom layer

P_{yld} = P to cause yield in reinforcing bar

$P_{yld\text{-}x\%}$ = P_{yld} with x% corrosion

$P_{yld\text{-}0}$ = P_{yld} with zero percentage corrosion

PI = partial interaction i.e. interface slip

RC = reinforced concrete

S_{cr} = crack spacing

$S_{cr\text{-}pr}$ = primary crack spacing

w_{cr} = crack width at level of reinforcing bar

α = angle of sliding wedge

χ = curvature

χ_{asc} = curvature at M_{asc}

χ_{des} = curvature at M_{des}

χ_{fail} = curvature at M_{fail}

χ_{yld} = curvature at M_{yld}

Δ = δ at crack face

Δ_b = Δ of bottom layer of tension reinforcement; $2\Delta_b$ is the crack width at level of bottom layer of tension reinforcement

Δ_t = Δ of top layer of tension reinforcement; $2\Delta_t$ is the crack width at level of top layer of tension reinforcement

δ = bond slip; deformation profile; longitudinal deformation in a beam

δ_1 = δ at δ_{max}

δ_{anch} = slip of anchorage; slip of mechanical anchorage; δ_{max} when only bond stress

δ_{ext} = extension of reinforcing bar due to debonded region; $\varepsilon_{IC}L_{db}$

δ_{max} = δ when τ tends to zero with increasing slip

δ_{max-0} = δ_{max} of uncorroded bar

$\delta_{max-x\%}$ = δ_{max} at x% corrosion

δ_{rb} = total deformation of reinforcing bar along L_{db}; $\delta_{max} + \varepsilon_{IC}L_{db}$

δ_{RC} = total deformation of RC member along L_{db} at the level of the debonded bar that is d_{tend} from neutral axis

ε = strain; strain profile

ε_{IC} = strain when force in bar is P_{IC}; $P_{IC}/(EA)_r$

ε_{pk} = train at peak concrete stress f_c

ε_{RC} = strain in RC member at level of the debonded reinforcement

ε_u = maximum softening strain when stress tends to zero

$\varepsilon_{u\text{-}model}$ = ε_u for L_{def} of segment being analysed

θ = rotation of a single cack face

θ_T = total rotation of segment imposed by Euler Bernoulli deformation;

σ = stress profile

σ_c = possible concrete stress profile

τ = bond shear stress

$\tau_{x\%}$ = bond shear stress at x% corrosion

τ_{max} = maximum bond shear strength

$\tau_{max\text{-}x\%}$ = τ_{max} at percentage corrosion

$\tau_{max\text{-}0}$ = τ_{max} of uncorroded bar

Figures

Tables

Introduction

Steel reinforcement corrosion is the principal form of deterioration in RC structures. Corrosion influences the longitudinal reinforcement in two ways: firstly the loss of area associated with corrosion leads to a reduction in the total force that can be carried; and secondly the products of corrosion exert stresses within the surrounding concrete leading to more extensive cracking and weakening of the bond between the reinforcement and the surrounding concrete (Al-Sulaimani et al., 1990; Almusallam 2001; Bhargava et al., 2007; Stanish et al., 1999). This latter reduction in bond leads to a loss of serviceability as it causes increased crack widths and a reduction in tension stiffening and, therefore, increased deflections. Moreover, the reduction in bond may lead to local or global debonding of the reinforcement (Haskett et al., 2008) thus limiting strength and ductility at the ultimate limit state which is the subject of this paper. While much experimental research exists particularly on the repair of corroded structures (Bertolini et al., 2013; Broomfield 2002; Lee et al., 2000; Miyagawa 1991), there is significantly less theoretical research, and thus guidance to practitioners, regarding the prediction through mechanics of the residual strength of members with corroded reinforcing bars (Castel et al., 2000; Coronelli and Gambarova 2004; Jin and Zhao 2001; Mangat, P S and Elgarf, M S 1999) particularly after partial debonding of the longitudinal bars (Eyre and Nokhasteh 1992; Yuan and Marosszeky 1991).

In previous research utilising published test results (Al-Sulaimani et al., 1990; Almusallam et al., 1996a; Amleh and Ghosh 2006; Cabrera and Ghoddoussi 1992; Fang et al., 2006; Jin and Zhao 2001; Lee et al., 2002; Yalciner et al., 2012), Feng et al. (2016b) developed a new local bond-stress/slip *(τ/δ)* relationship to describe the change in bond between corroded longitudinal bars and the surrounding concrete as illustrated in Figure 1 where: in the ordinate τ_C is the interface shear stress between the bar and adjacent concrete for reinforcement with *C*% corrosion by mass; τ_{max-0} is the maximum bond shear stress of an uncorroded bar that is with 0% corrosion; and in the abscissa δ is the slip between the longitudinal bar and adjacent concrete. The results of this research (Al-Sulaimani et al., 1990; Almusallam et al., 1996a; Amleh and Ghosh 2006; Cabrera and Ghoddoussi 1992; Fang et al., 2006; Jin and Zhao 2001; Lee et al., 2002; Yalciner et al., 2012) are summarised in Appendix 1.

The bond-slip O-A-B in Figure 1 is for the uncorroded longitudinal bar, that is C(0%), which can be determined through pull tests (Eligehausen et al., 1982) or from codes (CEB-FIP Model Code 1990: Design Code 1994). The maximum shear stress τ_{max-0} occurs at a slip of δ_1. The maximum slip capacity is δ_{max-0} and for slips greater than δ_{max-0}, the bond stress $\tau_{0\%}$ is zero. In regions of an RC beam where the bond slip is greater than δ_{max-0}, the bars will be referred to as unbonded or debonded such that the bars now acts as a tendon anchored at their ends in bonded regions. In regions of the beam where the slip is less than δ_{max-0} but greater than zero, the bars will be referred to as bonded and act as reinforcement and because there is interface slip these regions will also be referred to as partial interaction (PI) regions. Finally in regions of the beam where there is no interface slip that is δ is zero, the bars are also acting as reinforcement and these regions will be referred to as full interaction (FI) regions.

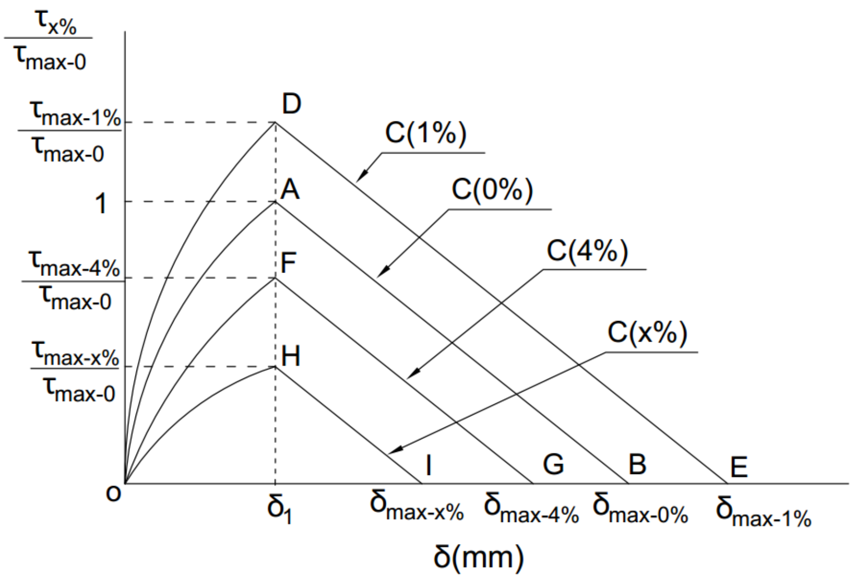

Figure 1 Change in interface bond/slip (τ/δ) due to corrosion

The corrosion level C(x%) in Figure 1 signifies the percentage loss of mass due to corrosion. At very low corrosion levels this can be beneficial (Al-Sulaimani et al., 1990; Almusallam et al., 1996a; Berto et al., 2008). This is illustrated at the 1% corrosion O-D-E where the maximum bond shear capacity $\tau_{max-1\%}$ is greater than τ_{max-0} and the slip capacity $\delta_{max-1\%}$ is greater than δ_{max-0}. After which, corrosion reduces both the interface shear capacity τ_{max} and slip capacity δ_{max} as shown for the 4% and C(x%) corrosion levels for O-F-G and O-H-I respectively.

From the bond-slip properties due to corrosion as illustrated in Figure 1, Feng et al. (2016b) used partial interaction (PI) intermediate crack (IC) debonding mechanics (Oehlers et al., 2015) to quantify the IC debonding resistance of a bar with x% corrosion, $P_{IC-x\%}$; this occurs when the bond-slip properties in Figure 1 are fully developed such that the maximum slip is that for x% corrosion that is $\delta_{max-x\%}$. The bar force $P_{IC-x\%}$ is the maximum force that the interface bond for x% corrosion in Figure 1 can apply to the bar as any further attempt to increase the force in the bar will simply cause greater slip without an increase in force (Haskett et al., 2008; Oehlers and Seracino 2004). The force in the bar is also limited by the yield capacity of the reinforcement $P_{yld-x\%}$, that is the yield stress times the cross-sectional area of the bar less the area lost through corrosion such that P_{yld-0} is the yield capacity prior to corrosion.

The variation in the strength of the corroded reinforcement is illustrated in Figure 2. The ordinate is either: $P_{IC\text{-}x\%}/P_{yld\text{-}0}$ that is the maximum force in the steel reinforcing bar as limited by the IC debonding strength at x% corrosion $P_{IC\text{-}x\%}$ as a proportion of the yield capacity prior to corrosion $P_{yld\text{-}0}$ that is at C = 0% corrosion; or $P_{yld\text{-}x\%}/P_{yld\text{-}0}$ that is the maximum force in the steel reinforcing bar as limited by the yield strength $P_{yld\text{-}x\%}$ as a proportion of $P_{yld\text{-}0}$.

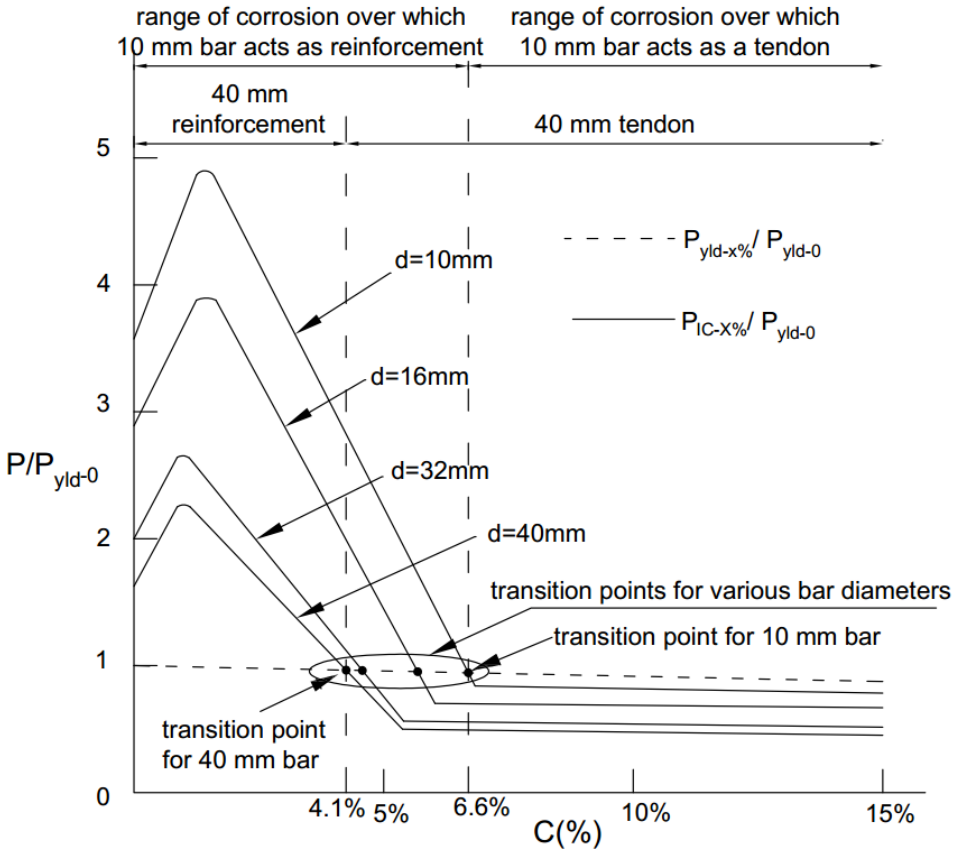

Figure 2 Capacities of corroded reinforcing bars (Feng et al., 2016b)

The broken line $P_{yld\text{-}x\%}/P_{yld\text{-}0}$ in Figure 2 shows the reduction in the yield capacity due to corrosion which depends only on the reduced cross-sectional area due to corrosion. The unbroken lines $P_{IC\text{-}x\%}/P_{yld\text{-}0}$ show the change in the IC debonding resistances for various bar diameters d that range from 10 mm to 40 mm. It can be seen that P_{IC} initially increases with corrosion as small amounts of corrosion improve the bond (Al-Sulaimani et al., 1990; Almusallam et al., 1996a; Berto et al., 2008) after which there is a rapid reduction in P_{IC} with corrosion which is followed by a gradual reduction. Where $P_{IC\text{-}x\%}/P_{yld\text{-}0}$ is greater than $P_{yld\text{-}x\%}/P_{yld\text{-}0}$, yield will occur before debonding and vice versa. It can be seen that these transition points, shown as dot points in Figure 2, range from 4.1% corrosion for 40 mm diameter bars to 6.6% for 10 mm diameter bars where the scatter of this range is given elsewhere (Feng et al., 2016b). Hence small diameter bars can sustain a higher amounts of corrosion than large diameter bars before debonding. Furthermore after debonding, the smaller diameter bars can resist a higher proportion of their yield capacity than larger diameter bars as shown by the variation after the transition point.

It may be worth noting in Figure 2 that for corrosion levels less than the transition point, the steel bar is acting as bonded reinforcement. In contrast, with corrosion levels greater than the transition point the steel bars are now debonded and subsequently act as tendons. Examples are given for 10 mm bar diameters at the top of Figure 2 where it can be seen that for corrosion levels up to 6.6% the bars remains bonded and act as reinforcement and for higher corrosion levels they acts as tendons. The ranges for 40 mm bars are also shown where the transition occurs at a lower percentage of 4.1%.

In this paper, a new analysis procedure based on the fibre reinforced polymer (FRP) plate debonding work of (Oehlers et al., 2015, 2016) is developed to predict both the strength and ductility of beams with: either bonded bars in which the bars acts as reinforcement that is the longitudinal stress in the bar varies along its bonded length; or with regions of unbonded bars in which the unbonded bars act as tendons with uniform stress along the debonded length. There is already much experimental work on RC beams with bonded bars (Almusallam et al., 1996b; Jin and Zhao 2001; Val et al., 1998) and on RC beams with regions of unbonded bars (Cabrera 1996; Coronelli and Gambarova 2004; Mangat, Pritpal S and Elgarf, Mahmoud S 1999). The aim of this paper is to provide the fundamental mechanics that govern and quantify both behaviours and their interaction. Hence the emphasis of this paper is on simulating the mechanisms that has already been recognised in practice.

In the following, the mechanics of reinforcement debonding is first explained along with a generic procedure for predicting the capacity of beams with unbonded reinforcement. A generic segmental approach, previously developed by the authors (Oehlers et al., 2014a, 2014b), is then summarised as it provides a technique for obtaining through the mechanics of partial interaction: the necessary sectional behaviours of a member with either bonded or unbonded reinforcement; and can directly incorporate the reduction in tension stiffening and increase in crack widths due to deterioration of bond. Examples of the application of the segmental and member approaches are then provided to illustrate the transition from bonded to unbonded behaviour that occurs through corrosion.

Debonding of reinforcement

Consider the half span of a beam in Figure 3(b) to which a distribution of moment *M* in Figure 3(a) is applied. The behaviour of the reinforcing bars in the beam in Figure 3(b) are analogous to the pull test in Figure 3(c) in which the reinforcing bars are encased in a prism of width *b* and depth *h* as shown on the right hand side of Figure 3(b); full descriptions of this analogy are given elsewhere (Oehlers et al., 2015, 2016). Figures 3(c-e) describe the stages of debonding.

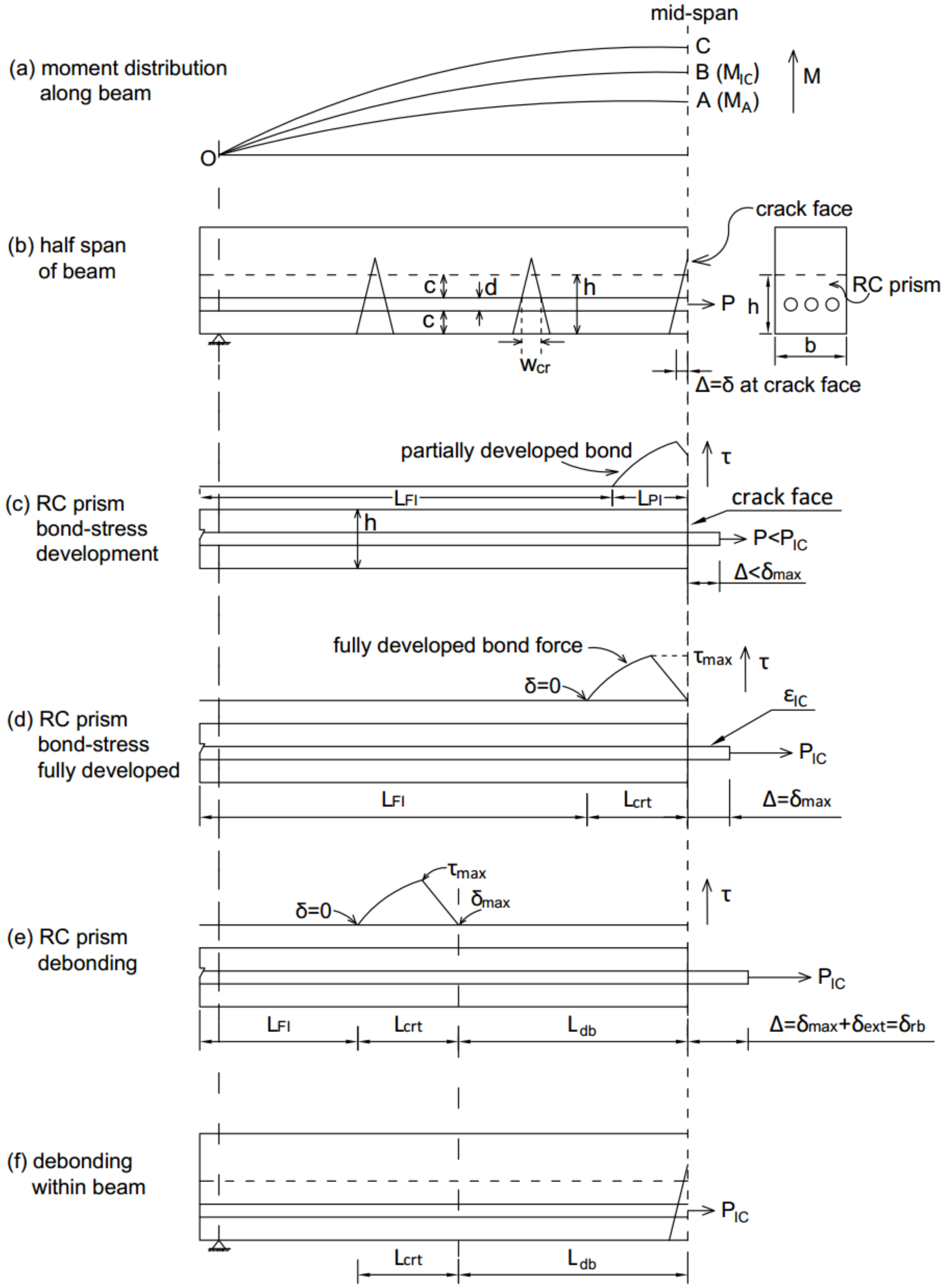

Figure 3 Member debonding mechanism

Consider at first the moment distribution OA in Figure 3(a) where the maximum moment M_A, that is at the mid-span at A, is less than the IC moment M_{IC} which is the moment when the force in the bar first reaches P_{IC}. In this case, the force in the reinforcing bar P in Figure 3(b) is less than P_{IC} for that reinforcing bar of diameter d and corrosion level x%. The force P in Figure 3(b) induces an interface slip δ which at the crack face will be referred to as Δ as shown and which is also half the crack width w_{cr} at the level of the reinforcing bar. The analogous pull test (Oehlers et al., 2015, 2016) is shown in Figure 3(c) where the slip of the bar from the crack face is Δ for the force *P*. The relationship between *P*, Δ and the distribution of τ over the length L_{PI}, in which there is partial interaction that is slip, can be derived from PI tension stiffening numerical analyses (Oehlers et al., 2014a) using the appropriate bond-slip characteristics in Figure 1. As *P* in Figure 3(c) is less than P_{IC}, the bond stresses τ are not fully developed, that is the integral of these shear stresses over the bonded area along L_{PI} has not reached its maximum value, because the slip Δ is less than δ_{max}.

Now consider the moment distribution OB in Figure 3(a) where the maximum moment is M_{IC} such that the bar force *P* in Figure 3(b) is now P_{IC} and the half crack width at the level of the reinforcement δ is now δ_{max} as shown in Figure 3(d). In this case, the shear stresses τ in Figure 3(d) are fully developed over a length of L_{crt}. The strain in the bar at the crack face due to P_{IC} is ε_{IC} that is $P_{IC}/(EA)_r$ where $(EA)_r$ is the axial rigidity of the reinforcing bar. Any further increase in Δ beyond δ_{max} in Figure 3(d) as in Figure 3(e) results in no change in the bond stress distribution, that is the force in the bar remains at P_{IC}. However, the further extension of the bar δ_{ext} in Figure 3(e) can only be accommodated through debonding over length L_{db} in Figure 3(e), such that extension of the bar δ_{ext} is equal to $\varepsilon_{IC}L_{db}$ so that the total slip of the bar relative to the crack face Δ is given by

$$\delta_{rb} = \delta_{max} + \varepsilon_{IC} L_{db} \tag{1}$$

The slip δ_{rb} in Figure 3(e) is the half crack width at the level of the bar. Within the length L_{db}, the bar is debonded because the slip is greater than δ_{max}. Within L_{crt}, the bar is bonded but because the slip is finite there is partial interaction and beyond L_{crt} where the slip δ is zero, in the region labelled L_{FI}, there is full interaction.

Following debonding in the beam in Figure 3(b), the flexural cracks close within the debonded region L_{db} (Liu et al., 2007; Oehlers et al., 2015, 2016) as in Figure 3(f). The force within the reinforcement is constant at P_{IC} over the debonded region L_{db}. Consequently, the beam within the debonded region L_{db} acts as a passively prestressed member with a passive prestress P_{IC} (Oehlers et al., 2015, 2016), that is the bars within L_{db} now act as tendons with a constant axial load P_{IC}. In the passively prestressed region as per the analogy with the pull test in Figure 3(e), the total extension of the bar over the unbonded region L_{db} is given by Eq. 1. In order to satisfy the requirements of compatibility, the total deformation of the RC beam at the level of reinforcement δ_{RC} over the length L_{db} must be equal to the total deformation of the tendon δ_{rb}, that is

$$\delta_{RC} = \int_0^{L_{db}} \varepsilon_{RC} = \delta_{rb} \tag{2}$$

where ε_{RC} is the effective strain in the RC beam at the level of the tendon.

To determine the capacity of the beam with unbonded reinforcement in Figure 3(f), it is a question of varying the moment distribution in Figure 3(a) until either total debonding of the reinforcement occurs or the moment capacity is satisfied through concrete softening. It is important to note that in order for the force P_{IC} to be developed in the reinforcement, a portion of the bar of length L_{crt} in Figure 3(f) must be bonded. Closed form solutions (Haskett et al., 2008) for L_{crt} and P_{IC} are given in Appendix 2, although, in this paper they have been determined through numerical analyses (Oehlers et al., 2014a).

It is necessary to develop an analysis procedure which can simulate the sectional behaviour of a member with corroded reinforcement in both the bonded and unbonded state. Here a segmental analysis procedure previously developed and validated widely for conventional and prestressed members by the authors (Knight et al., 2013b) is summarised as a potential solution technique in the following. However any analysis procedure capable of simulating the mechanics of the segmental analysis can be applied.

Segmental analysis

The segmental analysis procedure has been previously developed by the authors to simulate the full range of behaviours of RC (Oehlers et al., 2014b) and prestressed concrete (Knight et al., 2013b) members. The benefit of the approach is that it directly simulates the localised behaviours that control the global behaviour of reinforced concrete through the application of established partial interaction theory (Oehlers et al., 2014a); inputs of which are the local bond stress slip τ / δ relationship and concrete softening. This approach directly simulates crack formation, widening and tension stiffening and can through mechanics directly simulate the time effects of creep and shrinkage (Knight et al., 2013a; Visintin et al., 2013) although these time effects will not be considered in this paper. Moreover, either through the direct application of shear friction theory

(Visintin et al., 2012), or through the use of a size dependent stress strain relationships (Chen et al., 2013), the approach simulates the formation and failure of concrete softening hinges. As the approach is now well established and validated, only a brief presentation is given here and readers are referred to (Oehlers et al., 2014a, 2014b) for a more detailed explanation and discussion. However as already stated above, any convenient approach could be used to derive the sectional properties required for the debonding analysis, that is the debonding analysis does not depend specifically on the results from a segmental analysis.

Segmental analysis prior to reinforcement debonding

A segment of length L_{def} in Figure 4(b) has been extracted from an RC beam such as in Figure 3(b) (Oehlers et al., 2014b; Visintin et al., 2012); the segment length L_{def} in Figure 4(b) needs to encompass the length of the concrete softening wedge L_{wdg} which equals $d_{NA}/\tan\alpha$ (Oehlers et al., 2014b) where α is the angle of the sliding wedge as shown and can be taken as 26^{o}. Imposing the Euler Bernoulli deformation in Figure 4(c) on the right hand side of the segment in Figure 4(b) causes a total rotation of the segment end of θ_T in Figure 4(c) which is equal to the sum of rotations at each crack face; in the case shown θ_T is equal to 3θ where θ is the rotation of an individual crack face. For analysis, it is now a matter of determining the corresponding moment M to achieve θ_T.

In the uncracked regions of the beam in Figure 4(b) that is within the depth d_{NA}, the longitudinal deformation in Figure 4(c) divided by L_{def} gives the strain profile in Figure 4(d). Based on this distribution of strain, the distribution of stress in Figure 4(e) in the uncracked region can be determined from: the compression reinforcement secant moduli that is the stress strain relationship whether linear or non-linear; the concrete secant moduli prior to compression softening as in Distribution *A* in Figure 4(g) (Hognestad et al., 1955); and the size dependent effective concrete moduli (Chen et al., 2013) after softening as in Distribution *B* which allows for the formation of wedges. From the stress distributions in Figure 4(e) can be determined the resultant compressive force in the concrete that is P_{cc} in Figure 4(f) and that in the reinforcement P_{rc}. The analysis could include the tensile force in the uncracked concrete just below d_{NA} but it is common practice to ignore this at the ultimate limit state.

For reinforcement crossing a crack in Figure 4(b), the strain in the reinforcement is not equal to the strain in the concrete at the same level, that is full interaction cannot be assumed. For example in the top layer of the tension reinforcement, the tensile reinforcement force P_{rtt} shown in Figure 4(f) is a function of the slip of the reinforcement from an individual crack face Δ_t in Figure 4(b). The relationship between P_{rtt} and Δ_t is the crack opening stiffness K_t and can be determined from established partial interaction theory applied either numerically (Knight et al., 2013a; Visintin et al., 2013) or from mechanics (Muhamad et al., 2012) or from semi mechanical expressions (Zhang et al., 2016) and which depend on the bond-slip properties (τ/δ). Similarly for the bottom layer of tension reinforcement, P_{rtb} in Figure 4(f) depends on Δ_b in Figure 4(b) that is the slip at an individual crack face and not the total slip $3\Delta_b$ in Figure 4(c).

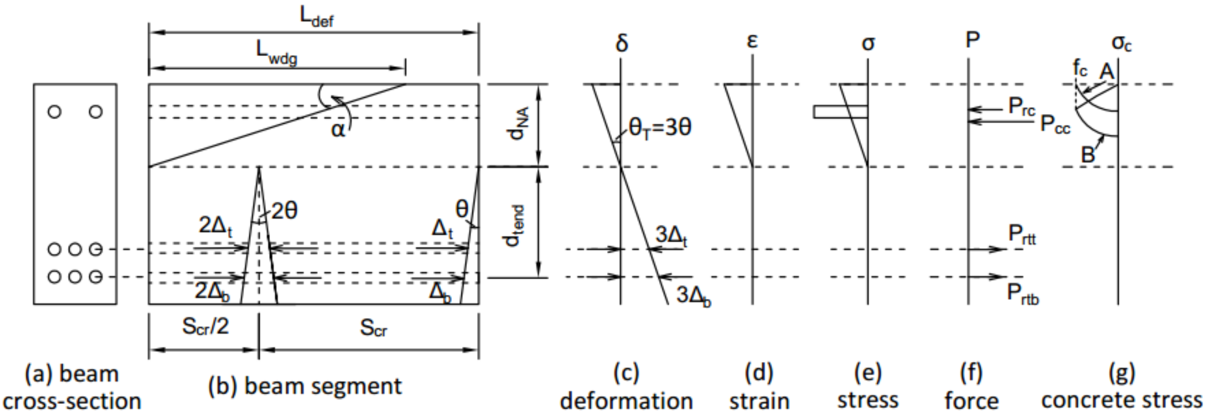

Figure 4 Segmental analysis prior to debonding

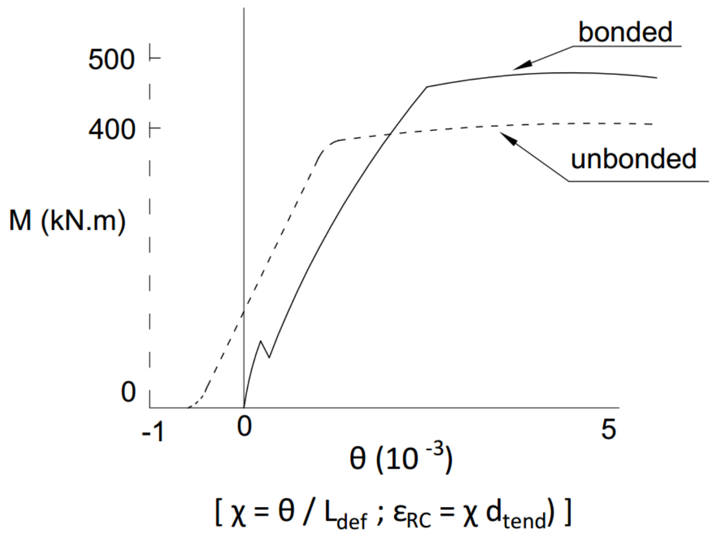

Figure 5 Results of segmental analyses – M/θ and M/χ

Having determined the longitudinal forces in the reinforcement and concrete in Figure 4(f), the Euler Bernoulli deformation in Figure 4(c) can be moved up or down until equilibrium of longitudinal forces is obtained. After which, the moment corresponding to the rotation of the segment end θ_T in Figure 4(c) can be determined by taking moments of the forces in Figure 4(f) at any level. The above analysis can be repeated for a range of rotations to produce the full moment rotation M/θ

relationship such as the unbroken line in Figure 5 labelled 'bonded'; dividing the rotation θ by the half segment length L_{def} in Figure 4(b) gives the moment effective curvature relationship M/χ in Figure 5. Importantly this moment effective curvature relationship is different from that obtained from a classical full-interaction moment curvature relationship as it directly allows for bond slip and hence tension stiffening of the reinforcement through the application of partial interaction theory as well as the effects of concrete softening. This bonded analysis can also be used to determine the moment at which debonding of the reinforcement may commence M_{IC}, should it occur, by setting the corresponding force in the reinforcement to P_{IC}.

Segmental analysis for unbonded reinforcement

When tension bars debonds that is where the slip exceeds the slip capacity δ_{max}, then the bars now act as tendons with a prestress of P_{IC}. Hence if the bottom layer of tension reinforcement in Figure 4(b) debonds then it is no longer acting as reinforcement but as a prestressing tendon with a force P_{IC}. There are numerous approaches to performing the analysis of a prestressed member (Oehlers et al., 2016). One way is to: simply replace P_{rtb} in Figure 4(f) with P_{IC}; repeat the analysis described above for the unbonded case that is to move the neutral axis d_{NA} in Figure 4(b) until equilibrium is achieved i.e. the sum of forces is zero; after which moments must be taken at the level of the tendon, that is at d_{NA} plus d_{tend} from the compression face, to obtain the applied moment for the imposed rotation θ_T. Should both layers of tension reinforcement debond, then the force in the second layer P_{rtt} in Figure 4(f) is also replaced by P_{IC} for that layer. Equilibrium is obtained and the moment taken about the position of the resultant of both prestressing forces.

The above analysis can then be repeated for increasing rotations to produce the moment rotation relationship M/θ shown as the broken line in Figure 5 labelled 'unbonded'. From which, dividing θ by L_{def} gives the moment curvature relationship M/χ for the unbonded case. Furthermore, multiplying the curvature χ by d_{tend} in Figure 4(b) gives the strain in the RC member at the level of the tendon ε_{RC} that is required for the ensuing member debonding analysis.

Member analysis

A member debonding analysis is illustrated in Figure 6 for a half span of a symmetrically load simply supported beam. The distribution of moment is shown in Figure 6(a) where distances are measured from mid-span. The maximum applied moment in Figure 6(a) at mid-span is M_{max} which is greater than M_{IC} to ensure debonding. Consequently the force in the debonded reinforcement, that is the tendon, is P_{IC}. The following procedure first assumes that all of the tension reinforcement is debonded, that is it is acting as a tendon with a force P_{IC}, and then the length of the debonded region L_{db} is determined through mechanics.

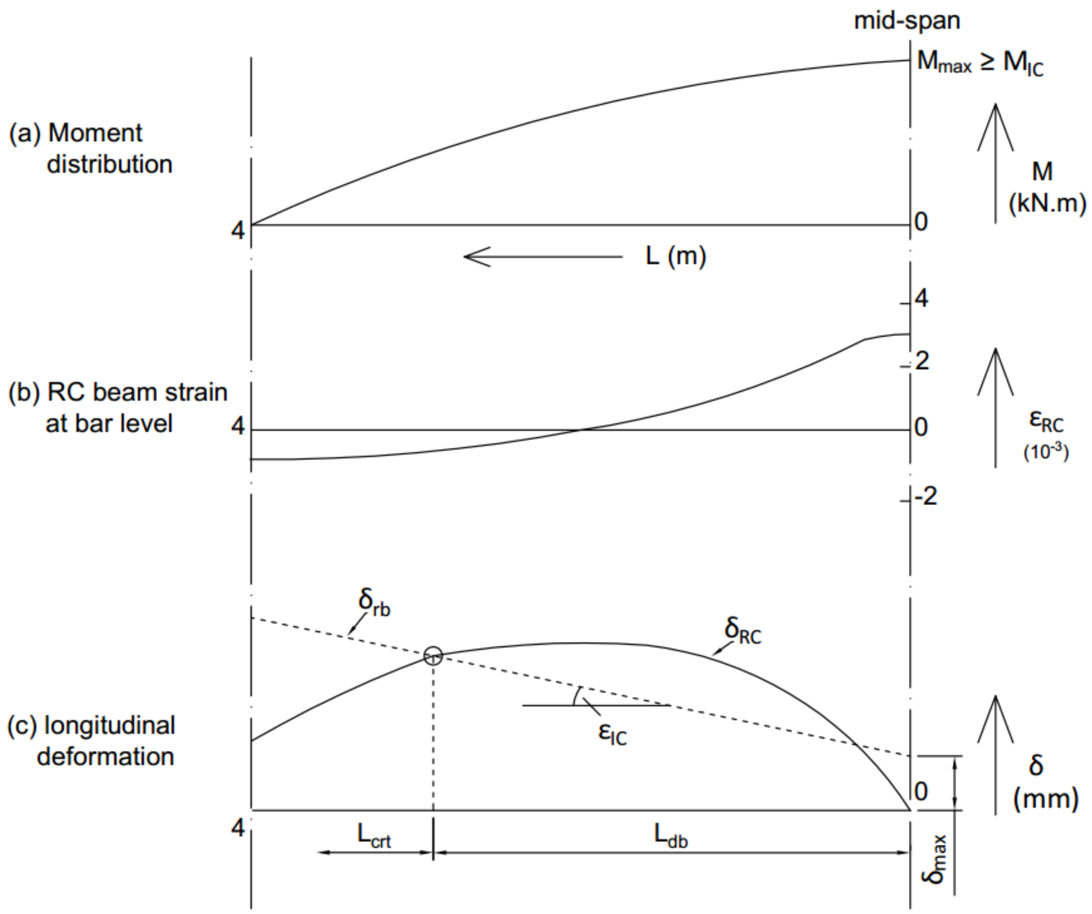

Figure 6 Member debonding analysis through deformations

The variation in the longitudinal strain in the RC beam at the level of the tendon ε_{RC} along the length of the beam is shown in Figure 6(b); this can be derived from the distribution of ε_{RC} with moment in Figure 5. From Eq. 2, integrating the strains in Figure 6(b) gives the RC beam deformation δ_{RC} in Figure 6(c) with respect to mid-span. This is the deformation of the RC beam within a debonded region which in this case is assumed to be the whole half span. From Eq. 1, the deformation of the reinforcement δ_{rb} in Figure 6(c) is the accumulation of slip within L_{crt} in Figure 3(e) which is δ_{max} plus the extension of the unbonded plate $\varepsilon_{IC}L_{db}$. Hence the slope of δ_{rb} is ε_{IC} as shown in Figure 6(c) where ε_{IC} is $P_{IC}/(EA)_r$. The intercept of δ_{rb} and δ_{RC} in Figure 6(c) is the length of the debonded region from mid-span L_{db} required for compatibility.

It may be worth noting that δ_{max} in Figure 6(c) is the slip accumulated within the bonded region L_{crt} in Figure 3(e) for which closed form solutions are given in Appendix 2, although, in this paper they have been determined numerically (Knight et al., 2013a). Hence there must be a bonded region of at least L_{crt} beyond L_{db} in Figure 6(c) as shown, otherwise, the bar force of P_{IC} could not be obtained purely through the bond stresses. If the remaining length was less than L_{crt} then mechanical anchors could be used (Oehlers et al., 2016) in which case δ_{max} would be the slip of the mechanical anchor δ_{anch}. However this scenario will not be considered further in this paper.

The analysis in Figure 6(c) is shown in Figure 7 for a range of distributed moments in Figure 6(a) in which the maximum moment M_{max-x} ranges from M_{max-1} to M_{max-6}. Each concrete deformation graph δ_{RC} in Figure 7 has been labelled with the maximum moment M_{max-x}. As the reinforcing bar deformation δ_{rb} is independent of the applied moment as can be seen in Eq. 1, there is only one variation A-B-C-D to consider as shown for a specific δ_{max-1}.

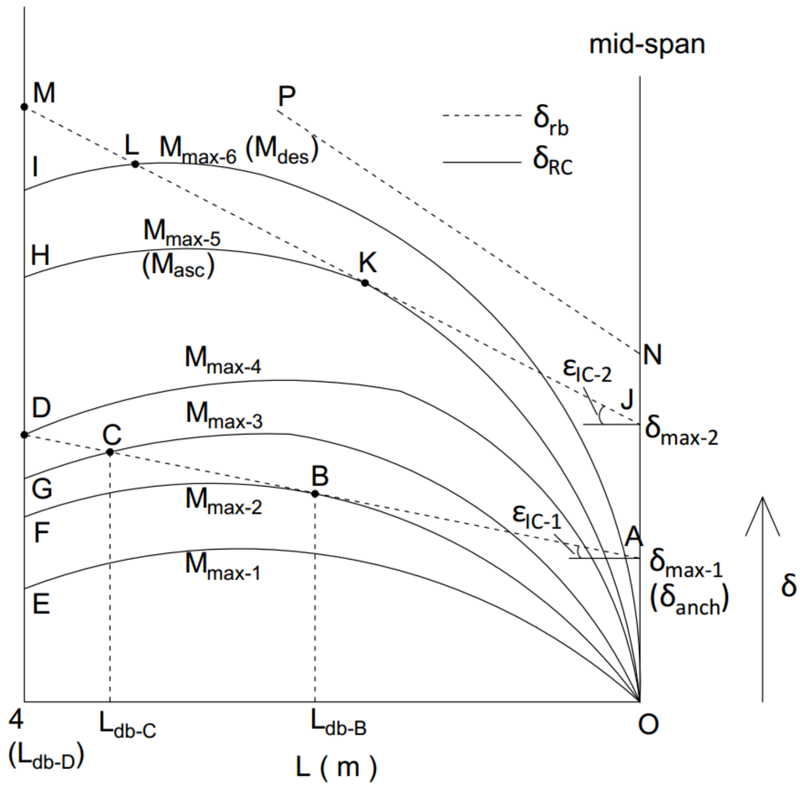

Figure 7 Interpreting the results of member debonding analyses

From a segmental analysis, the moment at which the force in the bottom layer of the tension reinforcing bars in Figure 4(b) reaches P_{IC} can be determined as M_{IC}. Let M_{max-1} in Figure 7 be M_{IC}, that is the reinforced concrete deformation δ_{RC} in Figure 7 is given by O-E. As the RC deformation O-E lies below the reinforcing bar deformation A-B-C-D, member debonding does not occur as the deformation capacity of the reinforcing bar can easily accommodate that of the RC beam. Increasing the maximum moment to M_{max-2} causes an intercept at Point B. Hence when the applied moment distribution reaches M_{max-2} there is rapid unstable debonding from mid-span over the length L_{db-B} and which then stabilises at the intercept L_{db-B}. It can now be seen that there are two mechanisms that control member debonding; the onset of P_{IC}; and compatibility at the intercept of δ_{rb} and δ_{RC}. Both are required for member debonding.

Increasing the maximum moment to M_{max-3} in Figure 7 causes stable debonding from Points B to C, that is the debonded region gradually increases with increasing applied moment from L_{db-B} to L_{db-C}. A further increase in the applied moment to M_{max-4} causes debonding to the beam end. This is theoretically impossible as, as explained previously, a bonded length of L_{crt} is required to achieve P_{IC}. However if the reinforcing bar is mechanically anchored at its ends, as might occur with a bend in the bar, such that this mechanical anchor can resist P_{IC} with a slip $\delta_{anch} = \delta_{max}$ then the analysis is valid. However if this is not the case, then the mechanics of anchored members can be applied as explained elsewhere (Oehlers et al., 2016).

Now apply a maximum moment that is equal to the RC beam moment capacity M_{asc}, that is when the ascending branch of the concrete compressive stress/strain is fully developed as in Distribution *A* in Figure 4(g) (Visintin et al., 2012). This is shown as $M_{max-5} = M_{asc}$ that is O-K-H in Figure 7. As O-K-H always lies above A-B-C-D, that is there is no intercept, compatibility cannot be achieved, hence M_{asc} cannot be achieved as the reinforcing bar cannot accommodate the required RC beam deformation. Applying a further rotation to the beam segment will eventually cause the concrete softening stresses in Distribution *B* in Figure 4(g) to be fully developed. The moment at which this occurs M_{des} (Oehlers et al., 2014b; Visintin et al., 2012) is usually slightly less than M_{asc} but it is the moment capacity at maximum ductility. To achieve this moment requires an increase in the RC beam elongation from O-K-H to O-L-I in Figure 7 and once again there is no intercept with the reinforcement elongation emanating from δ_{max-1} and, therefore, cannot be achieved.

It may be worth noting that a reduced corrosion increases δ_{max} in Figure 1. Hence a reduced corrosion may increase δ_{max-1} in Figure 7 to say δ_{max-2}. Furthermore a reduced corrosion increases P_{IC} in Figure 2 consequently increasing ε_{IC} from say ε_{IC-1} to ε_{IC-2} as shown in Figure 7 which raises the reinforcement deformation to J-K-L-M. This allows the intercepts K and L such that in the debonded region of the beam a hinge can start and complete to allow additional ductility. From this analysis it can be seen that corrosion reduces both the strength and ductility and can be designed for. Finally when the reinforcement deformation such as N-P always lies above the reinforced concrete deformation then member debonding does not occur such that the properties of the beam can be derived from a segmental bonded analysis.

As explained previously, rapid and unstable debonding occurs from mid-span to L_{db-B} in Figure 7 when the maximum applied moment is M_{max-2}. After which, stable debonding occurs with increased moment. Hence a large amount of corrosion could occur within L_{db-B} without affecting the moment capacity except in reducing the cross-sectional area which is easily accounted for. Hence the critical region in a beam is not adjacent to the position of maximum moment as might be expected but is in the region that lies outside $L_{db\text{-}B}$.

Application of member debonding analyses

The above segmental and member debonding analyses have been applied to RC beams with the cross-section in Fig. 8(a). The beam is simply supported with a span of 8m, the steel reinforcement is allowed to strain harden after yielding, and the beam is subjected to a uniformly distributed load. Full details of the analyses are given by Feng et al. (2016b) and examples of the properties used are summarised in Appendix 3.

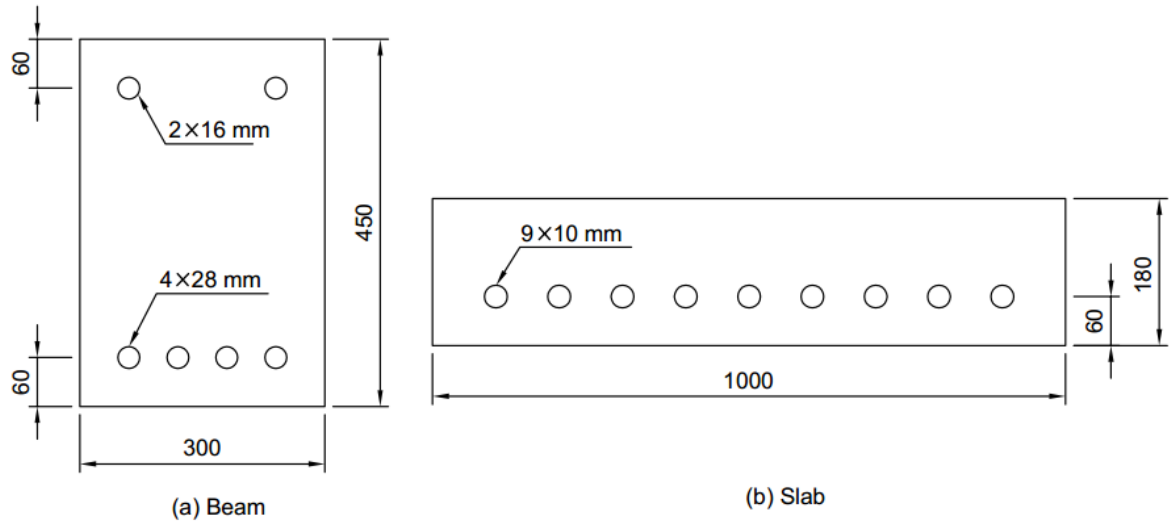

Figure 8 RC beam sections used in member analyses

For the 28 mm tension reinforcing bars in Figure 8(a): P_{yld} for different corrosion levels are listed in Column (3) in Table 1; and P_{IC} from numerical simulations (closed form solutions in Appendix 2 could have been used but would give slightly different values) using the bond properties of the corroded reinforcement in Appendix 1 are listed in Column (2) in Table 1. A comparison of P_{yld} with P_{IC} shows that the transition point, that is when the yield capacity exceeds the IC debonding resistance with increasing corrosion as illustrated in Figure 2, lies between 4% and 6% in Table 1; the actual value being 5.7%. Hence debonding does not occur with corrosion levels less than 5.7% for these 28 mm reinforcing bars. Consequently a bonded analysis, as illustrated in Figure 4, applies for the corrosion levels of 0%, 1% and 4% in Table 1 and the remaining higher corrosion levels require an unbonded analysis.

The results of an unbonded analysis using the approach illustrated in Figure 7 and for the section in Figure 8(a) with 8% corrosion in the tension reinforcement, is shown in Figure 9. Increasing the corrosion level to 8% that is beyond the transition point of 5.7% means that P_{IC} occurs before P_{yld}.

Consequently member debonding may possibly but not necessarily occur, bearing in mind that the following two criteria are required for member debonding: the attainment of P_{IC}; and compatibility along the debonded region.

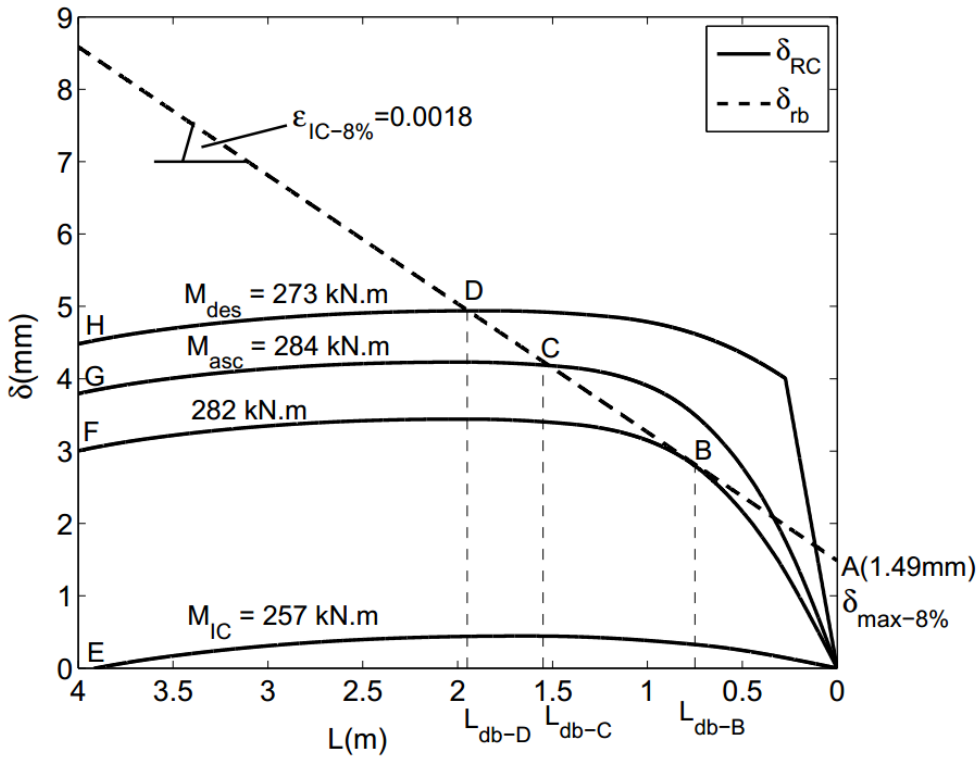

Figure 9 Member debonding analysis of beam with 8% corrosion

As previously explained, the reinforcement deformation δ_{rb} in Figure 9 is independent of the applied moment being dependent on: $\delta_{max\text{-}8\%}$ which in this case is 1.49 mm as shown at the intercept of δ_{rb} with the ordinate; and $\varepsilon_{IC\text{-}8\%}$, which is $P_{IC\text{-}8\%}/(EA)_r$ as explained in Figure 6(c) and which in this case is 0.0018 that is the slope as shown. When the maximum moment M_{IC} = 257 kNm that is when P_{IC} is first achieved, all of δ_{RC} labelled O-E in Figure 9 lies below δ_{rb} labelled A-B-C-D so that the deformation of the reinforcement can easily accommodate the RC deformation. Hence member debonding will not occur even though P_{IC} is attained because compatibility is not achieved. Increasing the applied moment with a maximum of 282 kNm that is deformation O-B-F, causes an intercept at *B* which occurs at $L_{db\text{-}B}$ = 0.75 m. Hence rapid and unstable debonding will occur along the length $L_{db\text{-}B}$ of 0.75 m when this moment distribution is applied. As there is unstable debonding within $L_{db\text{-}B}$, pockets of severe corrosion within this region are not important as the reinforcement has debonded. What is important is the corrosion in the remainder of the beam beyond $L_{db\text{-}B}$ as this affects stable debonding. Hence the critical region is not within $L_{db\text{-}B}$ but outside this region.

A further increase in moment to M_{asc} = 284 kNm to deformation O-C-G in Figure 9 will cause stable debonding from L_{db-B} = 0.75 m to L_{db-C} = 1.51 m; this assumes that the bonded region to the left of L_{db-C} is greater than L_{crt}. Increasing the applied deformation to the beam to allow a hinge to form such that M_{des} = 273 kNm will cause stable debonding to L_{db-D} = 1.95m. Any further increase in applied deformation to the beam will cause a rapid reduction in the moment capacity so that for all intents and purposes the failure capacity M_{fail} is in this case M_{des} = 273 kNm.

An analysis with 40% corrosion in the beam in Figure 8(a) is shown in Figure 10. In this case, maximum moment capacity M_{asc} is achieved with debonding to L_{db-B} of 3.48 m but the greatest ductility at M_{des} is not achievable due to debonding to the end of the beam. If the end of the reinforcement is anchored such as at a hook, then the strength and ductility depends on the properties of the anchor which if known can be used to quantify the beam behaviour using an alternative approach (Oehlers et al., 2016) but this will not be covered in this paper.

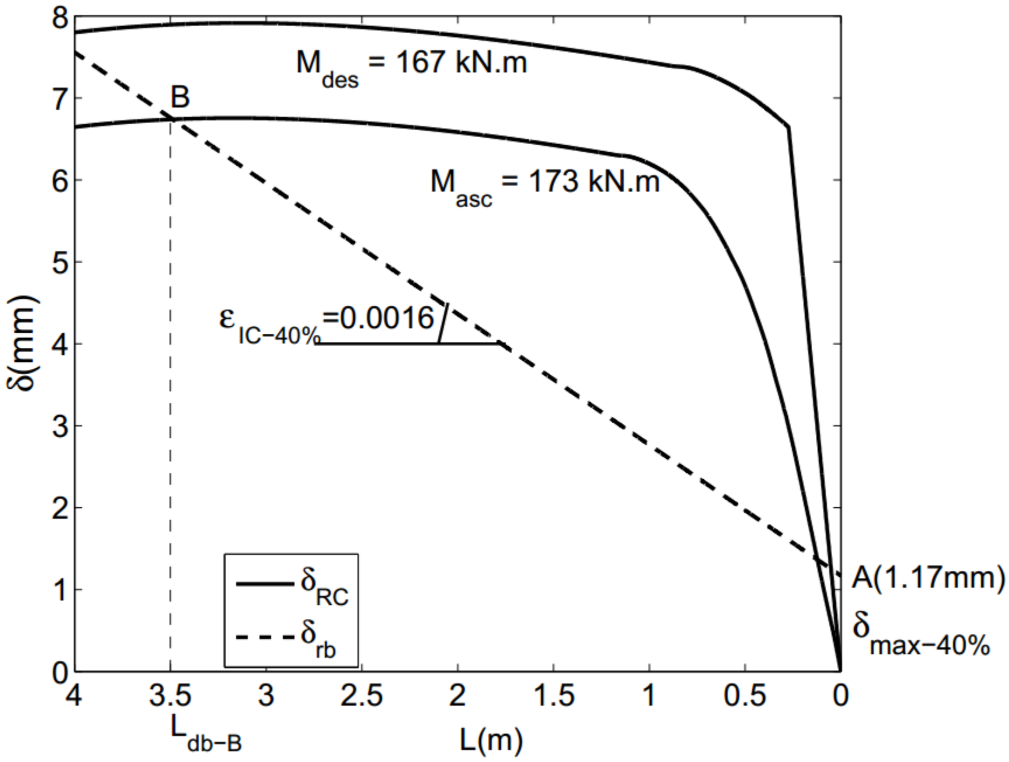

Figure 10 Member debonding analysis of beam with 40% corrosion

The beam in Figure 8(a) has been analysed with varying corrosion levels and the results summarised in Table 1. The corrosion levels in Column (1) range from 0% to 40%. For each corrosion level, the IC debonding capacity P_{IC} is tabulated in Column (2) and the yield capacity P_{yld} in Column (3). A comparison of P_{IC} and P_{yld} shows that $P_{IC} > P_{yld}$ for corrosion levels up to and including 4% so that a segmental bonded analysis applies in contrast to a segmental and member unbonded analysis for corrosion levels of 6% and more. At 0% corrosion, the failure moment M_{fail} in Column (12) is equal to M_{des} in Column (10) of 430 kNm and this occurs at a curvature χ_{fail} = 2.86x10^{-5} mm^{-1}. It may be worth noting that as rotation θ is the curvature χ times L_{def} where L_{def} is in effect the hinge length then the curvature at failure is directly proportional to the rotation capacity and consequently is a measure of the ductility. At 4% corrosion, M_{fail} reduces slightly to 409 kNm and the curvature rises slightly to 3.08x10^{-5} mm^{-1} such that there is only a minor reduction in strength with corrosion and no reduction in ductility.

Increasing the rotation to 6% gives the results in Table 1 from an unbonded segmental analysis. The ability to achieve these values from an unbonded segmental analysis depends on member debonding which itself depends on the debonded length. It can be seen that increasing the corrosion to 6% causes M_{fail} In Column 12 to reduce by 32% to 280 kNm. However the curvature increases by 57% to 4.84x10^{-5} mm^{-1} that is the major reduction in strength is in part compensated by a very large increase in ductility which is important for the absorption of energy and the redistribution of moment. At 20% corrosion, M_{fail} has reduced by 46% but the ductility has increased by 104% compared with 0% corrosion. However at 40% corrosion complete debonding of the reinforcement now governs, causing a major reduction in both strength and ductility; that is member debonding once it occurs can severely reduce both flexural capacity and ductility. Also worth noting is that the debonded region increases with corrosion at failure. In this example, the limit to the ductility due to member debonding is reached somewhere between 20% and 40% corrosion.

The analysis of the simply supported slab or shallow beam in Figure 8(b) of 4m span and with 8% corrosion is shown in Figure 11. In this case, member debonding occurs as soon as the maximum of the applied moment reaches M_{IC}. There is unstable debonding over $L_{db\text{-}B}$ = 0.58 m and then stable debonding until M_{des} is achieved at $L_{db\text{-}D}$ = 1.59m.

The results of the analysis of the slab in Figure 8(b) with varying degrees of corrosion are given in Table 2. By comparing P_{IC} with P_{yld} for the 10 mm bar, it can be seen that the transition point occurs between 7% and 8%. At 7% corrosion, the bonded moment capacity M_{fail} is 47 kNm at a curvature χ_{fail} of 18.7x10^{-5} mm^{-1}. At 8% corrosion the unbonded moment capacity reduces to 36 kNm that is a 23% reduction from that at 7% which is much less than the step change of 32% that occurred in the previous beam analysis. However, the curvature increases to 24.3x10^{-5} mm^{-1} that is an increase of 30%. The debonded region is 80% of the span and this increases as corrosion increases to 93% when the degree of corrosion is 15%. It can be seen in Table 2 that at 20% corrosion, member debonding prevents the full ductility from being achieved. Hence the limit due to member debonding is achieved somewhere between 15% and 20% corrosion.

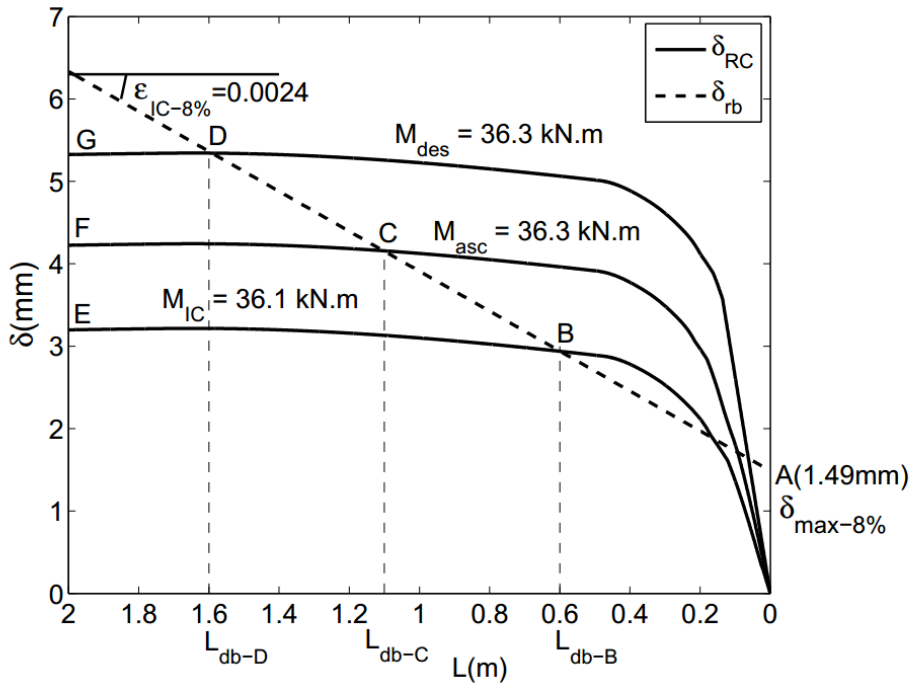

Figure 11 Member debonding analysis of slab with 8% corrosion

Conclusions

It has been shown that the flexural capacity and flexural ductility capacity that is rotation capacity of a beam with corroded steel reinforcing bars is governed by the following complex partial interaction mechanisms:

- The behaviour whilst the corroded bar acts as bonded reinforcement which can be determined from a segmental analysis.
- The transition from bonded behaviour in which the bar is acting as reinforcement to unbonded in which the bar is acting as a tendon. This transition is governed in part by the IC debonding resistance and the yield capacities of the reinforcing bars.
- The behaviour whilst the corroded bar acts as a tendon which can be determined from a segmental unbonded analysis.
- And finally debonding along the member which can limit the capacities from the segmental unbonded analysis.

A numerical analysis for quantifying the flexural capacity and flexural ductility of RC beams with corroded steel reinforcement has been described. The numerical analysis can quantify: whether member debonding can occur; the strength and ductility should member debonding not occur; and the strength and ductility should member debonding occur and the limits on these capacities due to the span of the members.

It has been demonstrated that the transition from the steel bar acting as reinforcement to acting as a tendon can cause a sudden reduction in the moment capacity which is quantifiable. However this is to some degree compensated by a substantial increase in ductility also quantifiable. It is shown through mechanics that the critical region for corrosion may not necessarily be adjacent to the position of maximum moment as may be thought at first instance. Instead it lies outside a mechanically quantifiable distance where unstable crack propagation occurs. The eventual aim of this research is to provide numerical models to help in the assessment of corroded RC beams and in their retrofitting and in developing simple assessment rules for RC beams and slabs with known corrosion levels.

Appendix 1 Bond-slip properties of corroded steel reinforcement

The research of (Feng et al., 2016b) derives the change in the bond-slip properties of steel reinforcement due to corrosion as illustrated in Figure 1. Its application requires the bond-slip properties prior to corrosion that is τ_{max-0} and δ_{max-0} in Figure 1 which can be obtained from tests or from Codes (CEB-FIP Model Code 1990: Design Code 1994). The bond-slip model with corrosion effects consists of a non-linear ascending branch and a linear-descending branch.

In the ascending branch in Figure 1, that is where the slip varies from 0 to δ_1, δ_1 may be considered as a constant valued at 0.175 mm. The bond shear stress at corrosion level *C(x%)* that is $\tau_{x\%}$ is given by

$$\tau_{x\%} = \tau_{max-x\%}\left(\frac{\delta}{\delta_1}\right)^{0.4} \text{ when } 0 \le \delta \le \delta_1 \tag{A1-1}$$

in which $\tau_{max-x\%}$ is the maximum shear stress at δ_1 for corrosion level *of x%* and which is given by

$$\tau_{max-x\%} = k_t\tau_{max-0} \tag{A1-2}$$

where k_t is given by either

$$k_t = \left(-0.032\frac{c}{d} + 0.576\right)x\% + 1,\ when\ 0 < x\% < 0.3(x\%)_{1-2} \tag{A1-3}$$

or

$$k_t = \left(0.0137\frac{c}{d} - 0.247\right)x\% + 1.42 + 0.0475\frac{c}{d} - 3.94\times10^{-3}(\frac{c}{d})^2,$$

$$when\ 0.3(x\%)_{1-2} < x\% < (x\%)_{2-3}$$

(A1-4)

or

$$k_t = -0.0016C + 0.224,\ when\ x\% > (x\%)_{2-3} \tag{A1-5}$$

in which: *x%* is the level of corrosion in terms of percentage mass loss; *c/d* is the ratio of cover to the edge of the bar *c* and the bar diameter *d*; $(x\%)_{1-2}$ is the transition point of corrosion level where the peak bond starts to descend with corrosion; and $(x\%)_{2-3}$ is the transition point where peak bond starts to level off despite increasing of corrosion level. The transition points $(x\%)_{1-2}$ and $(x\%)_{2-3}$ are calculated as follows.

$$(x\%)_{1-2} = 0.288\frac{c}{d} + 1.72 \tag{A1-6}$$

$$(x\%)_{2-3} = \frac{-1.20 - 0.0475\frac{c}{d} + 3.94\times10^{-3}(\frac{c}{d})^2}{0.0137\frac{c}{d} - 0.245} \tag{A1-7}$$

The coefficient τ_{max-0} in Eq. (A1-2) is the peak bond in bond-slip model when there is no corrosion which is suggested by the CEB model (CEB-FIP Model Code 1990: Design Code 1994) as

$$\tau_{max-0} = 7\times(\frac{f_c}{25})^{0.25} \tag{A1-8}$$

where f_c is measured in MPa.

The descending branch of the bond-slip model with corrosion is described in Eq. (A1-9), where δ_1 is a constant valued at 0.175 mm and $\delta_{max-x\%}$ is shown in Eq. (A1-10).

$$\tau = -0.161\tau_{max-0}\delta + 0.0282\,\tau_{max-0} + \tau_{max-C} \quad \delta_1 \le \delta \le \delta_{max-x\%} \tag{A1-9}$$

$$\delta_{max-x\%} = 0.175 + 6.21k_t \tag{A1-10}$$

Appendix 2 IC debonding properties

The IC debonding properties in this paper were derived from numerical analyses that can cope with any bond-slip shape. However, it may be worth noting that there are numerous closed form solutions for the IC debonding properties which depend on specific assumed shapes of the bond-slip (Haskett et al., 2008; Muhamad et al., 2011). The simplest solution is to assume that δ_1 in Figure 1 tends to zero that is we are only dealing with the linear descending branch (Haskett et al., 2008). In this case, the IC debonding resistance is given by

$$P_{IC} = \sqrt{\tau_{max-x\%}\delta_{max-x\%}}\sqrt{L_{per}(EA)_r} \tag{A2-1}$$

where L_{per} is the circumference of the reinforcing bar prior to corrosion and $(EA)_r$ is the axial rigidity of the reinforcing bar in which the cross-sectional area is reduced allowing for corrosion. Furthermore the critical length required to develop P_{IC} is given by

$$L_{crt} = \frac{\pi}{2\sqrt{\frac{\tau_{max-x\%}L_{per}}{\delta_{max-x\%}(EA)_r}}} \tag{A2-2}$$

Appendix 3 Examples of member properties and analyses

Full details of all the assumed properties and calculations are given elsewhere (Feng et al., 2016a). As an example of the material properties, those for the beam in Figure 8(a) with 8% corrosion in the tension reinforcement are given below.

concrete properties: compressive cylinder strength f_c = 40 MPa; elastic modulus E_c = 23.5 GPa; ascending branch of stress (σ)/strain (ε) provided by Hognestad (1951) $\sigma=[2\varepsilon/\varepsilon_{pk}-(\varepsilon/\varepsilon_{pk})^2]$ where ε_{pk}= $(-0.067f_c+29.9f_c+1053)10^{-6}$; linear descending branch (Visintin and Oehlers 2016) starts at $\varepsilon_{pk} = f_c$ and terminates at $\varepsilon_u = 0$ where $\varepsilon_u = \varepsilon_{u\text{-}model}$ x100/L_{def} where L_{def} is defined in Figure 4 and $\varepsilon_{u\text{-}model} = \varepsilon_0$ + $(3+1000\varepsilon_0)/(77f_c-500)$ where $\varepsilon_0 = 4.76\text{x}10^{-6}f_c + 2.13\text{x}10^{-3}$.

steel properties: tensile yield strength f_y = 520 MPa; elastic modulus E_s = 200 GPa,; and the strain hardening modulus E_{sh} = 2.6 GPa.

bond properties: maximum shear capacity at zero corrosion $\tau_{max\text{-}0}$ = 7.87 MPa; maximum slip capacity at zero shear stress $\delta_{max\text{-}0}$ = 6.34 mm; slip at τ_{max} that is δ_1 = 0.175 mm; maximum bond shear stress at 8% corrosion $\tau_{max\text{-}8\%}$ = 1.66 MPa; slip capacity at 8% corrosion $\delta_{max\text{-}8\%}$ = 1.49 mm; transition point in Figure 2 is 5.7%; length of softening wedge L_{wdg} = 237 mm.

Partial interaction pseudo material properties: Primary crack spacing $S_{cr\text{-}pr}$ = 182 mm; IC debonding resistance of 8% corroded bar $P_{IC\text{-}8\%}$ = 804 kN; critical bond length at 8% corrosion $L_{crt\text{-}8\%}$ = 1468 mm; crack opening stiffness at 8% corrosion $K_{8\%}$ = 400x10^6 N/mm

Reference

Al-Sulaimani, G, Kaleemullah, M, Basunbul, I and Rasheeduzzafar (1990) Influence of corrosion and cracking on bond behavior and strength of reinforced concrete members. *ACI Structural Journal*, 87(2): 220-231.

Almusallam, AA (2001) Effect of degree of corrosion on the properties of reinforcing steel bars. *Construction and Building Materials*, 15(8): 361-368.

Almusallam, AA, Al-Gahtani, AS, Aziz, AR, Dakhil, FH and Rasheeduzzafar (1996a) Effect of reinforcement corrosion on flexural behavior of concrete slabs. *Journal of materials in civil engineering*, 8(3): 123-127.

Almusallam, AA, Al-Gahtani, AS, Aziz, AR and Rasheeduzzafar (1996b) Effect of reinforcement corrosion on bond strength. *Construction and Building Materials*, 10(2): 123-129.

Amleh, L and Ghosh, A (2006) Modeling the effect of corrosion on bond strength at the steel-concrete interface with finite-element analysis. *Canadian Journal of Civil Engineering*, 33(6): 673-682.

Berto, L, Simioni, P and Saetta, A (2008) Numerical modelling of bond behaviour in RC structures affected by reinforcement corrosion. *Engineering Structures*, 30(5): 1375-1385.

Bertolini, L, Elsener, B, Pedeferri, P, Redaelli, E and Polder, RB (2013) Corrosion of steel in concrete: prevention, diagnosis, repair, *John Wiley & Sons*, U.S.

Bhargava, K, Ghosh, A, Mori, Y and Ramanujam, S (2007) Corrosion-induced bond strength degradation in reinforced concrete—Analytical and empirical models. *Nuclear engineering and design*, 237(11): 1140-1157.

Broomfield, JP (2002) Corrosion of steel in concrete: understanding, investigation and repair, *CRC Press*.

Cabrera, J (1996) Deterioration of concrete due to reinforcement steel corrosion. *Cement and concrete composites*, 18(1): 47-59.

Cabrera, J and Ghoddoussi, P (1992), The effect of reinforcement corrosion on the strength of the steel/concrete bond, *International conference on bond in concrete,* Riga Technical University, pp. 11-24.

Castel, A, François, R and Arliguie, G (2000) Mechanical behaviour of corroded reinforced concrete beams—Part 1: experimental study of corroded beams. *Materials and structures*, 33(9): 539-544.

CEB-FIP Model Code 1990: Design Code, (1994), Thomas Telford, London.

Chen, Y, Visintin, P, Oehlers, D and Alengaram, U (2013), Size-dependent stress-strain model for unconfined concrete, *Journal of Structural Engineering*, 140(4): 04013088.

Coronelli, D and Gambarova, P (2004) Structural assessment of corroded reinforced concrete beams: Modeling guidelines. *Journal of Structural Engineering*, 130(8): 1214-1224.

Eligehausen, R, Popov, EP and Bertero, VV (1982), Local bond stress-slip relationships of deformed bars under generalized excitations, *Proceedings of the 7th European Conference on Earthquake Engineering,* Techn. Chamber of Greece, Athens, vol. 4, pp. 69-80.

Eyre, J and Nokhasteh, M (1992) Strength assessment of corrosion damaged reinforced concrete slabs and beams. *Proceedings of the Institution of Civil Engineers-Structures and Buildings*, 94(2): 197-203.

Fang, C, Lundgren, K, Plos, M and Gylltoft, K (2006) Bond behaviour of corroded reinforcing steel bars in concrete. *Cement and concrete research*, 36(10): 1931-1938.

Feng, Q, Visintin, P and Oehlers, DJ 2016a, *Behaviour of RC beams with corrosion induced debonded reinforcement*, no. Research Report R193, School of Civil, Environmental and Mining Engineering, The University of Adelaide, Australia.

Feng, Q, Visintin, P and Oehlers, DJ (2016b) Deterioration of bond–slip due to corrosion of steel reinforcement in reinforced concrete. *Magazine of Concrete Research*, 68(15): 768-781.

Haskett, M, Oehlers, DJ and Mohamed Ali, M (2008) Local and global bond characteristics of steel reinforcing bars. *Engineering Structures*, 30(2): 376-383.

Hognestad, E, Hanson, NW and McHenry, D (1955) Concrete stress distribution in ultimate strength design. *Journal Proceedings*, 52(12): 455-480.

Jin, WL and Zhao, YX (2001) Effect of corrosion on bond behavior and bending strength of reinforced concrete beams. *Journal of Zhejiang University SCIENCE*, 2(3): 298-308.

Knight, D, Visintin, P, Oehlers, D and Jumaat, M (2013a) Incorporating residual strains in the flexural rigidity of RC members with varying degrees of prestress and cracking. *Advances in Structural Engineering*, 16(10): 1701-1718.

Knight, D, Visintin, P, Oehlers, D and Mohamed Ali, M (2013b) Short-Term Partial-Interaction Behavior of RC Beams with Prestressed FRP and Steel, *Journal of Composites for Construction*, 18(1): 04013029.

Lee, C, Bonacci, J, Thomas, MD, Maalej, M, Khajehpour, S, Hearn, N, Pantazopoulou, S and Sheikh, S (2000) Accelerated corrosion and repair of reinforced concrete columns using carbon fibre reinforced polymer sheets. *Canadian Journal of Civil Engineering*, 27(5): 941-948.

Lee, H-S, Noguchi, T and Tomosawa, F (2002) Evaluation of the bond properties between concrete and reinforcement as a function of the degree of reinforcement corrosion. *Cement and concrete research*, 32(8): 1313-1318.

Liu, I, Oehlers, D and Seracino, R (2007) Study of intermediate crack debonding in adhesively plated beams. *Journal of Composites for Construction*, 11(2): 175-183.

Mangat, PS and Elgarf, MS (1999) Bond characteristics of corrding reinforcement in concrete beams. *Materials and structures*, 32(2): 89-97.

Mangat, PS and Elgarf, MS (1999) Flexural strength of concrete beams with corroding reinforcement. *Structural Journal*, 96(1): 149-158.

Miyagawa, T (1991) Durability design and repair of concrete structures: chloride corrosion of reinforcing steel and alkali–aggregate reaction. *Magazine of Concrete Research*, 43(156): 155-170.

Muhamad, R, Ali, MM, Oehlers, D and Sheikh, AH (2011) Load-slip relationship of tension reinforcement in reinforced concrete members. *Engineering Structures*, 33(4): 1098-1106.

Muhamad, R, Ali, MM, Oehlers, DJ and Griffith, M (2012) The tension stiffening mechanism in reinforced concrete prisms. *Advances in Structural Engineering*, 15(12): 2053-2069.

Oehlers, D and Seracino, R (2004) Design of FRP and steel plated RC structures: retrofitting beams and slabs for strength, stiffness and ductility, *Elsevier*, London.

Oehlers, DJ, Visintin, P, Chen, JF and Ibell, TJ (2014a) Simulating reinforced concrete members. Part 1: partial interaction properties. *Proceedings of the Institution of Civil Engineers: Structures and Buildings*, 167(11): 646-653.

Oehlers, DJ, Visintin, P, Chen, JF and Ibell, TJ (2014b) Simulating reinforced concrete members. Part 2: displacement-based analyses. *Proceedings of the Institution of Civil Engineers-Structures and Buildings*, 167(12): 718-727.

Oehlers, DJ, Visintin, P and Lucas, W (2015), Flexural Strength and Ductility of FRP-Plated RC Beams: Fundamental Mechanics Incorporating Local and Global IC Debonding, *Journal of Composites for Construction*, 04015046.

Oehlers, DJ, Visintin, P and Lucas, W (2016) Fundamental mechanics governing FRP retrofitted RC beams with anchored and prestressed FRP plates. *Journal of Composites for Construction*, 10.1061/(ASCE)CC.1943-5614.0000710: 04016047.

Stanish, K, Hooton, R and Pantazopoulou, S (1999) Corrosion effects on bond strength in reinforced concrete. *ACI Structural Journal*, 96(6): 915-921.

Val, DV, Stewart, MG and Melchers, RE (1998) Effect of reinforcement corrosion on reliability of highway bridges. *Engineering Structures*, 20(11): 1010-1019.

Visintin, P, Oehlers, D and Haskett, M (2013) Partial-interaction time dependent behaviour of reinforced concrete beams. *Engineering Structures*, 49: 408-420.

Visintin, P, Oehlers, D, Wu, C and Haskett, M (2012) A mechanics solution for hinges in RC beams with multiple cracks. *Engineering Structures*, 36: 61-69.

Visintin, P and Oehlers, DJ (2016) Mechanics closed form solutions for moment redistribution of RC beams. *Structural Concrete, Accepted*.

Yalciner, H, Eren, O and Sensoy, S (2012) An experimental study on the bond strength between reinforcement bars and concrete as a function of concrete cover, strength and corrosion level. *Cement and concrete research*, 42(5): 643-655.

Yuan, Y-S and Marosszeky, M (1991) Analysis of corroded reinforced concrete sections for repair. *Journal of Structural Engineering*, 117(7): 2018-2034.

Zhang, T, Visintin, P and Oehlers, DJ (2016) Partial-interaction tension-stiffening properties for numerical simulation. *Advances in Structural Engineering, Accepted*.

Table 1. Beam results with varying corrosion

C (%) (1)	P_{IC} (kN) (2)	P_{yld} (kN) (3)	M_{IC} (kNm) (4)	$\chi_{IC} 10^{-5}$ (mm^{-1}) (5)	M_{yld} (kNm) (6)	$\chi_{yld} 10^{-5}$ (mm^{-1}) (7)	M_{asc} (kNm) (8)	$\chi_{asc} 10^{-5}$ (mm^{-1}) (9)	M_{des} (kNm) (10)	$\chi_{des} 10^{-5}$ (mm^{-1}) (11)	M_{fail} (kNm) (12)	$\chi_{fail} 10^{-5}$ (mm^{-1}) (13)	L_{db}/L (%) (14)
0	1586	1280	-	-	429	1.32	444	1.43	430	2.86	430	2.86	0
1	1663	1267	-	-	428	1.32	435	1.43	431	2.86	431	2.86	0
4	1384	1229	-	-	421	1.32	424	1.43	409	3.08	409	3.08	0
6	828	1203	261	0.68	-	-	292	2.31	280	4.84	280	4.84	46
8	805	1178	257	0.68	-	-	284	2.42	273	4.95	273	4.95	48
10	782	1152	256	0.68	-	-	277	2.42	264	5.16	264	5.16	50
15	726	1088	252	0.70	-	-	258	2.64	247	5.49	247	5.49	58
20	671	1024	238	0.69	-	-	240	2.75	231	5.82	231	5.82	65
40	472	768	174	0.62	-	-	173	3.74	167	7.47	173	3.74	-

Table 2. Slab results with varying corrosion

C (%)	P_{IC} (kN)	P_{yld} (kN)	M_{IC} (kNm)	$\chi_{IC} 10^{-5}$ (mm^{-1})	M_{yld} (kNm)	$\chi_{yld} 10^{-5}$ (mm^{-1})	M_{asc} (kNm)	$\chi_{asc} 10^{-5}$ (mm^{-1})	M_{des} (kNm)	$\chi_{des} 10^{-5}$ (mm^{-1})	M_{fail} (kNm)	$\chi_{fail} 10^{-5}$ (mm^{-1})	L_{db}/L (%)
0	518	367	-	-	40.9	2.13	53	12.8	54	16.3	54	16.3	0
1	577	364	-	-	40.2	2.06	55	12.4	55	15.8	55	15.8	0
4	482	353	-	-	39.0	2.21	51	13.3	51	17.1	51	17.1	0
7	383	342	-	-	38.5	2.35	47	14.4	47	18.7	47	18.7	0
8	315	338	36	2.51	-	-	36	18.4	36	24.3	36	24.3	80
10	307	331	35	2.48	-	-	35	19.5	35	25.4	35	25.4	88
15	287	312	33	2.43	-	-	33	20.6	33	27.2	33	27.2	93
20	268	294	31	2.38	-	-	31	21.7	31	29.0	31	21.7	-

CHAPTER 3

Manuscript

Feng, Q, Visintin, P and Oehlers, D (2016) A mechanics prediction of reinforcement corrosion in RC beams through the measurement of crack widths. Submitted to Structural Concrete.

Statement of Authorship

Title of Paper	A mechanics prediction of reinforcement corrosion in RC beams through the measurement of crack widths
Publication Status	☐ Published ☐ Accepted for Publication ☑ Submitted for Publication ☐ Unpublished and Unsubmitted work written in manuscript style
Publication Details	Feng, Q, Visintin, P & Oehlers, DJ 2016, A mechanics prediction of reinforcement corrosion in RC beams through the measurement of crack widths, Submitted to Journal of Structural concrete

Principal Author

Name of Principal Author (Candidate)	Qian Feng
Contribution to the Paper	Performed analysis on data processing and programming of numerical models, interpreted data and wrote manuscript.
Overall percentage (%)	75%
Certification:	This paper reports on original research I conducted during the period of my Higher Degree by Research candidature and is not subject to any obligations or contractual agreements with a third party that would constrain its inclusion in this thesis. I am the primary author of this paper.
Signature	Date 19/08/2016

Co-Author Contributions

By signing the Statement of Authorship, each author certifies that:

i. the candidate's stated contribution to the publication is accurate (as detailed above);

ii. permission is granted for the candidate in include the publication in the thesis; and

iii. the sum of all co-author contributions is equal to 100% less the candidate's stated contribution.

Name of Co-Author	Phillip Visintin
Contribution to the Paper	Supervised work progress, gave suggestions and acted as corresponding author.
Signature	Date 19/08/2016

Name of Co-Author	Deric Oehlers
Contribution to the Paper	Supervised work progress, helped wrote and edited the manuscript
Signature	Date 19/08/2016

Please cut and paste additional co-author panels here as required.

A mechanics prediction of reinforcement corrosion in RC beams through the measurement of crack widths

Q. Feng, P. Visintin and D.J. Oehlers

Abstract

The corrosion of steel reinforcement in reinforced concrete beams is a common occurrence and can be of major concern. The latter stages of corrosion can be detected visually through the occurrence of splitting cracks in line with the reinforcement. This paper shows that a more effective way of monitoring reinforcement corrosion is in measuring the flexural crack widths as this is a direct measure of the deterioration in bond due to corrosion. This paper describes a mechanics based approach for the detection and quantification of steel reinforcing bar corrosion via monitoring of the variation in flexural crack widths under serviceability loading with time. It is shown that continuous measurement of crack widths is a very effective way of monitoring steel corrosion as: it can detect small local areas of corrosion in beam lengths as small as the crack spacings; it is relatively easy to physically measure crack widths; the effects of shrinkage can be easily accounted for; and crack widths are unaffected by concrete creep. In contrast monitoring deflections due to corrosion is difficult as: the results are clouded by concrete creep; it is physically difficult to monitor the whole beam deflection; and beam deflections are insensitive to the effects of localised corrosion and hence the results are only of use should the reinforcement be corroding along the whole span.

Keywords: steel reinforcing bars; corrosion; reinforcement corrosion; reinforced concrete beams; monitoring crack widths; crack widths; time effects.

Notation

A_c = cross-sectional area of concrete prism

A_r = total cross-sectional area of tension reinforcement

B_n = bond force in n^{th} element of prism

C = percentage corrosion by weight

C_n = concrete force in n^{th} element of prism

C_0 = 0% corrosion

$C_{1\text{-}2}$ = C at transition from Stage 1 to Stage 2; C at start of rapid reduction in bond

$C_{2\text{-}3}$ = C at transition from Stage 2 to Stage 3; C at end of rapid reduction in bond

c = distance from tension reinforcement to tension face; half prism depth

D_{co} = deflection of beam due to corrosion throughout

$D_{co\text{-}pt}$ = deflection of beam de to corrosion in part

D_{cr} = deflection of beam due to creep

D_{sh} = deflection of beam due to shrinkage

E_c = concrete modulus

E_r = reinforcement modulus

k = bond-slip stiffness

$k(C_0)$ = k at C_0

$k(C_{2\text{-}3})$ = k at $C_{2\text{-}3}$

L_{def} = deformation length in a segmental analysis

L_{per} = total circumferential length of tension reinforcement

L_s = length of prism segment

M = moment

M_s = serviceability moment

P_{cc} = concrete compressive force

P_{cr} = force in reinforcing bars at a flexural crack

P_n = reinforcement force in n^{th} prism element

P_{rc} = force in reinforcing bar in compression

S_{cr} = flexural crack spacing

T = time

T_0 = time at first monitoring

w_{cr} = crack width

w_{cr0} = crack width first measured

Δ_{cr} = reinforcement slip at crack face; half crack width w_{cr}

Δ_n = slip in n^{th} prism element

$\delta\Delta_n$ = increase in slip in n^{th} element

δ_1 = bond slip at τ_{max}

δ_{max} = slip when bond descends at τ=0

$\delta_{max}(C)$ = δ_{max} for 0% corrosion

ε_c = concrete strain

ε_r = reinforcement strain

ε_{cn} = mean concrete strain in n^{th} element

ε_{rn} = mean reinforcement strain in n^{th} element

ε_{sh} = shrinkage strain

ε_{sh0} = ε_{sh} when first measured

ϕ_0 = creep coefficient when first measured

θ = rotation

τ = bond shear stress

τ_{max} = bond shear strength

$\tau_{max}(C_0)$ = τ_{max} at C_0

$\tau_{max}(C_{2\text{-}3})$ = τ_{max} at $C_{2\text{-}3}$

Figures

Introduction

The corrosion of reinforcement affects virtually all aspects of the behaviour of reinforced concrete. At the serviceability limit state corrosion leads to a degradation of the bond between the reinforcement and the concrete (Almusallam et al., 1996; Cabrera 1996; Feng et al., 2016c; Val et al., 1998), which leads to reduced tension stiffening and increased deflections and crack widths. At the ultimate limit state corrosion leads to a loss of reinforcement area and hence a reduction in strength (Feng et al., 2016a; Jin and Zhao 2001; Mangat and Elgarf 1999). Additionally the degradation of the bond between the reinforcement and concrete may lead to global debonding of reinforcement resulting in a loss of strength and ductility (Eyre and Nokhasteh 1992; Feng et al., 2016b; Val et al., 1998). Given the consequences of corrosion on the performance of reinforced concrete structures, it is vital that engineering practitioners have reliable methods for predicting the level of corrosion of reinforcement.

While several non-destructive electrochemical and transient based techniques are available for predicting reinforcement corrosion (Montemor et al., 2003), these have been reported to be imprecise (Khan et al., 2014). An alternative approach proposed by several researchers (Khan et al., 2014; Rodriguez et al., 1996; Vidal et al., 2004; Zhang et al., 2010) is the prediction of corrosion via correlation of measured longitudinal corrosion crack widths with empirical observations of crack width for known corrosion levels.

In this paper an alternate technique is suggested where it is shown that by monitoring the variation in flexural crack width over time the average level of corrosion between two flexural cracks can be predicted. Importantly this approach, which is based on the mechanics of partial interaction theory, can allow for the combined influence of corrosion and concrete shrinkage and creep (Knight, D et al., 2015; Knight et al., 2013; Visintin et al., 2013a). It also directly makes use of the significant quantity of research available which quantifies the variation in the bond between reinforcement and concrete with corrosion, as well as the influence of reinforcing bar diameter, reinforcement cover and concrete strength (Almusallam et al., 1996; Cabrera 1996; Feng et al., 2016c).

The proposed scenario in this paper is that the structural engineer can monitor with time, pairs of adjacent flexural cracks in reinforced concrete (RC) beams or slabs that are in regions of that beam in which there is concern with regard to corrosion. The purpose of this paper is to provide mechanics based approaches for interpreting these monitored results and extracting from them the amount of corrosion. Once the structural engineer has extracted the amount of corrosion, this paper can be used to quantify the effect of the corrosion on serviceability and other published approaches (Eyre and Nokhasteh 1992; Feng et al., 2016b; Yuan and Marosszeky 1991) can be used to determine the effect on the ultimate limit state. It is not the purpose of this paper to try and predict how corrosion will progresses with time. However any predictive model could be used in the analyses procedure described in this paper to predict the effect of further corrosion.

In this paper a partial interaction (PI) numerical segmental analysis of RC beams (Knight et al., 2013; Knight, Daniel et al., 2015; Visintin et al., 2013a) that incorporates the time dependent behaviour of concrete, that is, shrinkage, creep and reinforcement corrosion is first explained. This is followed by a description of the time dependent material properties that can be used in the numerical analyses. These material properties are presented as an example and the readers may substitute any material properties they consider better or more appropriate. The numerical model is then used to illustrate typical variations in crack widths with time which leads to the development of monitoring sheets to help the structural engineer interpret the results of crack width monitoring and, in particular, extract the amount of corrosion between two cracks.

PI time dependent mechanics of crack widths

Tension stiffening mechanics of crack widths

Consider a segment of an RC beam or slab between two flexural cracks of spacing S_{cr} as shown in Fig. 1(b). Each segment face B-B is subjected to an Euler-Bernoulli displacement A-A as shown that cause rotations θ, a constant moment M and a force in the tension reinforcement at the flexural crack of P_{cr} (Knight, Daniel et al., 2015; Oehlers et al., 2014; Visintin et al., 2013a). Because of the flexural cracks, the tension reinforcement slips relative to the adjacent concrete which is referred to as partial-interaction (PI). It is common practice (Knight et al., 2013; Visintin et al., 2013a) to simulate this PI mechanics using a tension-stiffening prism as in Fig. 1(d) where Δ_{cr} is the slip of the reinforcement relative to the crack face when the force in the reinforcement is P_{cr} and is equivalent to the half crack width at the level of the tensile reinforcement $w_{cr}/2$.

The tension stiffening prism in Fig. 1(c) has a total concrete cross sectional area A_c and is reinforced with a total area of tensile reinforcement A_r which has a total bonded perimeter L_{per}. For analysis the height of the tension stiffening prism is taken such that the reinforcement is located at the centroid c.

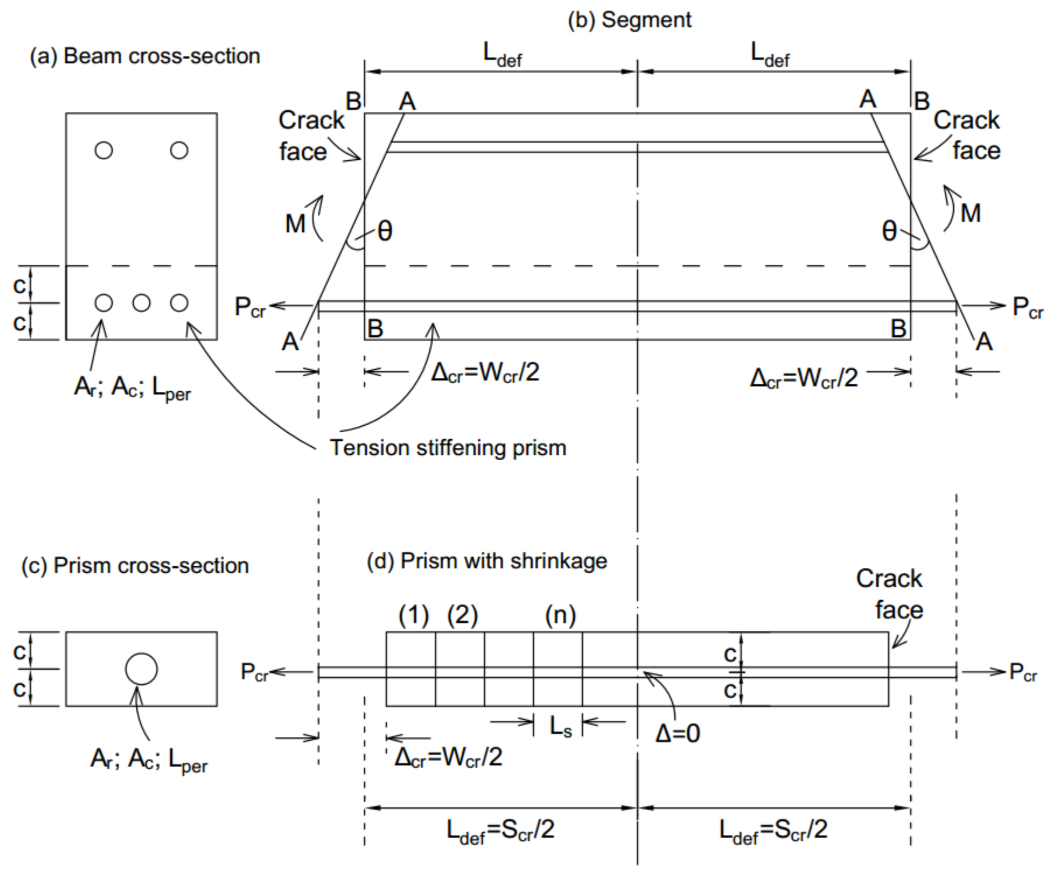

Figure 1 Beam segment components

The prism in Fig. 1(d) is divided into x small lengths of L_s as shown (Knight et al., 2013; Visintin et al., 2013a). The n^{th} element is shown in Fig. 2. Prior to concrete shrinkage, at a strain ε_{sh}, the left hand side (LHS) of the element is located at D-D and the right hand side (RHS) at A-A; the latter will also be used as a base line to measure all deformations. On the application of a concrete shrinkage strain ε_{sh}, the concrete face D-D, when unrestrained, will move to the right $\varepsilon_{sh}L_s$ to B-B shown in Fig. 2(b); this is the unstressed concrete state and any straining from this position ε_{cn} will cause a concrete stress. In contrast as the reinforcement does not shrink, any reinforcement straining ε_{rn} relative to D-D will cause a stress in the reinforcement.

The force in the reinforcement on the LHS of the n^{th} element in Fig. 2 is P_n and the slip is Δ_n as shown. The interface bond force B_n in Fig. 2(b) can be derived from the bond-slip properties for Δ_n and the surface over which it acts $L_{per}L_s$. Hence the force in the reinforcement reduces to P_n-B_n on the RHS. The mean of the reinforcement force can be used to derive the mean reinforcement strain ε_{rn} which causes an extension $\varepsilon_{rn}L_s$ as shown. The force on the concrete is C_n on the LHS and increases by B_n to that on the RHS as shown, and the mean strain in the concrete is ε_{cn} which causes an extension $\varepsilon_{cn}L_s$ also shown. Hence the change in slip $\delta\Delta_n$ as shown where the strain component in brackets is referred to as the slip strain $d\Delta/dx$.

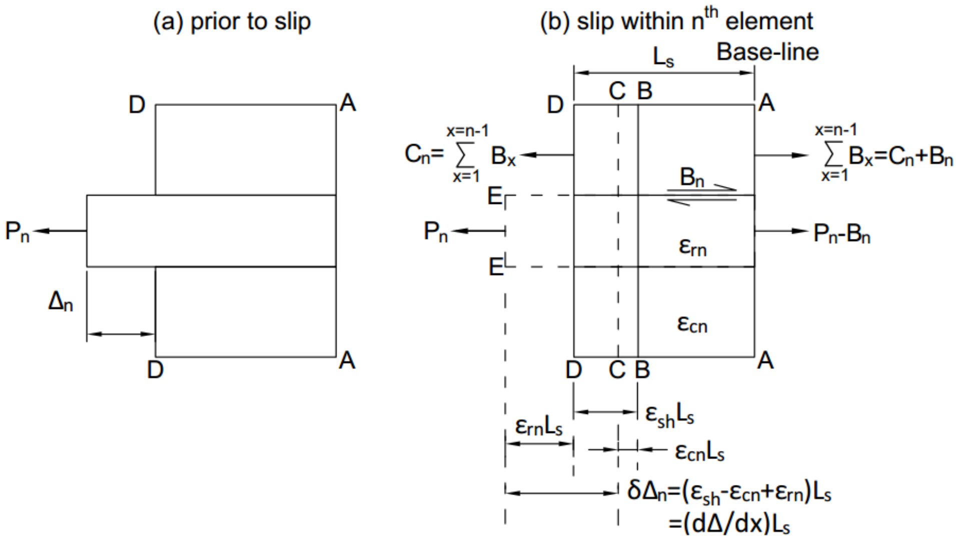

Figure 2 n^{th} prism element

The PI analysis depicted in Fig. 2 is applied to the first two elements in Fig. 1(d) in Fig. 3. Consider the first element which is adjacent to the flexural crack in Fig. 3(a). The steps in the numerical analysis are listed (A) to (G) below Element 1:

(A) At the crack face Δ_1 is equal to the slip of the reinforcement relative to the crack face Δ_{cr} which is equal to half the crack width that is $w_{cr}/2$. For analysis, a slip Δ_1 is imposed such that the problem is to derive the force P_1 to cause the slip Δ_1. Hence an initial guess for P_1 is made.

(B) As the analysis deals with serviceability loads, the bond slip properties can be considered to be linear (Muhamad et al., 2012; Visintin et al., 2013b) that is the relation between bond stress τ and bond slip Δ is a constant k. Hence for the imposed Δ_1, can be derived τ_1.

(C) From the known bond stress τ_1, the corresponding bond force B_1 within Element 1 can be derived.

(D) From equilibrium of forces across the element the change in concrete force and hence mean concrete strain ε_{c1} can be determined.

(E) Similarly, from equilibrium of forces across the element, the change in reinforcement force and hence mean reinforcement strain ε_{r1} can be determined.

(F) Knowing the concrete shrinkage strain and having determined the average strain in the concrete and the reinforcement, the slip strain $d\Delta_1/dx$ can be derived.

(G) Consequently the change in slip within the first element $\delta\Delta_1$ is known, from which the slip in the subsequent element Δ_2 can be determined.

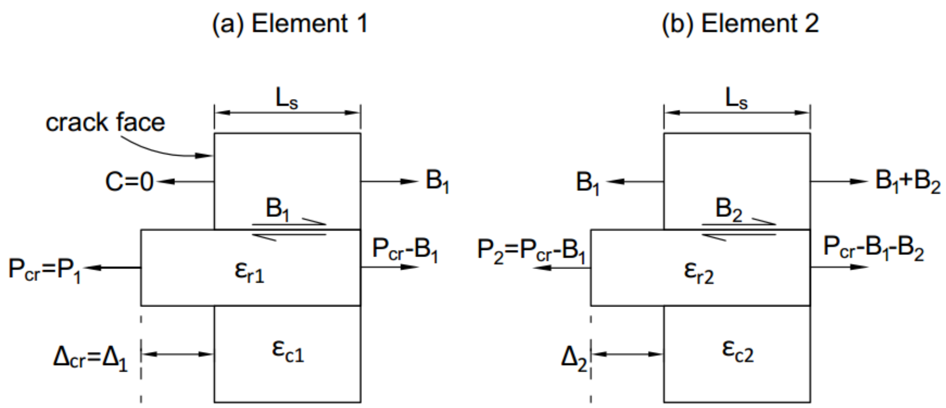

(A)	$\Delta_1=\Delta_{cr}=w_{cr}/2$	$\Delta_2=\Delta_1-\delta\Delta_1=\Delta_{cr}-(\varepsilon_{sh}-\varepsilon_{c1}+\varepsilon_{r1})L_s$
(B)	$\tau_1=k\Delta_1$	$\tau_2=k\Delta_2$
(C)	$B_1=\tau_1 L_{per} L_s$	$B_2=\tau_2 L_{per} L_s$
(D)	$\varepsilon_{c1}=(0+B_1)/(2E_cA_c)$	$\varepsilon_{c2}=(2B_1+B_2)/(2E_cA_c)$
(E)	$\varepsilon_{r1}=(2P_{cr}-B_1)/(2E_rA_r)$	$\varepsilon_{r2}=(2P_{cr}-2B_1-B_2)/(2E_rA_r)$
(F)	$d\Delta_1/dx=\varepsilon_{sh}-\varepsilon_{c1}+\varepsilon_{r1}$	$d\Delta_2/dx=\varepsilon_{sh}-\varepsilon_{c2}+\varepsilon_{r2}$
(G)	$\delta\Delta_1=(d\Delta_1/dx)L_s$	$\delta\Delta_2=(d\Delta_2/dx)L_s$

Figure 3 Tension stiffening analysis

The results from the analysis of Element 1 in Fig. 3(a) are now used in the analysis of Element 2 as listed below the element. This procedure is continued until the x^{th} element in Fig. 1(d) that is adjacent to the mid-length of the prism. By symmetry the slip at mid-length Δ is zero. Hence if slip Δ_x from the numerical analysis is not zero, then it is a question changing the guessed value of P_1 until it is.

Material properties

The mechanics of the tension stiffening analysis described above does not depend directly on the material properties used. For example Code values for the variation of shrinkage and creep with time could be used or any values the reader deems appropriate. A summary of material models can be found in (Gilbert and Ranzi 2011).

Of importance is the variation of the bond stiffness *k* with corrosion. Research by (Feng et al., 2016c) suggests that the bond strength τ_{max} varies with corrosion as shown in the three stages in Fig. 4 where: τ_{max0} is the bond strength with zero corrosion; *C* is the percentage corrosion by weight; C_0 signifies zero corrosion. The transition between the three stages in Fig. 4 can be defined by the points $C_{1\text{-}2}$ which is the percentage corrosion when the bond strength starts reducing rapidly and which is often the onset of the longitudinal splitting cracks; and $C_{2\text{-}3}$ which is the percentage corrosion when splitting cracks are fully developed, beyond which a gradual reduction in bond strength occurs.

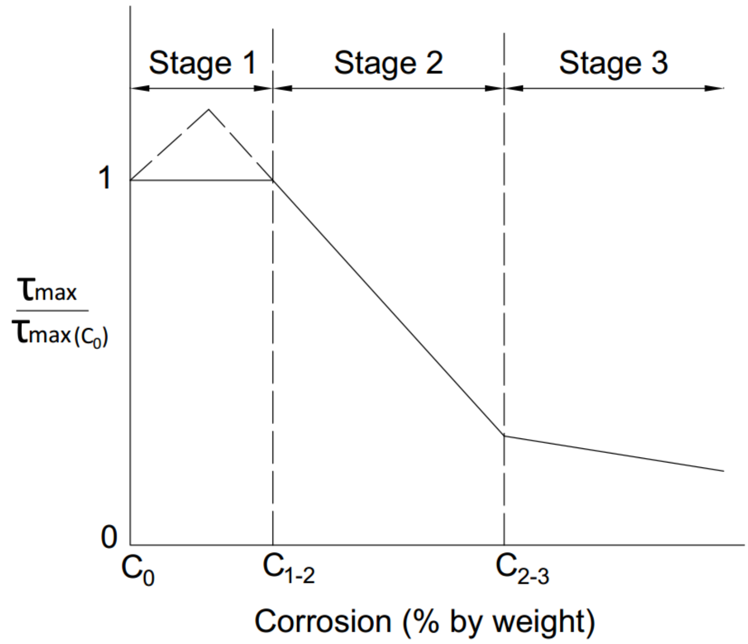

Figure 4 Variation of bond strength with corrosion

Again it is worth mentioning that much research has been conducted to quantify the variation in bond properties with corrosion (Albitar et al., 2016; Almusallam et al., 1996; Cabrera 1996; Feng et al., 2016c; Val et al., 1998) and any model deemed appropriate may be used in the analysis. Here the model of (Feng et al., 2016c) is presented as it was derived from the analysis of 377 data points from test results covering a broad range of material properties. The variation in bond-slip with corrosion

(Feng et al., 2016c) is shown in Fig. 5 where: δ_1 is the slip at τ_{max} as shown and can be taken as a constant value of 0.175 mm; and δ_{max} is the slip when the bond stress tends to zero.

The ultimate bond strength τ_{max} with corroded reinforcement is defined as

$$\tau_{max-C} = k_t \tau_{max-0} \tag{1}$$

Where the corrosion reduction factor k_t varies with the level of corrosion C as follows:

$$k_t = \left(-0.032\frac{c}{d} + 0.576\right)C + 1,\ when\ 0 < C < 0.3C_{1-2} \tag{2}$$

$$k_t = \left(0.0137\frac{c}{d} - 0.247\right)C + 1.42 + 0.0475\frac{c}{d} - 3.94\times10^{-3}(\frac{c}{d})^2,\ when\ 0.3C_{1-2} < C < C_{2-3} \tag{3}$$

$$k_t = -0.0016C + 0.224,\ when\ C > C_{2-3} \tag{4}$$

In which: C is the level of corrosion in terms of percentage of mass loss; c/d is the ratio of cover to the edge of the bar c and the bar diameter d; C_{1-2} is the transition point where splitting cracks form; and C_{2-3} is the transition point where to the residual bond strength after the formation of splitting cracks. The transition points C_{1-2} and C_{2-3} are calculated as follows.

$$C_{1-2} = 0.288\frac{c}{d} + 1.72 \tag{5}$$

$$C_{2-3} = \frac{-1.20 - 0.0475\frac{c}{d} + 3.94\times10^{-3}(\frac{c}{d})^2}{0.0137\frac{c}{d} - 0.245} \tag{6}$$

The coefficient τ_{max-0} is the bond strength when there is no corrosion and which has been suggested by the CEB Model Code (CEB-FIP Model Code 1990: Design Code 1994) to be

$$\tau_{max-0} = 7\times(\frac{f_c}{25})^{0.25} \tag{7}$$

It should be noted that Eq. 7 corresponds to the scenario in which where good bond conditions are present. The variation in bond strength with corrosion given Eq. 1-6 is independent of the definition of τ_{max-0} and hence Eq. 7 can be substituted for any bond model covering any initial conditions according to the best judgement of the reader.

As this paper is only dealing with serviceability, only the ascending branch in Fig. 5 needs to be considered as in Fig. 6. The serviceability bond stiffness at zero corrosion is shown as $k(C_0)$. From the work of (Feng et al., 2016c) who determined the average slip at peak stress is 0.175 It is suggested that $k(C_0)$ could be taken as

$$k(C_0) = 40\times(\frac{f_c}{25})^{0.25} \tag{8}$$

However, any appropriate value could be taken as it will be shown subsequently that the assessment procedure does not depend on an accurate value.

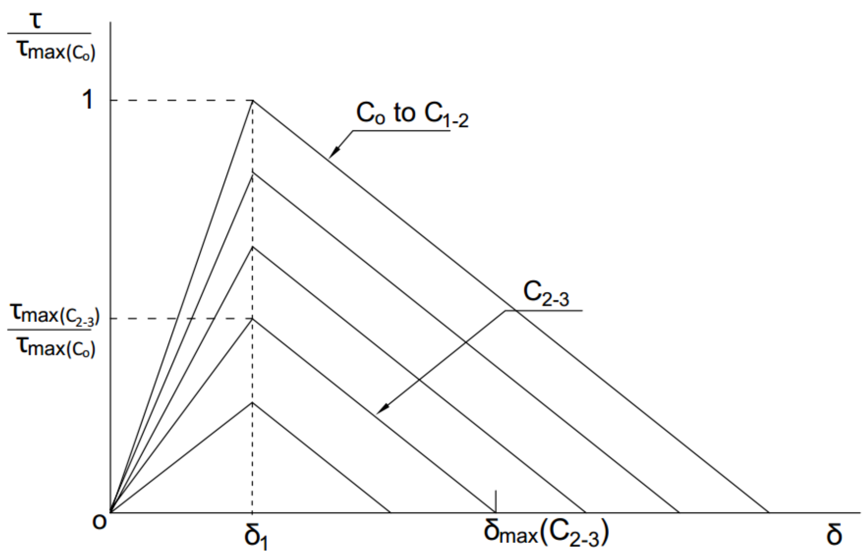

Figure 5 Variation in bond-slip with corrosion

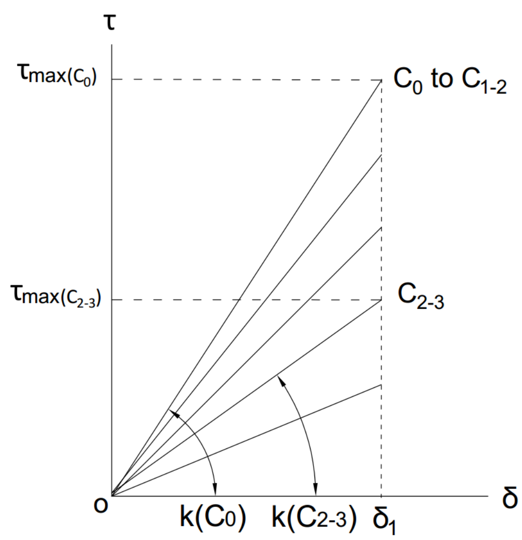

Fig. 6 Serviceability bond stiffness

Monitoring sheet

Consider a beam that is being monitored from an early stage starting at time T_0 such that corrosion has not yet started; other scenarios will be considered later. The existing RC beam has two visible adjacent flexural cracks of mean width w_{cr0} at a spacing S_{cr} as shown in Fig. 1(b). Let the moment acting on the beam in the vicinity of these flexural cracks be estimated as M_s and the shrinkage strain ε_{sh0} and creep coefficient ϕ_0 at T_0 be estimated from code variations (Gilbert and Ranzi 2010). For a given M_s, ε_{sh0} and ϕ_0 the force in the reinforcement can be determined as P_{cr} from any standard analysis technique such as the moment curvature approach *(Gilbert and Ranzi 2010)* or from any advance analysis technique such as the segmental approach which directly incorporates the influence of bond-slip and concrete time effects *(Knight et al., 2013; Visintin et al., 2013a)* or estimated by approximating the location of the neutral axis depth (Warner et al., 1998). A tension stiffening analysis as depicted in Fig. 3 can then be applied and the bond stiffness $k(C_0)$ adjusted until the crack width is equal to the measured value w_{cr0}.

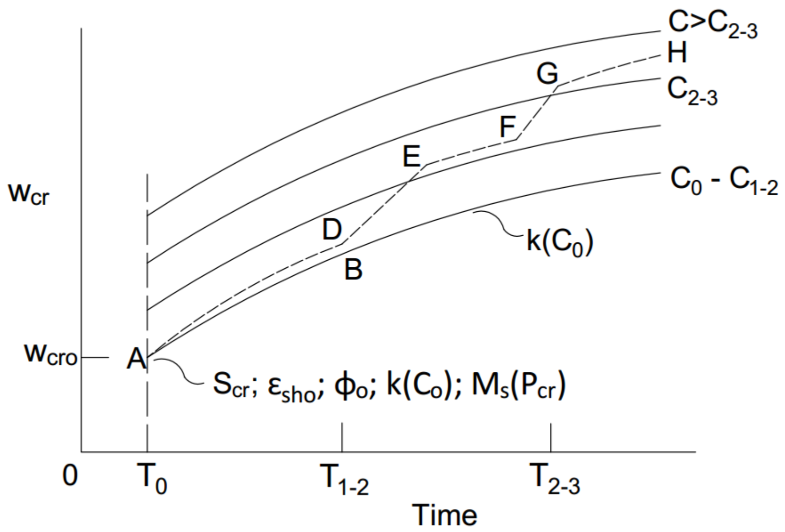

Figure 7 Monitoring corrosion from crack width

Assuming code values for the variation in shrinkage and creep with time, the tension stiffening analysis in Fig. 3 can be used to derive the variation A-B-C in Fig. 7 that is without corrosion. This variation will be assumed to be appropriate in Stage 1 in Fig. 4 that is from C_0 to $C_{1\text{-}2}$ where corrosion does not lead to a reduction in bond strength. Similarly, by simply varying k in Fig. 6 according to the level of corrosion the tension stiffening analysis can also be used to determine the variation in crack widths with increasing corrosion.

Plotting the measured flexural crack width time, which is shown by the dashed line in Fig. 7 it is therefore possible to predict the average level of corrosion between the flexural cracks. For example, should the measured crack widths lie along A-D that is not significantly diverged from the predicted A-B, then this would suggest that the measured crack widening can be attributed to shrinkage and creep. Should divergence occur such as along D-E, then this would suggest that Stage 2 in Fig. 4 has started at time $T_{1\text{-}2}$ in Fig. 7. A levelling off such as E-F in parallel with the predicted value would suggest that there was no further increase in corrosion. Path F-G suggests further corrosion and a shallower path G-H would suggest Stage 3 in Fig. 4 has been reached.

This monitoring procedure does give an indication of whether detrimental corrosion is occurring and also an indication of the percentage of corrosion. It will be shown later that this information can be used to assess the serviceability deflection and it can also be used to predict the ultimate flexural capacity (Feng et al., 2016b).

Monitoring crack widths

For a given RC beam, the tension stiffening analysis as explained above can be used to predict the variation in crack width with time for a range of bond stiffnesses *k* as in Fig. 8. The measured crack width w_{cr0} can then be used to predict the starting position Point A that is $k(C_0)$ and the application proceeds as explained previously. These tension stiffening analyses also showed that variations in creep does not affect the crack width even though it will be shown later that it has a significant effect on the deflection. Hence in quantifying the variation in crack width with time, only shrinkage and corrosion needs to be considered.

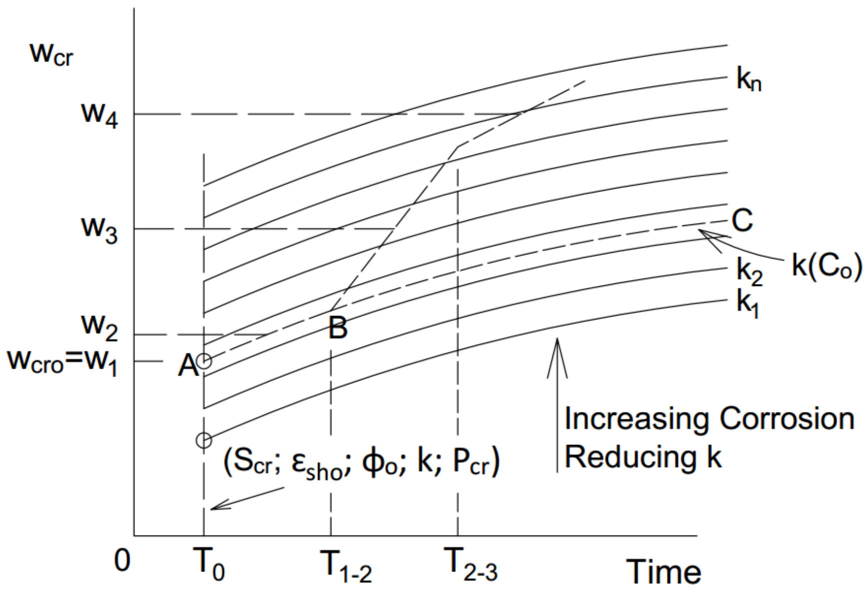

Figure 8 Monitoring sheet of crack width

The variation A-B-C in Fig. 8 is now the true $k(C_0)$ in Fig. 7. This is the value in Fig. 6 from which changes in bond stiffness due to corrosion are calculated. Hence it is the reduction in *k* above $k(C_0)$ in Fig. 8 that is due to corrosion as shown on the RHS of the figure. Consequently the variation in crack width due to corrosion shown as the dashed line relative to A-B-C can be used to predict the amount of corrosion as already explained using Fig. 7.

As an example of application of the proposed technique, consider the beam cross section in Fig. 9. The beam is constructed from concrete with a compressive strength of 25 MPa, a tensile strength at 2.8 MPa and a modulus of elasticity of 25 GPa. The diameter of reinforcement is 16 mm and has a modulus of elasticity of 200 GPa. The variation in the bond between the reinforcement and concrete has been taken as that defined by (Feng et al., 2016c) which is given by Eq. 1-7 and the variation in corrosion over has been taken as that experimentally recoded by (Vidal et al., 2007). Australian Standards (Australia 2009) have been used to define the variation in concrete shrinkage and creep with time.

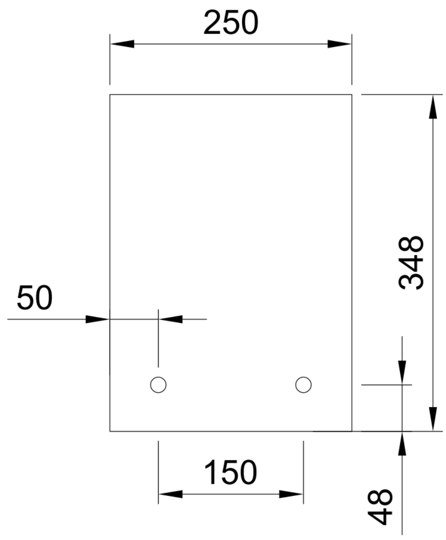

Figure 9 Dimensions of the cross-section

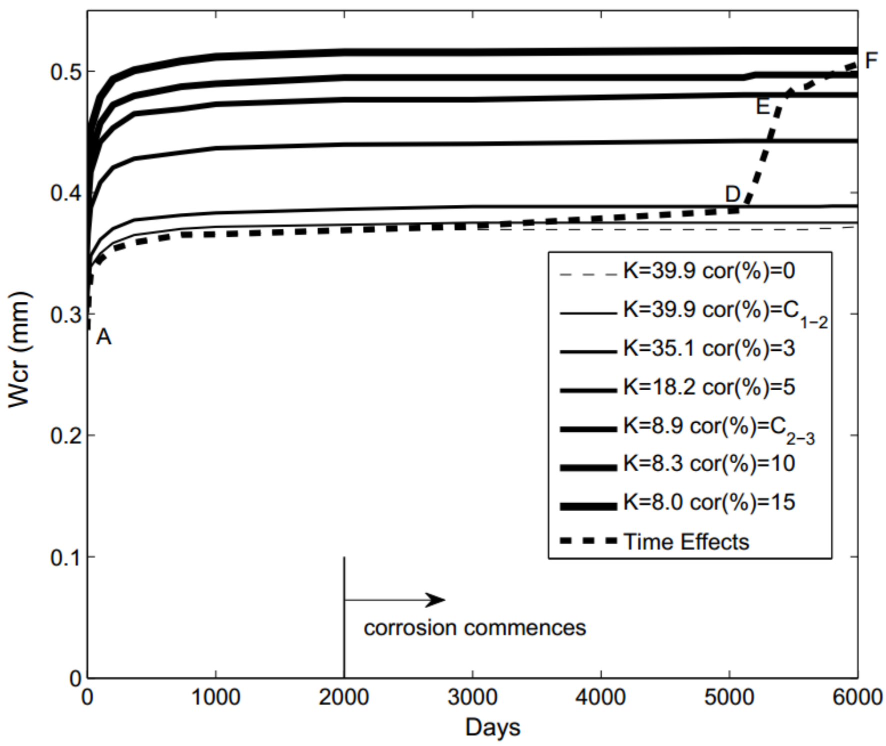

Figure 10 Variation in crack width with time

The monitoring sheet relating to the above mentioned scenario is shown in Fig. 10, where corrosion is varied from 0%-15%. In Fig. 10, Point A represents the application of load at day zero where concrete shrinkage and creep and reinforcement corrosion is zero. The crack width increases with concrete shrinkage up until day 2000 at which point corrosion commences. It can be observed that between day 2000 and day 5000 a gradual increase in crack width above that which is expected to occur due to concrete time effects alone occurs, that is, there is a deviation from the crack width corresponding to no corrosion. A rapid increase in crack width occurs at approximately day 5000. This point corresponds to a corrosion level of approximately 3%, which according to the model of (Feng et al., 2016c) results in the formation of splitting cracks. Finally, the widening of cracks is observed to slow between points E and F in Figure 10 which corresponds to the complete formation of splitting cracks and loss of significant confinement to the bar by the concrete cover beyond point C_{2-3} in Figure 4.

Up until this point we have considered the scenario where crack monitoring commenced when the corrosion level is in Stage 1 in Fig. 4 that is before $C_{1-2,}$ that is where the crack opening behaviour follows path A-B in Fig. 8 with time. Hence a crack width w_2 in Fig. 8 will give the same $k(C_0)$. However there is a difficulty when monitoring starts after Stage 1 in Fig. 4 as illustrated by w_3 or w_4 in Fig. 8. A solution to this problem is to monitor a pair of cracks in a region where corrosion is not expected as in Fig. 11(a) and also to monitor a pair of cracks in a region where corrosion is expected in Fig. 11(b).

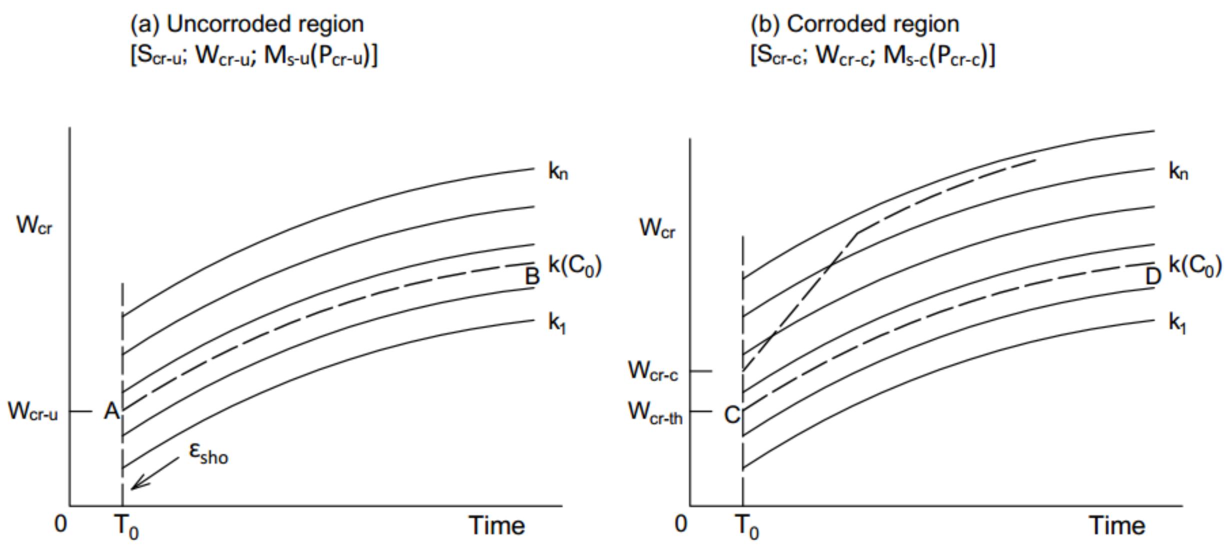

Figure 11 Monitoring two pairs of cracks

Each of the regions in Fig. 11 will have their unique crack spacing, crack width and moment as shown in the square brackets. The analysis depicted in Fig. 8 for the uncorroded region is shown in Fig. 11(a) from which can be derived $k(C_0)$. The variation for this stiffness are shown in Fig. 11(b) for the corroded region which is now the base line for predicting corrosion levels as described in Fig. 8. Hence in this approach the uncorroded region is used to determine $k(C_0)$ for the corroded region.

The above approach of monitoring in corroded and uncorroded regions can be taken one step further. Non-dimensionalising the ordinate in Fig. 11(a) by dividing w_{cr} by w_{cr-u} and that in Fig. 11(b) by w_{cr-th} and then comparing the variations at $k(C_0)$ generally shows little variation. This is because in the tension stiffening analyses all the material properties including the bond-slip are assumed linear. Hence it is only necessary to compare the proportional increase in crack width in the corroded region w_{cr}/w_{cr-u} with the proportional increase in the uncorroded region w_{cr}/w_{cr-th}. Any major divergence would signify corrosion after which the analysis in Fig. 11(b) could be performed to determine the amount of corrosion. Hence initially there is no need to plot the figures in Fig. 11 rather it is only necessary to compare the proportional increases in crack width. Once corrosion is detected then the figures will have to be plotted to determine the amount of corrosion.

Monitoring deflection

The segmental deformation in Fig. 1 can also be used to predict the effect of corrosion on the beam deflection. The RHS of the segment in Fig. 1(b) is shown in Fig. 12. The Euler-Bernoulli deformation A-A in Fig. 12(a), can be converted to a strain, stress and force distributions as shown to the right in order to derive the moment-curvature (M/χ) at serviceability; full descriptions of this numerical analysis are published and validated against experimental results elsewhere (Knight et al., 2013; Visintin et al., 2013a) and hence not repeated here. The tension stiffening analysis has shown that creep has virtually no effect on crack width. However creep will reduce the concrete modulus so that the Euler-Bernoulli deformation A-A needs to move to C-C with an increase in rotation due to creep $\Delta\theta_{cr}$. It can be seen how creep significantly increases the deflection but does not affect the crack width. Hence monitoring the crack width is more effective than monitoring the deflection.

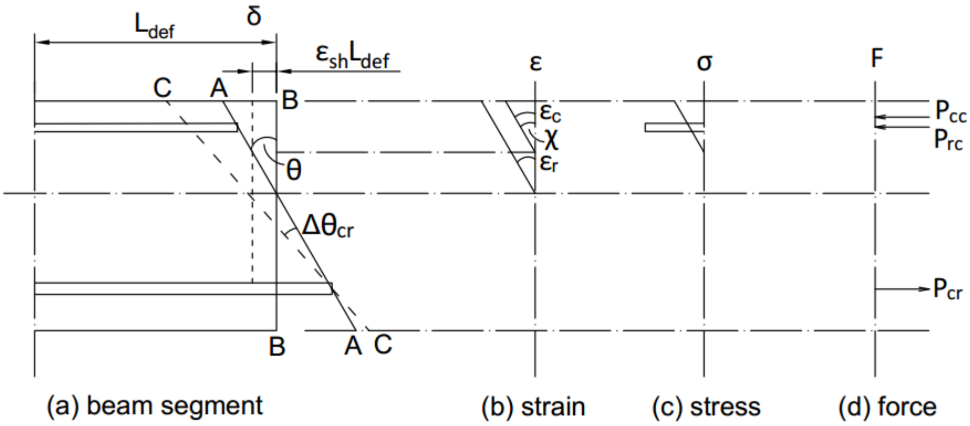

Figure 12 Segmental analysis

The moment curvature results from the analysis in Fig. 12 can then be used to predict the deflection of a beam with time as in Fig. 13. It can be seen at time T_2 that the deflection has three components: that due to creep D_{cr}; that due to shrinkage D_{sh}; and that due to corrosion D_{co}. When only part of the beam corrodes then the increase in deflection $D_{co\text{-}pt}$ is small and can be clouded by $D_{cr}+D_{sh}$ that is it would be difficult to detect. Additionally, the monitoring of crack widths allows the average corrosion between each pair of adjacent cracks to be easily determined while a monitored deflection alone does not yield a unique level of corrosion.

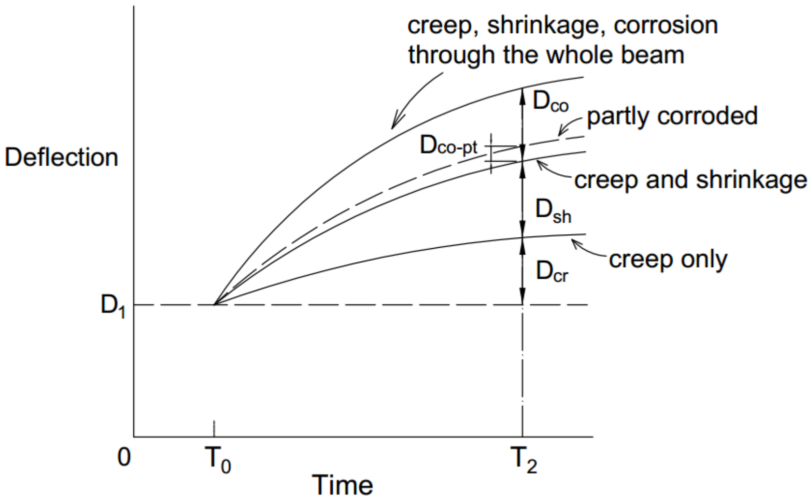

Figure 13 Time dependent beam deflection

By way of an example of application, again consider the cross section in Fig. 9 which is used to construct a beam with a span of 3500mm and which is loaded in 4 point bending with the loads applied at the third span. For an applied load which yields a stress in the tensile reinforcement of half of the yield strength, the variation of mid-span deflection with time is shown in Fig. 14 for three different corrosion scenarios (i) where uniform corrosion exists along the entire span as in Fig. 15(a);

(ii) where only 20% of the beam is corroded at mid-span as in Fig. 15(b); and (iii) where only the portion of the beam near the supports is corroded as is Fig. 15(c).

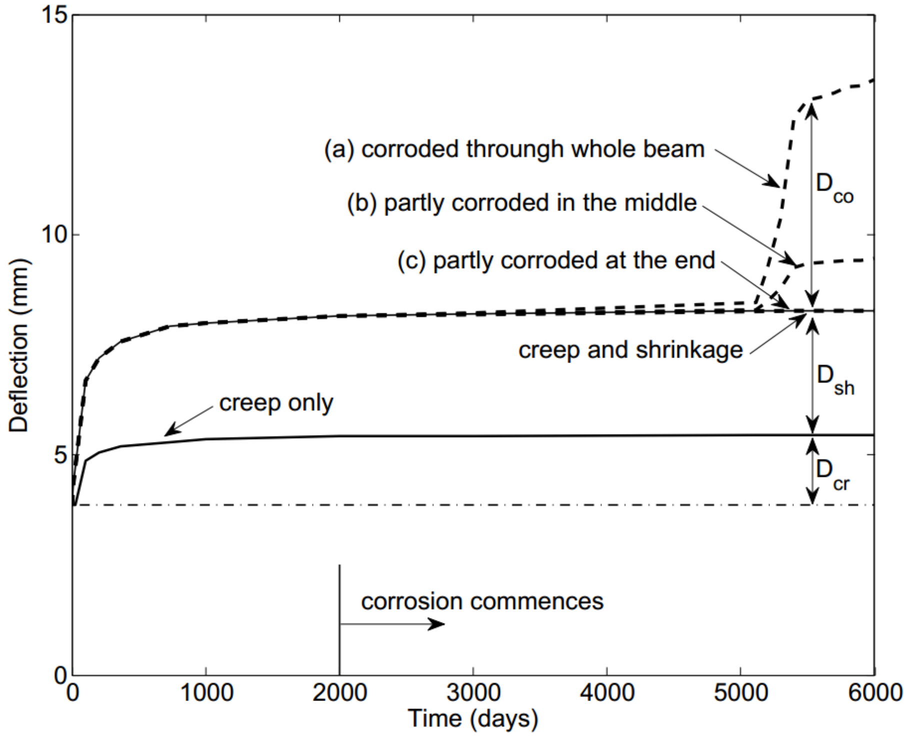

Figure 14 Change in Deflection with time

In Fig. 14 it can be seen that although corrosion commences at day 2000, even when the whole beam is considered to be uniformly corroded, no significant increase in deflection due to corrosion can be detected until splitting cracks form at approximately day 5200 where the corrosion level has reached 3%. This is particularly significant as the small variation in deflection due to corrosion could easily be lost in the variation in concrete creep and shrinkage strains which are known to vary by as much as 30% (Australia 2009).

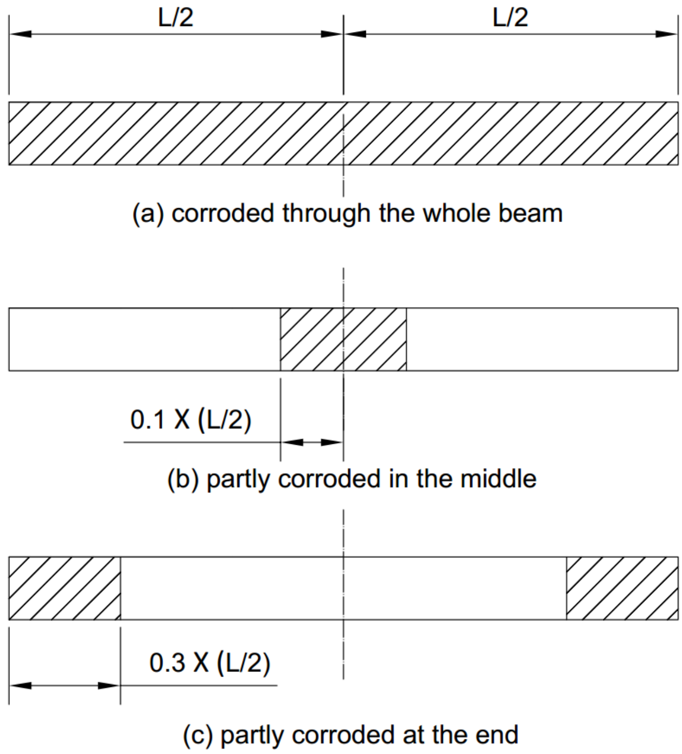

Figure 15 Varying extent of corrosion

The prediction of corrosion via the monitoring of member deflection is made more difficult when only a portion of the beam is corroded. For example consider the scenarios shown in Figures 15(b) and (c)where only the centre or the ends of the beam have corroded reinforcement. In these scenarios increases in deflection due to corrosion lie within the scatter expected from calculation of time effects, particularly when corrosion is concentrated in regions of low moment. As seen in the deflection measurement for end corrosion, it may therefore be difficult to estimate the level of corrosion from a measurement of deflection even after splitting cracks have formed.

Conclusions

It has been shown that monitoring crack widths is an effective procedure in monitoring steel reinforcement corrosion in RC beams and slabs because monitoring flexural crack widths can detect local areas of corrosion and the results are not clouded by creep. A partial interaction mechanics based approach that allows for changes in bond properties due to corrosion as well as the effects of creep and shrinkage has been described. It is shown how this model can be used to provide charts for the variation in crack width with time to monitor existing flexural cracks in beams or slabs to predict when the effects of corrosion are deleterious and also to give a guidance to the amount of corrosion that exists. The approach does not predict future corrosion but it can be used in conjunction with future corrosion predictions to estimate their effect on the structure.

References

Albitar, M, Visintin, P, Mohamed Ali, M, Lavigne, O and Gambowa, E (2016) Effects of corrosion on the bond between reinforcement and class-F fly ash based geopolymer concrete. *ASCE Materials in Civil Engineering. Accepted for publication.*

Almusallam, AA, Al-Gahtani, AS, Aziz, AR and Rasheeduzzafar (1996) Effect of reinforcement corrosion on bond strength. *Construction and Building Materials*, 10(2): 123-129.

Australia, S (2009) Australian Standards: Concrete structures.

Cabrera, J (1996) Deterioration of concrete due to reinforcement steel corrosion. *Cement and concrete composites*, 18(1): 47-59.

CEB-FIP Model Code 1990: Design Code, (1994), Thomas Telford, London.

Eyre, J and Nokhasteh, M (1992) Strength assessment of corrosion damaged reinforced concrete slabs and beams. *Proceedings of the Institution of Civil Engineers-Structures and Buildings*, 94(2): 197-203.

Feng, Q, Visintin, P and Oehlers, D (2016a) Quantifying through bond mechanics the effect of steel bar corrosion on the flexural capacity of RC beams. *Submitted to Proceedings of the Institution of Civil Engineers-Structures and Buildings*.

Feng, Q, Visintin, P and Oehlers, D (2016b) Quantifying through bond mechanics the effect of steel bar corrosion on the flexural capacity of RC beams. *Submitted to Structures and Buildings*.

Feng, Q, Visintin, P and Oehlers, DJ (2016c) Deterioration of bond–slip due to corrosion of steel reinforcement in reinforced concrete. *Magazine of Concrete Research*, 68(15): 768-781.

Gilbert, RI and Ranzi, G (2010) Time-dependent behaviour of concrete structures, *CRC Press*.

Gilbert, RI and Ranzi, G (2011) Time-dependent behaviour of concrete structures, *Spoon Press*.

Jin, W-l and Zhao, Y-x (2001) Effect of corrosion on bond behavior and bending strength of reinforced concrete beams. *Journal of Zhejiang University SCIENCE*, 2(3): 298-308.

Khan, I, François, R and Castel, A (2014) Prediction of reinforcement corrosion using corrosion induced cracks width in corroded reinforced concrete beams. *Cement and concrete research*, 56: 84-96.

Knight, D, Visintin, P and Oehlers, D (2015) Displacement ‐ based simulation of time ‐ dependent behaviour of RC beams with prestressed FRP or steel tendons. *Structural Concrete*, 16(3): 406-417.

Knight, D, Visintin, P, Oehlers, D and Jumaat, M (2013) Incorporating residual strains in the flexural rigidity of RC members with varying degrees of prestress and cracking. *Advances in Structural Engineering*, 16(10): 1701-1718.

Knight, D, Visintin, P and Oehlers, DJ (2015) Displacement - based simulation of time - dependent behaviour of RC beams with prestressed FRP or steel tendons. *Structural Concrete*, 16(3): 406-417.

Mangat, P and Elgarf, M (1999) Bond characteristics of corrding reinforcement in concrete beams. *Materials and structures*, 32(2): 89-97.

Montemor, M, Simoes, A and Ferreira, M (2003) Chloride-induced corrosion on reinforcing steel: from the fundamentals to the monitoring techniques. *Cement and concrete composites*, 25(4): 491-502.

Muhamad, R, Ali, MM, Oehlers, DJ and Griffith, M (2012) The tension stiffening mechanism in reinforced concrete prisms. *Advances in Structural Engineering*, 15(12): 2053-2069.

Oehlers, DJ, Visintin, P, Chen, JF and Ibell, TJ (2014) Simulating reinforced concrete members. Part 2: Displacement-based analyses. *Proceedings of the Institution of Civil Engineers-Structures and Buildings*, 167(12): 718-727.

Rodriguez, J, Ortega, L, Casal, J and Diez, J (1996) Corrosion of reinforcement and service life of concrete structures. *Durability of building materials and components*, 7(1): 117-126.

Val, DV, Stewart, MG and Melchers, RE (1998) Effect of reinforcement corrosion on reliability of highway bridges. *Engineering Structures*, 20(11): 1010-1019.

Vidal, T, Castel, A and Francois, R (2004) Analyzing crack width to predict corrosion in reinforced concrete. *Cement and concrete research*, 34(1): 165-174.

Vidal, T, Castel, A and François, R (2007) Corrosion process and structural performance of a 17 year old reinforced concrete beam stored in chloride environment. *Cement and concrete research*, 37(11): 1551-1561.

Visintin, P, Oehlers, D and Haskett, M (2013a) Partial-interaction time dependent behaviour of reinforced concrete beams. *Engineering Structures*, 49: 408-420.

Visintin, P, Oehlers, D, Muhamad, R and Wu, C (2013b) Partial-interaction short term serviceability deflection of RC beams. *Engineering Structures*, 56: 993-1006.

Warner, R, Rangan, B, Hall, A and Faulkes, K (1998) Concrete structures.

Yuan, Y-S and Marosszeky, M (1991) Analysis of corroded reinforced concrete sections for repair. *Journal of Structural Engineering*, 117(7): 2018-2034.

Zhang, R, Castel, A and François, R (2010) Concrete cover cracking with reinforcement corrosion of RC beam during chloride-induced corrosion process. *Cement and concrete research*, 40(3): 415-425.

CONCLUSIONS

Corrosion strongly influences the performance of reinforced concrete structures at the serviceability and ultimate limit states due to a reduction in the cross-sectional area of reinforcement, a deterioration of bond between the reinforcement and concrete, the formation of splitting cracks and ultimately debonding of the reinforcement. This thesis has developed a (i) material model to quantify the deterioration of bond between concrete and reinforcement caused by corrosion; (ii) a numerical model to simulate the debonding behaviour of reinforced concrete in ultimate limit states and (iii) a monitoring technique to detect the corrosion condition of reinforcement at serviceability limit.

The mathematical model of bond-slip relationship with corrosion is built based on a database with 377 data points to show how the bond-slip relationship changes after corrosion of bars occurs. The model was applied to analyse the examples with different material properties and different corrosion level which shows that when corrosion level increases, debonding may happen before bar yielding and bars with large diameter is more easily to be influenced by corrosion than bars with small diameter.

The mathematical model of bond-slip with corrosion indicates that debonding occurs when corrosion amount of reinforcement increases. Then numerical models were presented to simulate the beam behaviour in ultimate limit state before and after debonding of reinforcement. The segmental approach was applied to simulate the capacity of reinforced concrete prior to debonding while the numerical model of debonding was presented to show how to compute the capacity of reinforced concrete beam after debonding, in which condition, the reinforcing bars work as prestressed tendon. The procedures indicates that with certain material properties, even when debonding exists between concrete and bars due to the amount of corrosion, there still might be considerable strength and ductility provided by the structures by the compatibility of deformation between reinforcement and the concrete at the level of reinforcement.

Besides, an effective way of monitoring corrosion in serviceability was introduced by measuring the flexural crack width. Although corrosion influences deflection, the problem with measuring deflection is that deflection is normally affected by creep and shrinkage dramatically. The mechanics based approach described in this thesis shows that crack width is obviously affected by corrosion while creep has very less impact on flexural crack width in contrast. The continuous measurement of crack width indicates the increase of corrosion of steel bars in small local area, while the shrinkage effects with time could be very easily computed from references like building codes. Furthermore, the measurement of crack width is much easier than measuring deflection. Hence, this analysis provides a more efficient way to monitor the increase of corrosion of reinforcement inside the structures.

In summary, this thesis provides the mathematical model of bond-slip with corrosion effects, which quantified the reinforced concrete structural behaviour not only in ultimate limit states but also in serviceability limit states. Hence, the contribution of this thesis to future research work could includes these aspects: (1) the study of debonding behaviour of reinforced concrete with small local area of corrosion; (2) the study of the ultimate limit state behaviour of reinforced concrete with prestressed tendon based on the numerical models of segmental approach and the debonding model; (3) the experimental work of stirrup effects on bond with corroded reinforcement.